FINAL REPORT

ELECTROPHORESIS EXPERIMENT FOR SPACE

(NASA-CR-149925) ELECTROPHORESIS EXPERIMENT FOR SPACE Final Report (Lehigh Univ.) 87 p HC $5.00 CSCL 06A

N76-27837

Unclas

G3/52 44518

Contract No. NAS8-28654

April 1976

Prepared for:

George C. Marshall Space Flight Center
National Aeronautics and Space Administration
Huntsville, Alabama

by

Center for Surface and Coatings Research
Lehigh University
Bethlehem, Pa.

JUL 1976
RECEIVED
NASA STI FACILITY
INPUT BRANCH

Title: FINAL REPORT

ELECTROPHORESIS EXPERIMENT FOR SPACE

Prepared for: George C. Marshall Space Flight Center
National Aeronautics and Space Flight Center
Huntsville, Alabama

Prepared by:

John W. Vanderhoff, Principle Investigator

F. J. Micale, Co-Investigator

TABLE OF CONTENTS

		Page
INTRODUCTION		1
CHAPTER I	Analysis of the Apollo 16 Electrophoresis Experiment	2
CHAPTER II	Low-Electroosmotic Mobility Coatings	17
CHAPTER III	Resolution of Separation of Free-Fluid Electrophoresis	41
CHAPTER IV	Evaluation of the Beckman CPE with Standard Particles	72
CHAPTER V	Summary and Conclusions	80

LIST OF TABLES

Table		Page
I	Electrophoretic Mobilities and Observed Velocities of Latex Particles	9
II	Electroosmotic Flow in Coated Glass Capillaries	30
III	Electroosmotic Mobility of Coated Glass Capillary Tubes	33
IV	Electroosmotic Mobility of Coated Pyrex Glass Electrophoresis Columns	35
V	Electroosmotic Flow in Coated Plexiglas Cells	38
VI	Water Permeation Results	40

LIST OF FIGURES

Figure		Page
1.	Cell for Measuring Potential Gradient E	4
2.	Position of Apex of Parabola as a Function of Time	8
3.	Latex Parabolic Profile at 1, 2, 3, and 4 Minute Intervals	13
4.	Length of Parabolic Profiles as a Function of Time	14
5.	Free-fluid Electrophoretic Separation of Mixed 0.23μm and 0.80μm Monodisperse Polystyrene Latex Particles During Apollo 16 Mission	16
6.	Electrophoresis Cell with Removable Capillary Channel	19
7.	Lexan Electrophoresis Cell with Removable Rectangular Channel	20
8.	Electrophoresis Cell for Evaluation of Electroosmotic Flow in Split Columns	22
9.	Electrophoretic Mobility of Latexes as a Function of Height in Capillary	23
10.	Parabolic Flow of Polystyrene Latex in Uncoated Rectangular Lexan Channel	24
11.	Electroosmotic Flow in Union Carbide and Pierce Chemical Coated Capillaries	26
12.	Electroosmotic Flow in Dow Methocel, MC, Coated Capillaries	27
13.	Electroosmotic Flow in Coated Capillaries	29
14.	Minimum Difference in Particle Mobility Required for Separation as a Function of Relative Size of Sample Plug	43
15.	Variation of Reciprocal Viscosity with Temperature for Water and A-1 Buffer	49
16.	Variation of Dielectric Constant of Water with Temperature	50
17.	Variation of Ratio of Dielectric Constant to Viscosity Ratio with Temperature for A-1 Buffer	52
18.	Temperature Gradient Conditions Necessary for Maximum Resolution for Different Values of $U_{os}/U_{e_{max}}$	53

Figure		Page
19.	Variation of Resolution of Separation with Channel Wall Temperature for Forward Parabolic Velocity Profile as a Function of Electro-osmotic Mobility and Maximum Electrophoretic Mobility of the Particles	55
20.	Variation of Resolution of Separation with Channel Wall Temperature for Inverted Parabolic Velocity Profile as a Function of Electro-osmotic Mobility and Maximum Electrophoretic Mobility of the Particles	56
21.	Variation of Resolution of Separation with Electroosmotic Mobility as a Function of Maximum Electrophoretic Mobility of the Particles	57
22.	Electrophoretic Mobility Distributions of Fixed Red Blood Cells	59
23.	Computer Output of Free-Fluid Electrophoretic Separation Assuming Parabolic Distribution of Fixed Red Blood Cells	60
24.	Computer Output of Free-Fluid Electrophoretic Separation Assuming Straight Line Distribution of Fixed Red Blood Cells	61
25.	Computer Output of Free-Fluid Electrophoretic Separation Assuming Gaussian Distribution of Fixed Red Blood Cells	62
26.	Computer Output of Free-Fluid Electrophoretic Separation Assuming Parabolic Distribution of Fixed Red Blood Cells with $U_{os} = -0.3\mu m$ cm/volt sec and $\Delta T = 2°C$	64
27.	Computer Output of Free-Fluid Electrophoretic Separation Assuming Parabolic Distribution of Fixed Red Blood Cells with $U_{os} = -0.2\mu m$ cm/volt sec and $\Delta T = 2°C$	65
28.	Computer Output of Free-Fluid Electrophoretic Separation Assuming Parabolic Distribution of Fixed Red Blood Cells with $U_{os} = -0.1\mu m$ cm/volt sec and $\Delta T = 2°C$	66
29.	Computer Output of Free-Fluid Electrophoretic Separation Assuming Parabolic Distribution of Fixed Red Blood Cells with $U_{os} = 0.0\mu m$ cm/volt sec and $\Delta T = 2°C$	67
30.	Computer Output of Free-Fluid Electrophoretic Separation Assuming Parabolic Distribution of Fixed Red Blood Cells with $U_{os} = +0.05\mu m$ cm/volt sec and $\Delta T = 2°C$	68

Figure		Page
31.	Computer Output of Free-Fluid Electrophoretic Separation Assuming Parabolic Distribution of Fixed Red Blood Cells with $U_{os} = -0.20\mu m$ cm/volt sec and $\Delta T = 5°C$	69
32.	Computer Output of Free-Fluid Electrophoretic Separation Assuming Parabolic Distribution of Fixed Red Blood Cells with $U_{os} = -0.20\mu m$ cm/volt sec and $\Delta T = 0°C$	70
33.	Computer Output of Free-Fluid Electrophoretic Separation Assuming Parabolic Distribution of Fixed Red Blood Cells with $U_{os} = -0.20\mu m$ cm/volt sec and $\Delta T = -5°C$	71
34.	Schematic Representation of Flow Profiles Present in Electrolyte Curtain of CPE	74
35.	CPE Scan of the 1.01 Micron Polystyrene Latex for Different Applied Potentials	76
36.	CPE Scan of Six Latexes in BSB Buffer at 50 volts/cm	78
37.	CPE Scan of Three Colored Latexes 30 Volts Applied	79

INTRODUCTION

For a long time, the electrokinetic behavior of biological materials has been an active and productive area of research. As early as 1860, Kuhne and Jurgensen, in separate publications, demonstrated the electrokinetic properties of muscle tissue and biological cells. Since that time, biologists have shown that the electrical double-layer properties at the cell wall/liquid interface often reflect the biological characteristics of the cells. Electrophoresis, therefore, represents a potentially powerful tool for separating biological cells according to their biological properties.

It has long been recognized that electrophoretic separation in space would alleviate at least two major problems of ground-based separations which are due to the effect of gravity. The first and most serious problem is thermal convection, which is brought about by the joule heating resulting from the electric current in the liquid medium. The second problem is the settling of large biological particles of high density. A microgravity environment, such as exists in an earth orbit vehicle, is sufficient to eliminate both of these problems. The problems which remain are of an experimental nature and primarily involve the design of the electrophoresis cell so as to attain maximum resolution of separation along with the physical capability of efficiently collecting the separated fractions.

The major effort described in this report has been to analysis the Apollo 16 electrophoresis experiment results and to recommend to NASA the design features for the electrophoresis cell planned for the ASTP experiment which would increase the resolution of separation. This latter aspect of the program included a theoretical analysis of the resolution of free-fluid electrophoretic separation, the development of a low-electroosmotic-mobility coating to control electroosmosis in the electrophoresis cell, and a method for experimentally evaluating electroosmotic flow in the cell. The progression of this work has gradually led to a more thorough appreciation of not only free-fluid electrophoresis, but of all types of electrophoretic separations.

CHAPTER I

ANALYSIS OF THE APOLLO 16 ELECTROPHORESIS EXPERIMENT

A. Introduction

The Apollo 16 electrophoresis experiment was designed to demonstrate that colloidal particles of different surface charge could be separated more efficiently in space than on Earth. Although the eventual objective of this program is the separation of biological cells, monodisperse polystyrene latexes were chosen as model colloids for this experiment to simplify analysis of the experimental results. The objective of our work was to analyze the results of the Apollo 16 electrophoresis experiment and to help design future electrophoresis experiments for space. This chapter describes the analysis of the results of the Apollo 16 experiment.

B. Experimental Details

1) Apollo 16 Electrophoresis Cell

The Apollo 16 electrophoresis cell consisted of three parallel 10.2 cm-long Lexan tubes separated from the electrode compartments by semipermeable membranes. The two monodisperse polystyrene latexes (The Dow Chemical Co.) selected were Lot #LS-1200-B (0.80μm diameter) and Lot #LS-1047-E (0.23μm diameter). Prior to the start of the experiment, the latex samples were isolated in a cylindrical chamber separated from the cathode by a fixed semipermeable membrane and from the Lexan tube by a removable Kapton film. To start the experiment, the Kapton film was removed so that the latex particles were free to migrate up the Lexan tube. The inside radii of the Lexan tube and the sample chamber were 0.318 cm and 0.238 cm, respectively. The dispersion medium was a solution containing 0.008 M boric acid and 0.0016 M sodium hydroxide as buffer, as well as 0.1% formalin preservative and 0.02% sodium lauryl sulfate emulsifier. The potential applied across the platinum electrodes (11.5 cm apart) was 300 volts.

2) Electrophoretic Mobility of Polystyrene Latex Particles

The electrophoretic mobilities of the 0.80μm and 0.23μm diameter polystyrene latex particles were measured in a microcapillary electrophoresis apparatus (Rank Brothers Ltd.) at an applied potential of 1.7 volts/cm. The dispersion medium was various modifications of the borate buffer dispersion medium used in the Apollo 16 experiment. The cylindrical 2-mm diameter microcapillary cell had extremely thin walls (less than 0.1 mm), thus giving distortionless viewing at all levels without the necessity for any optical corrections. The zero-solvent-flow level in this cell was defined accurately by measuring the parabolic velocity profile across the diameter of the cell for particles of different electrophoretic mobility. The usual light source was a quartz-iodine lamp in the dark-field configuration. Since the 0.23μm diameter particles could not be detected with this light source, a 5 mv He·Ne laser (Model ML411, Metrologic Instruments, Inc.) was used as the light source for

REPRODUCIBILITY OF THE
ORIGINAL PAGE IS POOR

this sample, with remarkable success in detecting the primary particles. The advantage of the microcapillary electrophoresis is that the electrophoretic mobilities of a large number of individual particles can be measured directly

3) Potential Gradient in the Apollo 16 Electrophoresis Cell

An important parameter for evaluating the Apollo 16 electrophoresis experiment is the potential gradient E. Since a potential of 300 volts was applied across a distance of 11.5 cm, the calculated potential gradient is 26 volts/cm. Two possible factors that could reduce this value of E are the semipermeable membranes that were used to close both ends of the channel and the presence of bubbles both inside and outside the channel. An attempt was made to measure the potential gradient within the channel by inserting two electrodes into the channel of an electrophoresis cell identical to that used for the Apollo 16 experiment and measuring the potential across these electrodes. The value of E varied from 15 to 23 volts/cm because of the bubbles that were always present in the electrode compartments, these bubbles were the result of poor circulation of buffer (the circulation equipment used on the Apollo 16 flight was not available for this study).

A simplified electrophoresis cell was constructed from Lexan tubing to more easily eliminate bubbles from the channel and electrode compartments. The main features of this cell were identical to that used for the Apollo 16 experiment as shown in Figure 1. The three probe electrodes (A, B and C) were used to measure the potential gradient at different positions in the Lexan tube when a potential of 300 volts was applied across the main electrodes.

4) Electroosmosis in the Apollo 16 Electrophoresis Cell

The electroosmosis at the Lexan channel wall/buffer solution interface was measured by placing the apparatus shown in Figure 1 on a microscope stage and observing the particle velocity at 250 X magnification. Although the optical properties of the Lexan tubing were improved greatly by polishing the top surface to a flat configuration, some difficulty was encountered in observing the particles at different depths in the channel. Monodisperse polyvinyltoluene latex particles of 2μm diameter with an electrophoretic mobility of 10μm cm/volt sec were used to measure the velocity of the medium near the channel wall.

C. Theoretical Aspects of Electrophoresis

The observed velocity V_{obs} of a colloidal particle subjected to an applied potential in a closed cylindrical channel is defined by the equation:

$$V_{obs} = V_e + V \qquad (1)$$

where V_e = the velocity of the particle due to electrophoresis,
V = the solvent velocity due to electroosmosis.

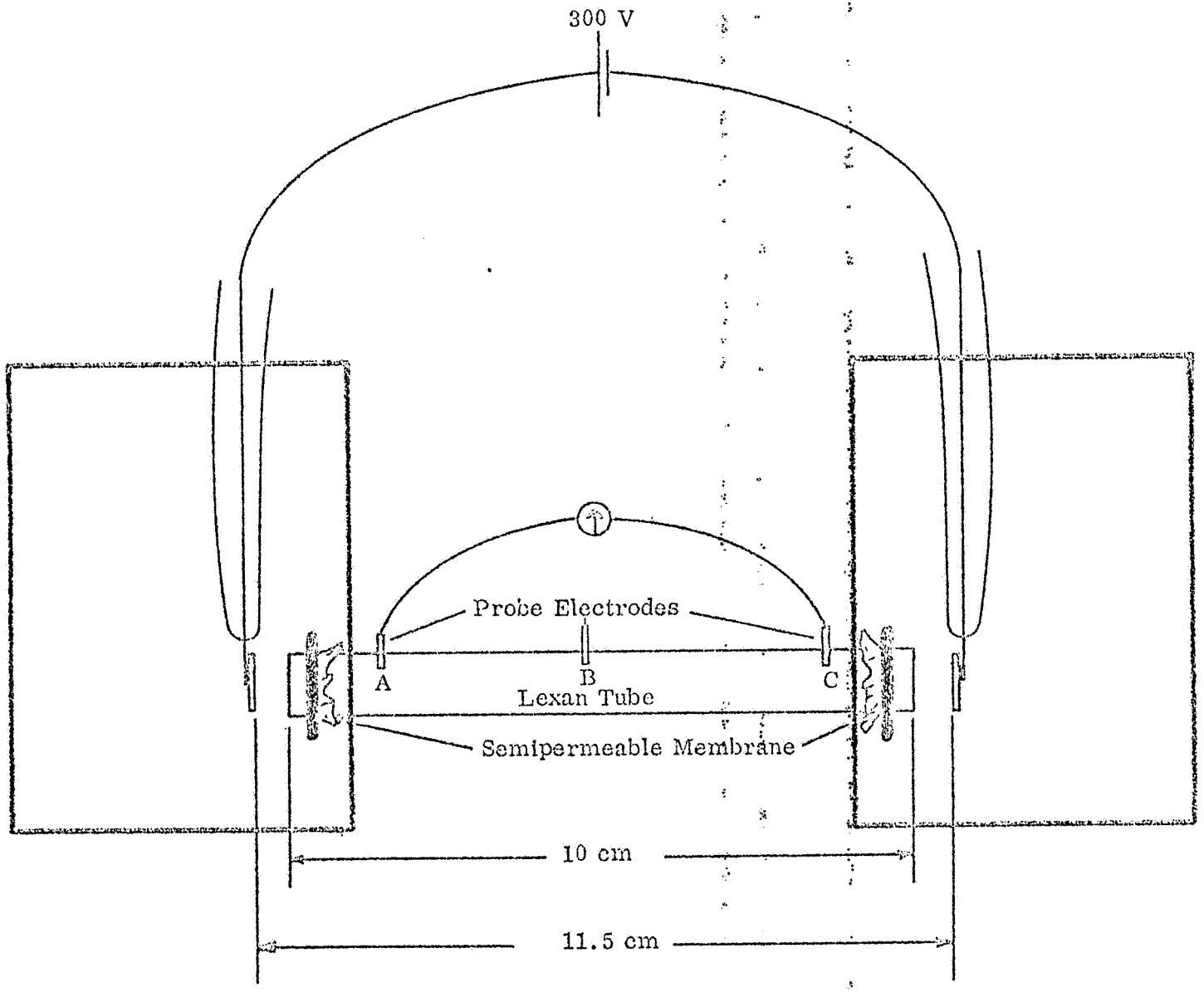

Figure 1. Cell for Measuring Potential Gradient $\underline{E}$

The solvent velocity $\underline{V}$ under these conditions is defined by the equation:

$$V = U\left[(2r^2/a^2) - 1\right] \tag{2}$$

where r = the distance from center of channel,
a = the radius of channel,
U = the electroosmotic velocity of solvent at the channel wall (i. e., where $\underline{r} = \underline{a}$).

Combining Equations 1 and 2 yields:

$$V_{obs} = V_e + U\left[(2r^2/a^2) - 1\right] \tag{3}$$

Equation 3 predicts that the observed particle velocity is a sensitive function of $\underline{r}$ and is described by a parabola that is symmetric about the center of the channel. Since information obtained from the Apollo 16 experiment was in the form of photographs taken every 20 seconds, the position that could be followed and measured accurately was the apex of the parabola at the center of the channel, i. e., at $\underline{r} = 0$. At $\underline{r} = 0$, Equation 3 reduces to:

$$V_{obs} = V_e - U \tag{4}$$

A potential of 300 volts applied to a cell of these dimensions gives a potential gradient of 26 volts/cm. However, there are "a posteriori" reasons for suspecting the constancy and absolute value of this potential gradient during the course of the experiment.

The potential gradient may be separated from the right hand side of Equation 4 as follows:

$$V_{obs} = (U_e - U_{os})\,E \tag{5}$$

where U_e = electrophoretic mobility of the particle,
U_{os} = electroosmotic mobility of the solvent,
E = potential gradient.

The particle velocity in the center of the channel, therefore, is a function of the electrophoretic mobility of the particles, the electroosmotic mobility of the solvent at the channel wall, and the applied potential gradient.

D. Ground-Based Experimental Results

1) Microcapillary Electrophoresis

The electrophoretic mobility of the 0.8μm (Sample A) and 0.23μm (Sample B) diameter polystyrene latex particles were 9.2 and 6.5μm cm/volt sec, respectively, in the standard

borate buffer solution. There was no detectable change in the electrophoretic mobility of these latex particles after storage for two weeks.

2) Electroosmosis in Lexan Tubes

The electroosmotic flow in Lexan tubes was determined by measuring the velocity of latex particles near the tube wall by means of the apparatus shown in Figure 1. The results showed that the particles changed direction near the channel wall, indicating that the electroosmotic velocity at the Lexan/buffer solution interface was greater than -10μm cm/volt sec. The negative sign indicates that the solvent moves toward the anode, as opposed to the negatively-charged polystyrene particles, which move toward the cathode. The experiment was repeated using Lexan tubing coated with collodion, which reduced, but did not eliminate, the electroosmosis.

3) Potential Gradient in the Apollo 16 Electrophoresis Apparatus

The potential gradient measurements obtained from the apparatus shown in Figure 1 with no bubbles present in the channel indicated that the semipermeable membranes used in the Apollo 16 experiment did not affect the potential gradient. When bubbles were introduced into the channel intentionally, the potential gradient was decreased by as much as 5%, depending upon the size of the bubble. When the bubble was inserted at the end of the channel in contact with the semipermeable membrane, the potential gradient was decreased by as much as 10%. These values may be in error, however, because of the tendency of the bubbles to rise and flatten out against the top of the channel, thus offering less resistance than would be expected in space where the absence of gravity allows air bubbles to assume a spherical shape.

Glass beads of 5 mm diameter were placed in the channel to approximate more closely the air bubbles of the Apollo 16 experiment. The results showed that the spherical glass beads had a much greater effect in reducing the potential gradient within the channel and that the decrease in $\underline{E}$ ($\Delta \underline{E}$) was inversely proportional to the cross-sectional area of the channel minus the cross-sectional area of the glass beads according to the equation $\Delta \underline{E} = K/(d_1^2 - d_2^2)$ where $\underline{K}$ is a constant, $\underline{d}_1$ the diameter of the channel, and $\underline{d}_2$ the diameter of the glass bead or air bubble. Since $\Delta \underline{E}$ was found to be 2.5 volts/cm for $\underline{d}_2 = 0.5$ cm, $\underline{K} = 0.4$.

The photographic record of the Apollo 16 experiment showed that the bubble diameters were 0.6 cm or greater. The foregoing equation predicts that the value of $\Delta \underline{E}$ will be 10 volts/cm when the bubble diameter is 0.60 cm and 15 volts/cm when the bubble diameter is 0.61 cm. Apparently, $\underline{E}$ decreases rapidly as the bubble diameter approaches the inside diameter of the channel. Experimental verification with glass beads larger than 0.5 cm in diameter was not possible because the geometric tolerances of the available beads were about 25%, with the result that the larger beads would not fit into the channel. Nevertheless, the foregoing theory and experimental results suggest that the air bubbles present in the Apollo 16 electrophoresis apparatus could have drastically reduced the potential gradient within the channel.

4) Analysis of Results of the Apollo 16 Electrophoresis Experiment

The details of the experimental apparatus and the flight photographs, which were the source of all experimental results, are not included in this report and can be found elsewhere (1). The photographs, numbered sequentially beginning with frame 17001, were taken automatically every 20 seconds. The experiment was initiated (i. e., time = 0) at frame 17003, and the current was first reversed at frame 17017 (280 seconds after the start of the experiment) when the fastest-moving particles approached the end of the channel. Although 52 photographs were taken during the four traversals of latex particles, the useful information for analysis was in the first 14 frames after the current was turned on.

The initial appearance of the latex particles (frame 17005, time = 40 seconds) showed that the observed velocity of the latex particles was influenced by electroosmotic solvent flow as evidenced by the sharp parabolic particle profile. The position of the apex of the parabola as a function of time is shown in Figure 2. Tube 1 contained the mixture of 0.23μm and 0.80μm diameter particles, while tube 2 contained the 0.80μm diameter particles and tube 3 the 0.23μm diameter particles. The linear variation of position with time for the first three minutes of the experiment shows that the particles were traveling at a constant velocity during this period. Extrapolation of the results to zero time, however, indicates that the latex particles in tubes 1 and 3 were delayed in the sample chamber for 7 and 9 seconds, respectively. The change in slope beyond three minutes indicates a sudden decrease in the potential gradient of all three tubes. This phenomenon can be explained by the presence of three large bubbles that were located initially at the center of each tube: when the current was turned on, the bubbles migrated toward the anode and reached the end of the tube three to four minutes later; when the bubbles contacted the semipermeable membrane, the resistance increased, resulting in a decrease in the potential gradient. The observed particle velocities at the center of each tube (i. e., at $r = 0$) calculated from the data of Figure 2 are given in Table I.

An evaluation of the Apollo 16 flight films requires the use of Equation 5 which predicts the observed particle velocity V_{obs} in the center of the channel as a function of the electrophoretic mobility of the latex particles U_e, the electroosmotic mobility at the channel wall/liquid interface U_{os}, and the potential gradient E:

$$V_{obs} = (U_e - U_{os})\, E \qquad (6)$$

Although V_{obs} and U_e are known accurately (Table I), there is some uncertainty in the values of both U_{os} and E. The value of U_{os} was found from laboratory experiments to be at least -10μm cm/volt sec (or -0.06 cm^2/volt min), while E was found to be less than the theoretical value of 26 volts/cm. Equation 5 was solved for E_1, E_2, and E_3, the potential gradients in tubes 1, 2, and 3, respectively, and the following ratios were set up, to estimate which tubes, if any, had identical values of E:

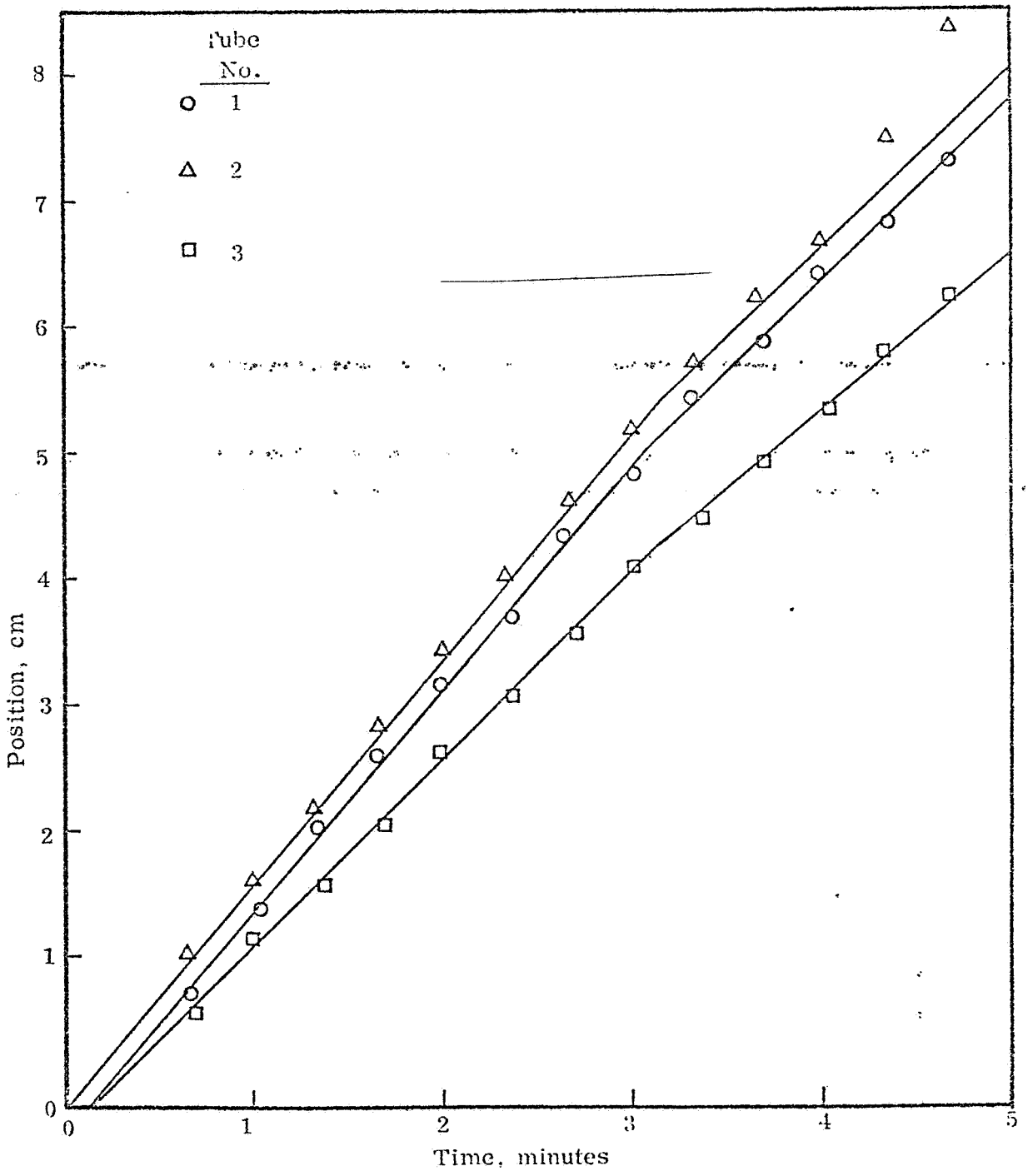

Figure 2 Position of Apex of Parabola as a Function of Time

Table I

Electrophoretic Mobilities and Observed Velocities of Latex Particles*

Tube No.	Latex Particles	Observed Particle Velocity, cm/min Initial	Observed Particle Velocity, cm/min Final	Electrophoretic Mobility,** cm^2/volt min
1	0.23μm + 0.80μm	${}_1V_{obs} = 1.72$	${}_1V'_{obs} = 1.45$	${}_AU_e = 0.0552$
2	0.80μm	${}_2V_{obs} = 1.79$	${}_2V'_{obs} = 1.43$	${}_AU_e = 0.0552$
3	0.23μm	${}_3V_{obs} = 1.49$	${}_3V'_{obs} = 1.26$	${}_BU_e = 0.0392$

* The observed particle velocity $\underline{V}_{obs}$ is taken at $\underline{r} = 0$.

** ${}_AU_e$ and ${}_BU_e$ are the electrophoretic mobilities of the 0.80μm and 0.23μm diameter latex particles, respectively.

$$\frac{E_2}{E_1} = \frac{{}_2V_{obs}}{{}_1V_{obs}} = 1.04 \tag{7}$$

$$\frac{E_1}{E_3} = \frac{{}_1V_{obs}}{{}_3V_{obs}} \frac{({}_BU_e - U_{os})}{({}_AU_e - U_{os})} = 1.155 \frac{(0.0392 - U_{os})}{(0.0552 - U_{os})} \tag{8}$$

$$\frac{E_2}{E_3} = \frac{{}_2V_{obs}}{{}_3V_{obs}} \frac{({}_BU_e - U_{os})}{({}_AU_e - U_{os})} = 1.200 \frac{(0.0392 - U_{os})}{(0.0552 - U_{os})} \tag{9}$$

When the approximate value of $\underline{U}_{os} = -0.06$ cm^2/volt min. is substituted into Equations 8 and 9, $\underline{E}_2/\underline{E}_1 = 1.04$, $\underline{E}_1/\underline{E}_3 = 0.99$, and $\underline{E}_2/\underline{E}_3 = 1.03$. These results show clearly that it is reasonable to assume that $\underline{E}_1 = \underline{E}_3$. Equation 5 may now be solved for $\underline{E}$ in tubes 1 and 3:

$$E_1 = \frac{{}_1V_{obs}}{({}_AU_e - U_{os})} \tag{10}$$

$$E_3 = E_1 = \frac{{}_3V_{obs}}{({}_BU_e - U_{os})} \tag{11}$$

Equations 10 and 11 may be equated and rearranged to solve for $\underline{U}_{os}$:

$$U_{os} = \frac{{}_3V_{obs}\,{}_AU_e - {}_1V_{obs}\,{}_BU_e}{{}_3V_{obs} - {}_1V_{obs}} \tag{12}$$

Substituting the data in Table I gives $\underline{U}_{os} = -0.0644$ cm^2/volt min. or -10.7μm cm/volt sec, in good agreement with the experimental approximation presented previously. Using this value of $\underline{U}_{os}$ and solving Equation 5 for $\underline{E}$, the potential gradient may be calculated separately for tubes 1, 2, and 3 as follows (see Table I for pertinent data):

$$E_1 = \frac{{}_1V_{obs}}{({}_AU_e - U_{os})} = 14.4 \text{ volts/cm} \tag{13a}$$

REPRODUCIBILITY OF THE
ORIGINAL PAGE IS POOR

$$E_2 = \frac{{}_2V_{obs}}{({}_AU_e - U_{os})} = 15.0 \text{ volts/cm} \tag{13b}$$

$$E_3 = \frac{{}_3V_{obs}}{({}_BU_{os} - U_{os})} = 14.4 \text{ volts/cm} \tag{13c}$$

The potential gradient $\underline{E'}$ beyond 3 minutes (past the inflection points of the curves of Figure 4) may be calculated for each tube from the following series of equations (see Table I for pertinent data):

$$E'_1 = \frac{{}_1V'_{obs}}{({}_AU_e - U_{os})} = 12.1 \text{ volts/cm} \tag{14a}$$

$$E'_2 = \frac{{}_2V'_{obs}}{({}_AU_e - U_{os})} = 12.0 \text{ volts/cm} \tag{14b}$$

$$E'_3 = \frac{{}_3V'_{obs}}{({}_BU_e - U_{os})} = 12.2 \text{ volts/cm} \tag{14c}$$

Furthermore, the six Equations 13a-c and 14a-c can be shown to be internally consistent.

Equation 3 may now be expressed in terms of a potential gradient that is not constant for all three tubes:

$$V_{obs} = U_eE + U_{os}E\left\{\frac{2r^2}{a^2} - 1\right\} \tag{15}$$

Since the values of all the parameters in Equation 15 are known, the particle velocity may be calculated as a function of position $\underline{r}$ in each tube where $\underline{a}$ = 0.318 cm. The results for the observed particle velocity $\underline{V}_{obs}$ expressed in cm/min are as follows:

Initial 3 minutes (frames 17004 - 17012)

Tube 1: $${}_1V_{obs} = 1.72 - 18.3\ r^2 \tag{16}$$

Tube 2: $${}_2V_{obs} = 1.79 - 19.1\ r^2 \tag{17}$$

Tube 3: $${}_3V_{obs} = 1.49 - 18.3\ r^2 \tag{18}$$

Final 100 sec of first traverse (frames 17013 - 17017)

Tube 1: $${}_1V'_{obs} = 1.45 - 15.4\ r^2 \tag{19}$$

Tube 2: $${}_2V'_{obs} = 1.43 - 15.3\ r^2 \tag{20}$$

Tube 3: $${}_3V'_{obs} = 1.26 - 15.5\ r^2 \tag{21}$$

Equations 16-21 give the parabolic shape and position of the latex particles in each tube as a function of time. The length of the tail of each parabola, however, requires a knowledge of how close the latex particles approach the channel wall. Since the radius of the sample chamber is smaller than the channel radius, the position of the particles in the channel is a function of the dimensions and solvent flow conditions of the sample chamber, i.e., at some maximum distance from the center of the sample chamber, the particle velocity will be zero so that only the particles at smaller distances may leave the sample chamber. Equation 15 may be utilized to predict the maximum distance $\underline{r}_{max}$ of the particles measured from the center of the chamber, by setting the observed velocity $\underline{V}_{obs}$ equal to zero and solving for $\underline{r}_{max}$:

$$r_{max} = \frac{a}{\sqrt{2}} \sqrt{\left(1 - \frac{U_c}{U_{os}}\right)} \tag{22}$$

where the radius of the sample chamber $\underline{a}$ is equal to 0.238 cm. Therefore, Equation 22 predicts that the maximum distances of the latex particles from the center of the channel will be 0.229, 0.229, and 0.214 cm for tubes 1, 2, and 3, respectively. These results, along with Equations 16-21, allow the latex-particle profile to be predicted as a function of time. Figure 3 compares the predicted profiles with the results of the Apollo 16 experiment for tubes 1, 2, and 3 at the indicated times of 1, 2, 3, and 4 minutes. The agreement between experiment and theory is remarkably good; however, the theory cannot explain the irregular particle profile observed in tube 3.

Another important parameter that can be evaluated from theory and compared with experiment is length of the latex parabolic profile as a function of time. The velocity of parabolic growth may be calculated by subtracting the velocity of the particles at the tail of the parabola (i.e., at $\underline{r} = \underline{r}_{max}$) from the velocity of the particles at the apex of the parabola (i.e., at $\underline{r} = 0$). For the case of tube 1, Equation 16 is used to calculate particle velocity at $\underline{r} = 0$, while Equation 18 is used to calculate the particle velocity at $\underline{r} = \underline{r}_{max}$. Equations 17 and 18 are used to calculate this difference in velocity for tubes 2 and 3, respectively. The results show that the lengths of the parabolas grow at a rate of 1.19, 1.00, and 0.83 cm/min for tubes 1, 2, and 3, respectively. These results, of course, are only valid for the first three minutes of the experiment, at which point the potential gradient decreases to a lower value. Equations 19, 20, and 21 may subsequently be used in a similar fashion to calculate the growth velocities of 0.89, 0.80, and 0.70 cm/min for tubes 1, 2, and 3, respectively, for the final 100 seconds of the first traverse. Figure 4 presents the theoretical

Figure 3 Latex Parabolic Profile at 1, 2, 3 and 4 Minute Intervals

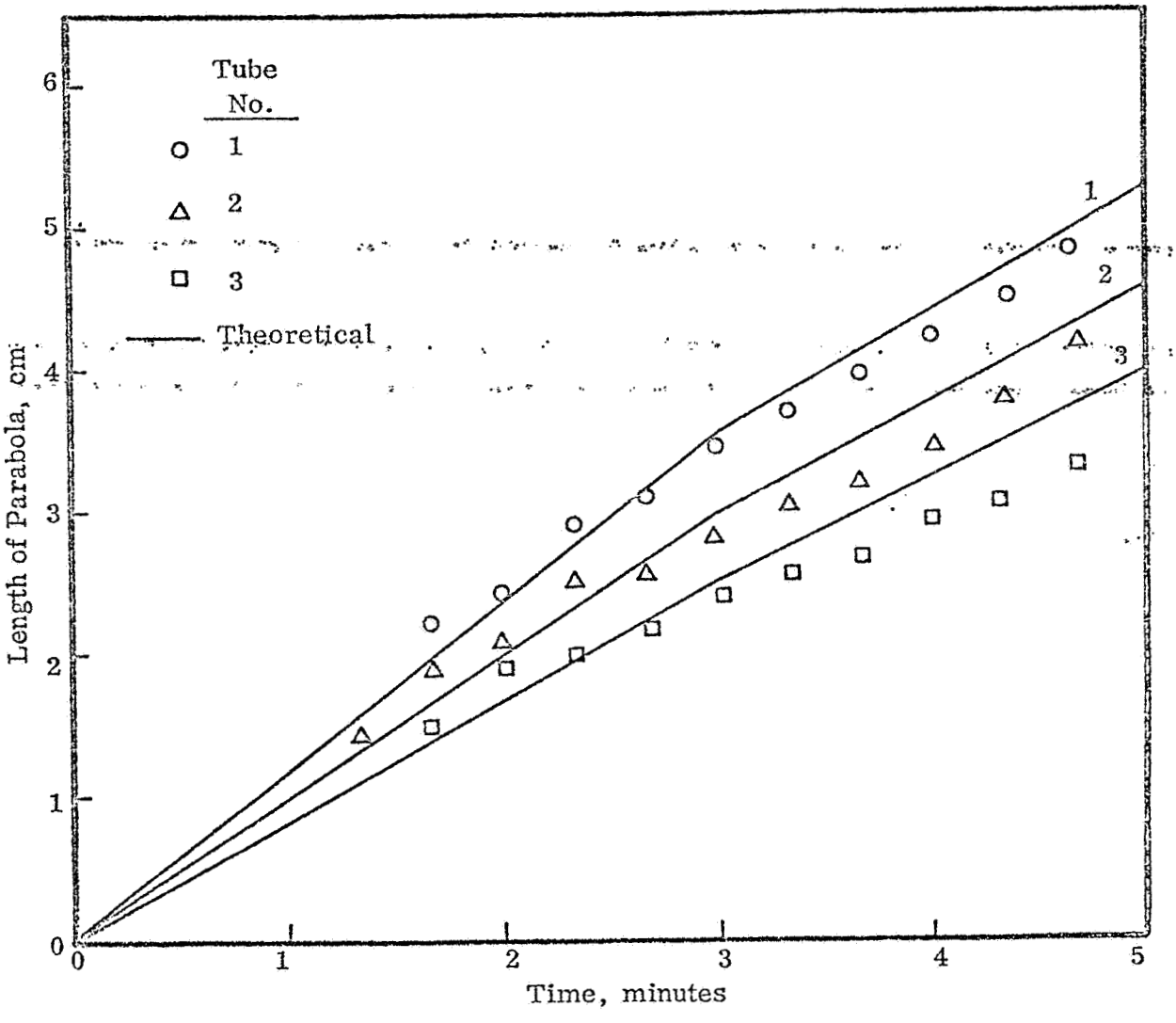

Figure 4 Length of Parabolic Profiles as a Function of Time

(solid lines) and experimental parabolic lengths measured from the Apollo 16 flight films. Although there was some difficulty in measuring the lengths of the parabolas from the photographs because of the fuzzy nature of the tails, the agreement with theory is very good. It should be emphasized that the particle velocity near the channel wall is a very sensitive function of the distance from the channel wall, so that small errors in $\underline{r}_{max}$ can lead to relatively large errors in the minimum particle velocity and the parabolic length as a function of time. The qualitative agreement between the experimental points and theory shown in Figure 4, therefore, may be taken as a reasonable confirmation of the validity of the theoretical approach and assumptions used in this report.

The concept of the separation actually taking place in tube 1, by means of the parabola of the slower moving particles being nested within the parabola of the faster moving particles, was further verified by a color densitometric scan of the photographic results after 3 minutes of separation (carried out by NASA). Figure 5B shows the calculated results corresponding to experimental results after 3 minutes of separation (Figure 5A). A black-and-white reproduction of the color densitometric scan of Figure 5A (Figure 5C) shows a high-density area in the region of the predicted overlap, which demonstrates that the separation of the two latexes did indeed take place.

Conclusions

1. The potential gradient in each channel was reduced by approximately 40%, probably because of the presence of bubbles.

2. Electroosmosis was pronounced at the Lexan/buffer-solution interface and was the primary factor that controlled the parabolic shape of the latex particles.

3. The latex particles behaved entirely according to the theory of electrophoresis and electroosmosis in closed cylindrical channels.

4. The separation of the 0.23μm and 0.80μm diameter latex particles in tube 1 did in fact occur according to theory, even though the separation was not in the desired practicable form.

5. A practicable separation of this type is greatly simplified in a gravity-free environment, but requires the development of a low electroosmotic coating.

A

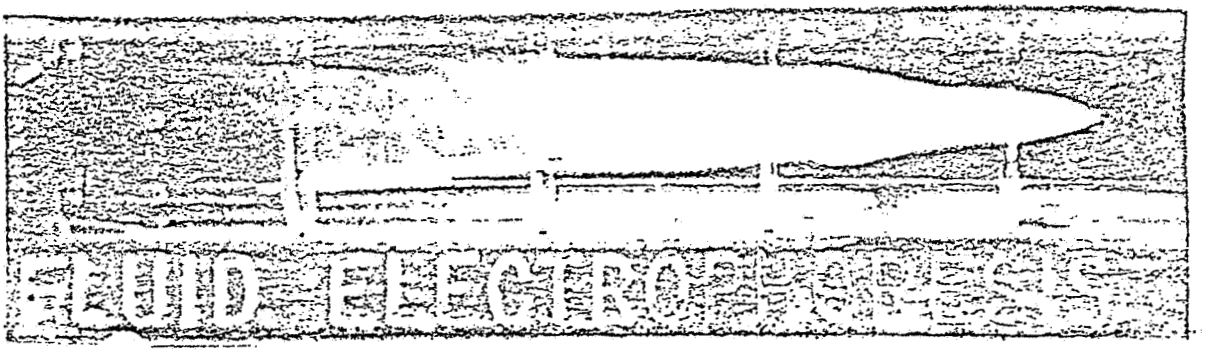

B

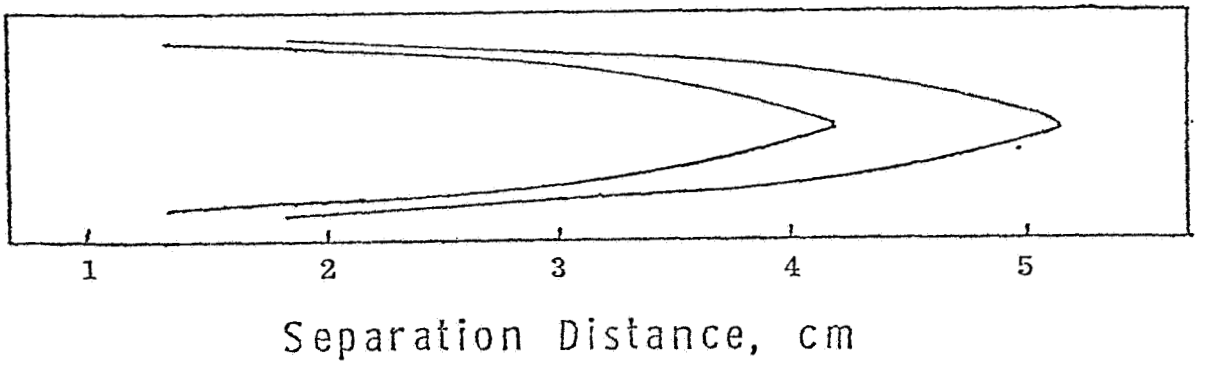

C

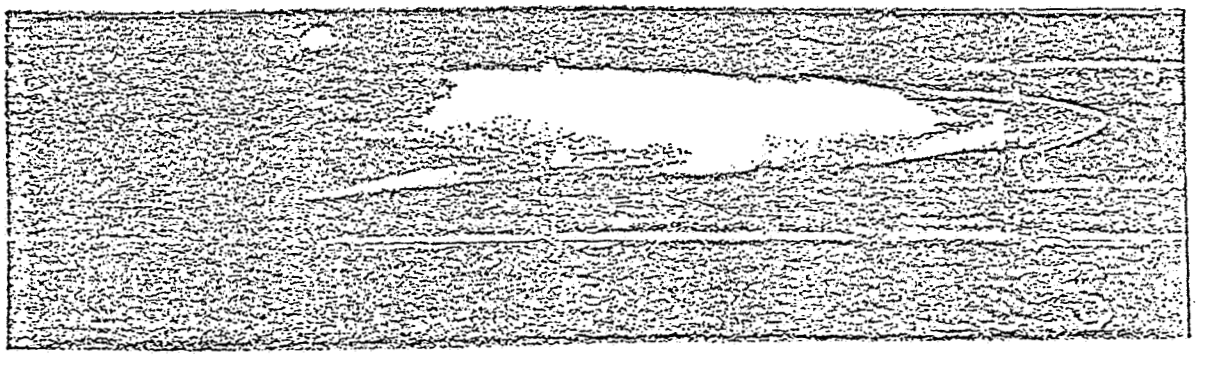

Figure 5 Free-fluid electrophoretic separation of mixed 0.23μm and 0.80μm monodisperse polystyrene latex particles during Apollo 16 mission: A. photograph of separation after minutes; B. theoretical prediction of separation shown in A.; C. black-and-white reproduction of color densitometric scan of photograph shown in A.

REPRODUCIBILITY OF THE
ORIGINAL PAGE IS POOR

CHAPTER II

LOW-ELECTROOSMOTIC-MOBILITY COATINGS

A. Introduction

The Apollo 16 Electrophoresis Experiment demonstrated the need for a low-electroosmotic-mobility coating in a free-fluid electrophoretic separation. Although the theoretical treatment of the resolution of separation as a function of electroosmosis in free-fluid electrophoresis (FFE) is derived in Chapter III, the photographs of the Apollo 16 experiment showed parabolic particle profiles that are characteristic of electroosmosis in the cell and which render a practical separation impossible. Therefore, a major effort was initiated to develop a coating that would reduce the zeta potential at the cell-wall/liquid interface to zero or near-zero, to eliminate the driving force responsible for electroosmotic flow in the presence of an applied electrical potential. The initial work was directed towards the electrokinetic behavior of different coatings on a variety of surfaces in the presence of different buffer systems because neither the buffer nor the electrophoresis cell material were decided upon until very late in the development of the ASTP experiment.

B. Experimental Details

1) Electrophoresis Cell-Wall Materials

The cell-wall materials which were coated and investigated for their electrokinetic properties during the course of this study included glass, Plexiglas, and Lexan. The glass was available in small capillaries with an inside diameter of 1.0 ± 0.05 mm and a wall thickness of 0.15 mm. Lexan and Plexiglas were not available in small capillaries, but tubes were obtained with an inside diameter of 6 mm and a wall thickness of 1 mm. Sheets of Plexiglas and Lexan of 1.6 and 1.0 mm thickness, respectively, were also obtained.

2) Buffers

The electrokinetic properties of the coated materials were investigated under a variety of ionic conditions. The buffers generally used were: (i) the borate buffer which was identical to that used for the Apollo 16 electrophoresis experiment; (ii) a phosphate buffer which contained 4.32% glucose, 0.18% Na_2HPO_4, and 0.02% KH_2PO_4; (iii) the A-1 buffer, a modification of the phosphate buffer, which was used for the biological ASTP electrophoresis experiments.

3) Experimental Method of Measuring Electroosmotic Flow in Cylindrical and Rectangular Channels

Several methods are available for measuring electroosmosis which depend upon the physical configuration of the sample under investigation. The method developed in this program was to construct both cylindrical and rectangular microelectrophoresis cells from

the materials under investigation and to measure directly the velocity of individual particles in an applied electric field as a function of position in the cell. Under these conditions, the observed electrophoretic velocity V_{obs} is equal to:

$$V_{obs} = V_e + V, \tag{23}$$

where V_e is the true electrophoretic velocity, which is constant, and V is the solvent velocity due to electroosmosis, which is a function of position in the channel. When the channel is cylindrical, the solvent velocity may be expressed as:

$$V = U\left(\frac{2r^2}{a^2} - 1\right), \tag{24}$$

where r is the distance from the center of the channel, a is the channel radius, and U is the electroosmotic velocity at the channel wall, i.e., at $r = a$. When the channel is rectangular, the solvent velocity may be expressed as:

$$V/U = 1 - 3\left[1 - (y^2/b^2)\right] \Big/ 2\left[1 - (192/\pi^5 K)\right], \tag{25}$$

where V is solvent velocity at the center of the channel, $K = a/b$ the ratio of channel width/channel height, a is one-half the channel width, b is one-half the channel height, and y is the height measured from the center of the channel.

The experimental design for these electrophoresis cells requires that the instrument have the channel be easily removable from the cell. Figure 6 shows a diagram of an electrophoresis cell designed for small capillaries constructed with threaded nylon caps and O-rings which seal the capillary channel into the cell and allow for quick disconnection and replacement of the capillary The platinum electrodes are similarly sealed in place to give a completely closed system. Standard glass capillary tubes with an outside diameter of 1.0-1.5 mm are coated as desired and inserted in the cell for determination of the electroosmotic flow under standard conditions. A metal cell holder was constructed to clamp the electrode compartments in a fixed position to support the cell. This cell was designed to fit into the constant-temperature bath of the Rank Brothers electrophoresis apparatus, replacing the conventional microcapillary electrophoresis cell. This apparatus was also modified to observe the particles in the dark-field configuration using a He-Ne laser as the light source.

Figure 7 shows a diagram of an analogous cell with a replaceable rectangular center channel constructed from 0.8 mm-thick Lexan or Plexiglas sheets. The replaceable channel was constructed by glueing strips of Lexan or Plexiglas sheets between two larger plates using ethylene dichloride as adhesive. The replaceable channel with a height of 0.8 mm and a width of 20 mm fits tightly into the two electrode compartments and is sealed into position with RTV. The channel can be replaced by simply stripping away the RTV rubber seal and separating the parts. Several replaceable channels were constructed and coated in various ways; each in turn was cemented into the cell and its electroosmotic mobility was measured.

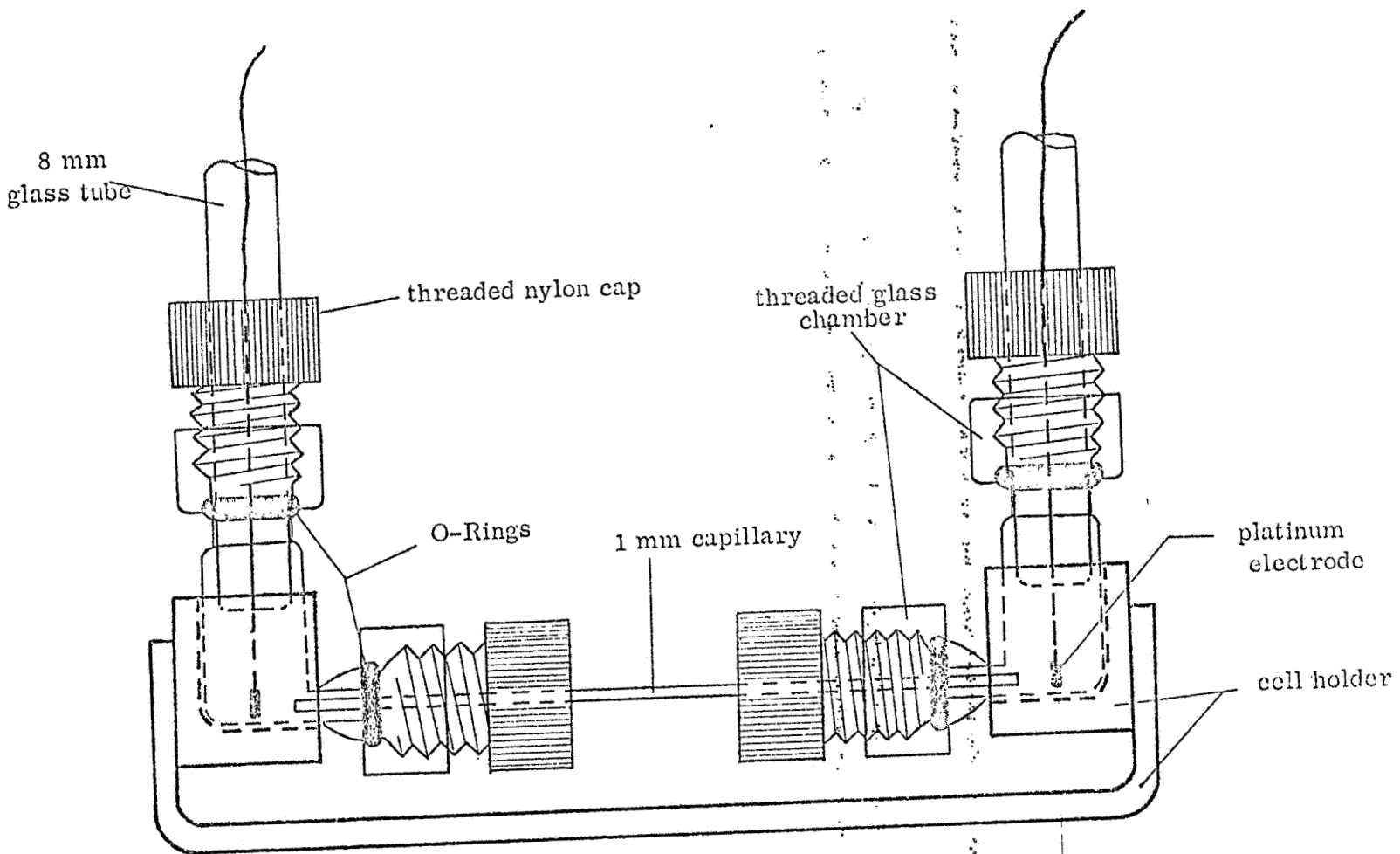

Figure 6. Electrophoresis Cell with Removable Capillary Channel

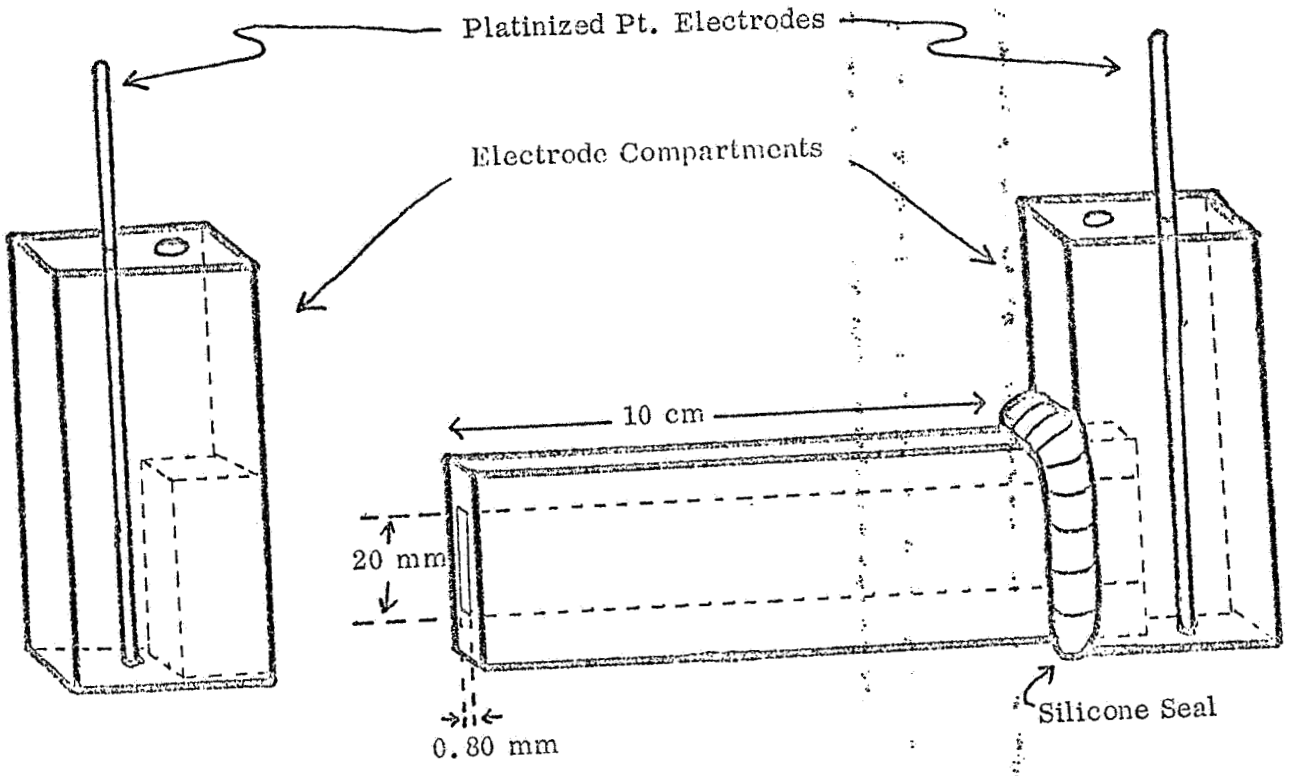

Figure 7. Lexan Electrophoresis Cell with Removable Rectangular Channel.

Figure 8 shows a diagram of the apparatus constructed to measure the electroosmotic mobility in the split columns of the ASTP electrophoresis experiment. The Lexan electrode compartments comprised two halves with rubber gaskets over the areas of contact. The end pieces of the split columns fit into the electrode compartments, which are clamped together with pressure plates. The filling ports are positioned so that the dispersion can be loaded into the cell without introducing air bubbles. The cell holder is designed so that the seam in the split columns does not interfere with the light source or the observation of the particles in the column. The whole assembly fits into the capillary constant-temperature compartment of the Rank microelectrophoresis instrument. The 5-mw He-Ne laser in the dark-field configuration is used as the light source in place of the usual tungsten-halogen lamp, which does not have sufficient intensity to penetrate the thick-walled columns. The particles were more easily discerned when a flat was ground in the tubes so that the wall thickness at the point of observation was less than 1 mm. A similar apparatus was constructed for measuring the electroosmotic flow in thick-walled Lexan and glass tubes which were not split.

The electrophoresis capillary cell (Figure 6) was tested by measuring the velocity profile of 0.8μm-diameter monodisperse polystyrene particles (LS-1200-B) in uncoated capillaries. Figure 9 shows the results for the latex particles dispersed in the borate buffer (pH = 8), the boric acid component of the buffer (pH = 4), and distilled water. The results are given as the velocity-distance^2 plot, which converts the parabolic velocity-distance relationship to a straight line. Only one half of the parabola is shown in Figure 9, although measurements of velocity were made across the entire width of the channel. This method of plotting allows comparison of straight lines with an intercept at the ordinate equal to the electroosmotic flow velocity and an intersection with the stationary level (height = $\pm$ 0.35 mm) equal to the electrophoretic mobility of the latex particles.

Figure 10 shows the results obtained with latex particles of known electrophoretic mobility in an uncoated rectangular Lexan channel in the electrophoresis cell shown in Figure 7. Figures 9 and 10 show that the plots of the electrophoretic velocity vs. the square of the distance are linear, indicating that the solvent velocity flow profile is parabolic, in agreement with Equations 24 and 25.

C. Experimental Results

1) Glass Surfaces

The rationale for the pretreatment of the glass capillaries depends upon an assumption of a mechanism of electrical double layer formation at the capillary wall interface. Since the capillary wall exhibits a negative charge over a wide pH range (as shown by experiments in this laboratory) the surface charge can arise from the adsorption of cations on the proton of silanol groups ($>$SiOH) or desorption of the silanol proton. The initial approach, therefore, was to render the active surface silanols inactive by specific chemisorption techniques, i.e., by alkylation of surface silanols according to the following mechanism:

$$>\mathrm{SiOH} + \mathrm{ROH} \longrightarrow >\mathrm{SiOR} + \mathrm{H_2O}$$

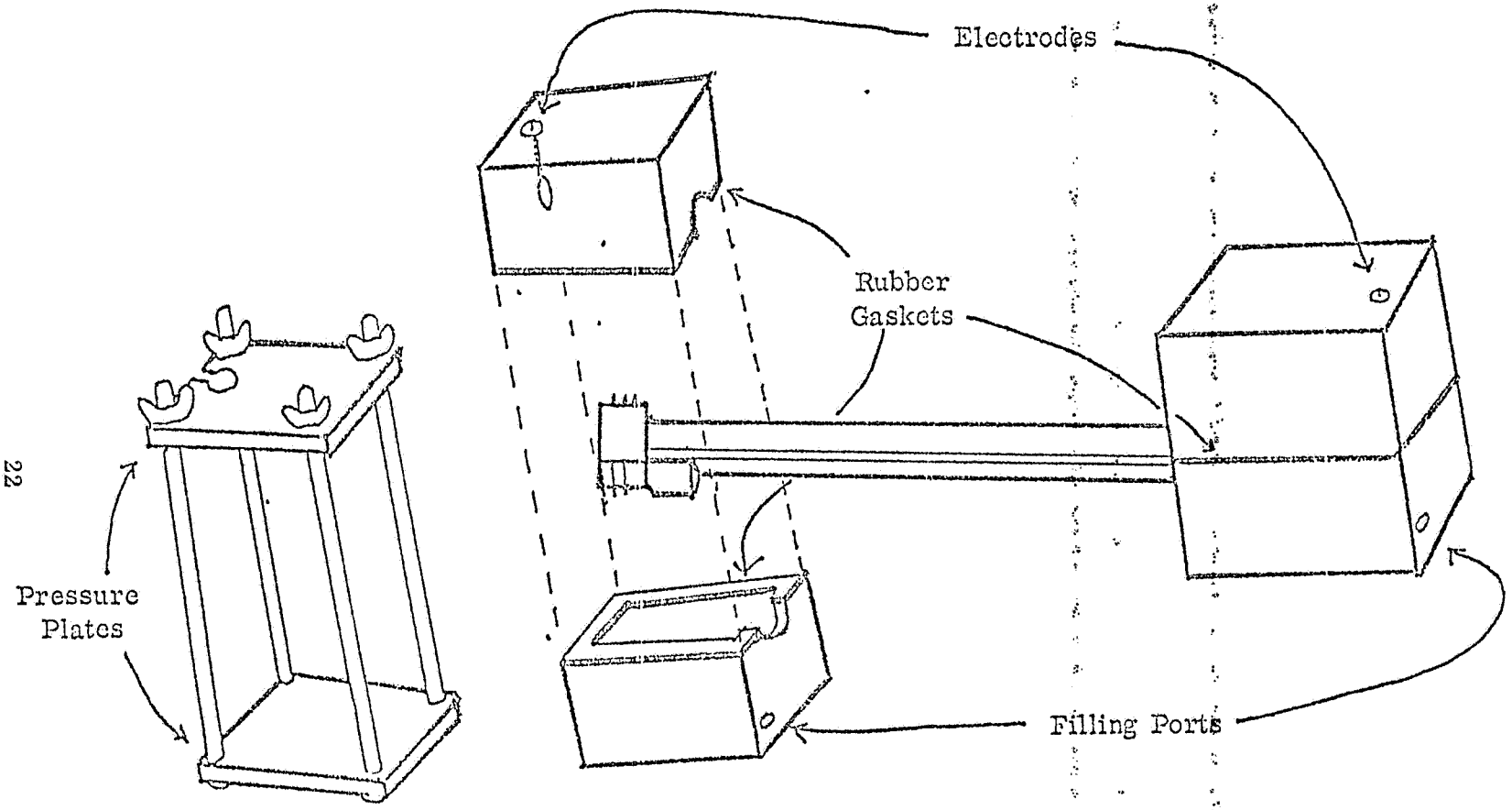

Figure 8. Electrophoresis Cell for Evaluation of Electroosmotic Flow in Split Columns

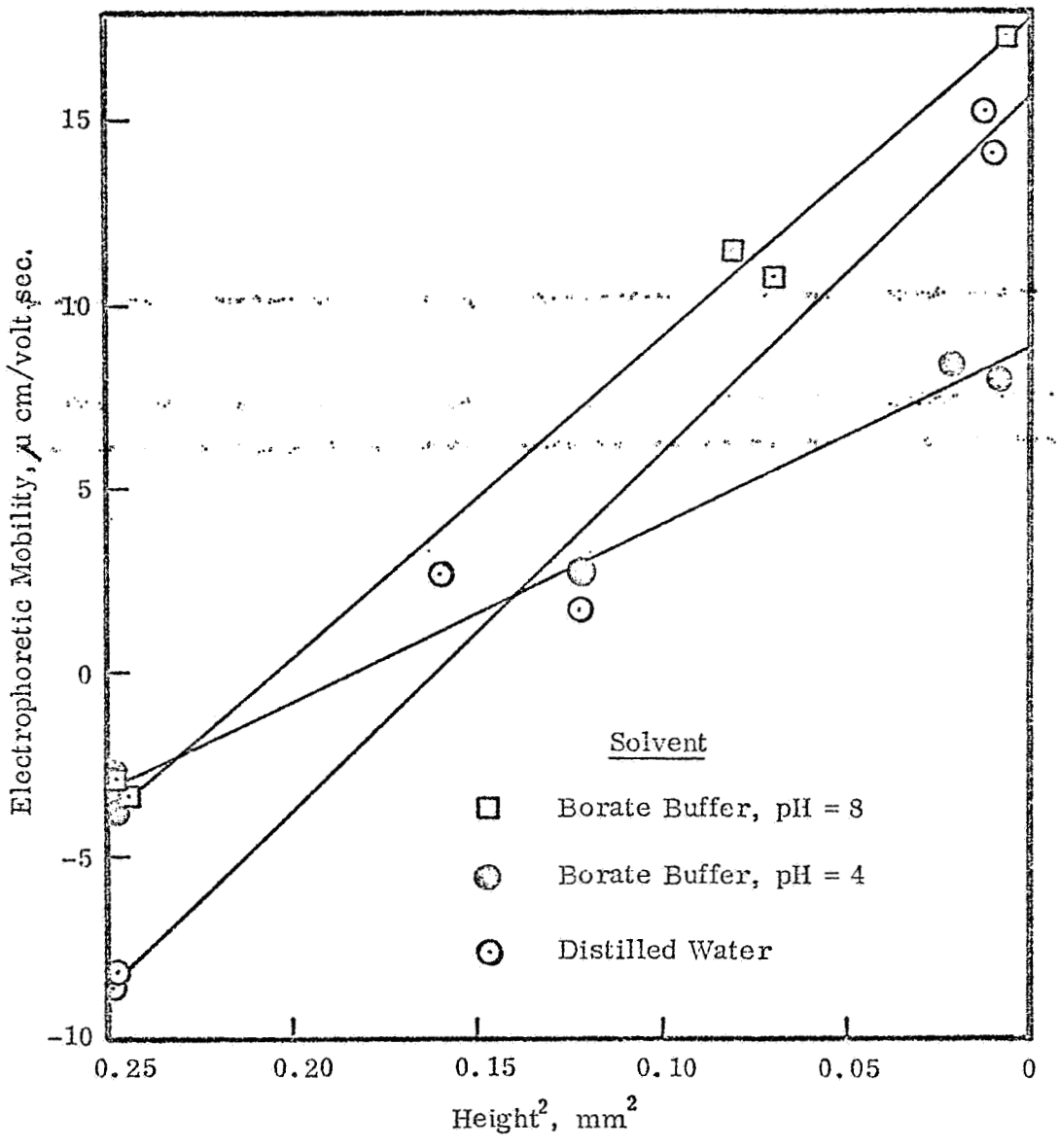

Figure 9. Electrophoretic Mobility of Latexes as a Function of Height in Capillary.

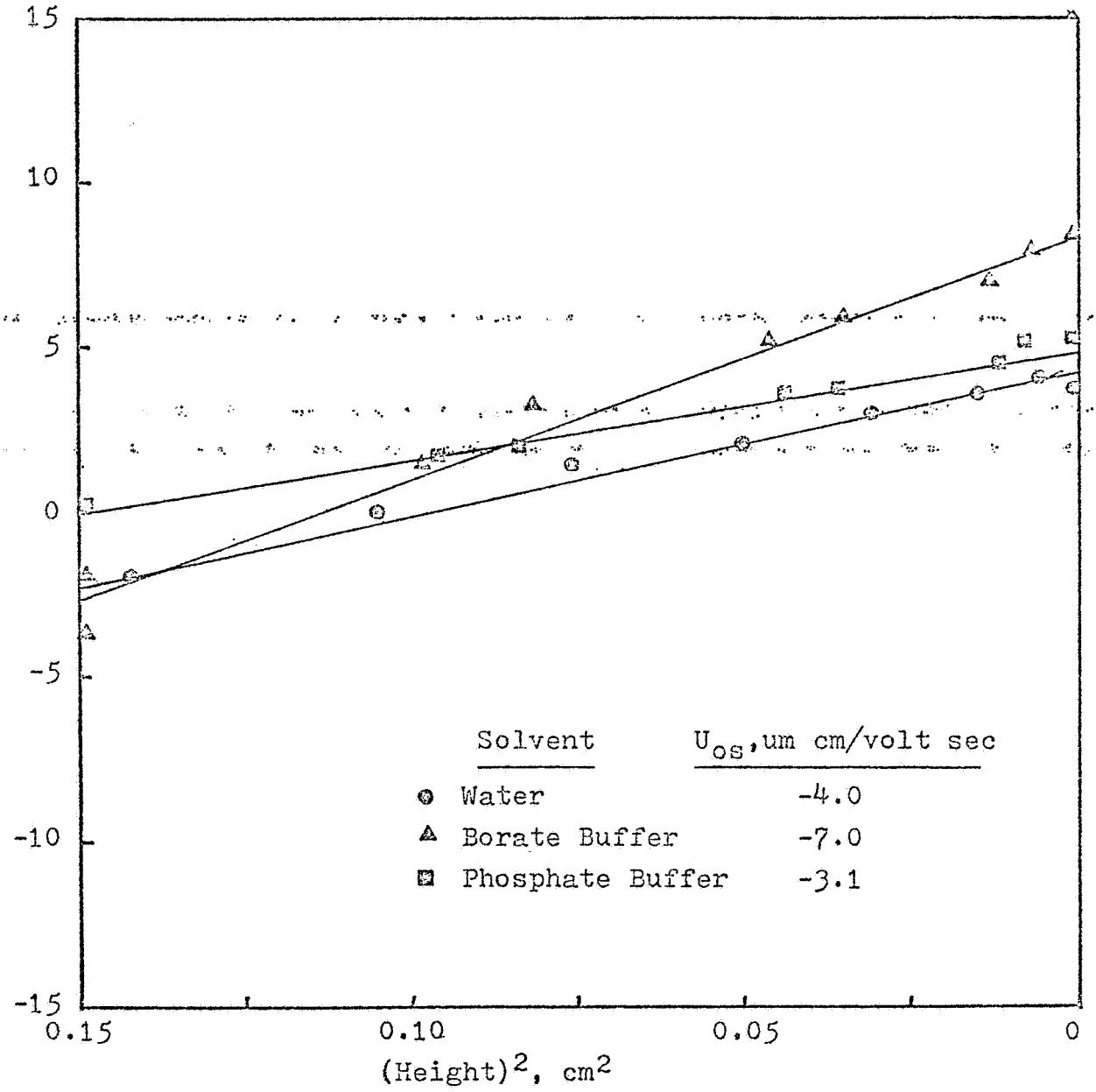

Figure 10. Parabolic Flow of Polystyrene Latex in Uncoated Rectangular Lexan Channel.

A number of experiments were performed with methanol (i. e., $R = CH_3$) by heating the glass capillary at 300° C in high vacuum and exposing the capillary to 30 mm of methanol vapor. Although the glass surface was rendered hydrophobic, the reaction appeared to be reversible in the presence of water, as evidenced by a steady decrease in hydrophobicity and an increase in surface charge.

Surface silanols can also be rendered hydrophobic by surface silylation. One of the more common silylating agents is hexamethyldisilazane (HMDS) which reacts with silanols according to the following mechanism:

$$2\,\text{SiOH} + (CH_3)_3 - Si - \overset{H}{\overset{|}{N}} - Si - (CH_3)_3 \longrightarrow 2\,\text{Si-O-Si-}(CH_3)_3 + NH_3.$$

This reaction is expected to be quantitative. A number of glass capillaries were treated with HMDS and although the surface charge was nominally reduced the results were not consistent.

Another organo-silane coating which was evaluated was γ-Aminopropyl-triethoxysilane (Union Carbide Co., A-1100; Pierce Chemicals). The coating procedure comprised rinsing the capillary with the A-1100 solution, drying, and curing at 150° C. The values of electroosmotic mobility for these A-1100-coated capillaries were erratic. Some capillaries showed extremely low mobility values, actually approaching zero, while others showed values corresponding to uncoated capillaries. This anomalous behavior was investigated further by taking two capillaries coated with the Union Carbide and the Pierce Chemicals coating materials, respectively, and measuring their electroosmotic flow profiles after exposure of the coatings to different ionic media. The results are shown in Figure 11, in which the order of measurement of each capillary is designated by the appropriate number. A negative slope indicates a reversal of the parabola velocity profile, which means that the surface has changed from negative to positive values. These results show that the zeta potential is dependent upon the pH of the media and the pH history of the sample. The uncertainties involved in the use of this coating were found to be unacceptable for a low-electroosmotic-mobility coating.

Glass capillaries were coated with methylcellulose (Dow Methocel) with molecular weights in the range 11×10^4 by drying an aqueous solution of Methocel and baking for 15 hours at 150° C to reduce its solubility (Methocel is insoluble in hot water and soluble in cold water). The media used were distilled water, borate buffer with and without sodium lauryl sulfate (pH=8), and borate buffer without sodium borate, i. e., boric acid (pH=4).

Samples of monodisperse polystyrene latex (LS-1200-B; 0.80μm diameter) showed little or no movement at the stationary level in the microelectrophoresis, independent of voltage gradient, solvent composition or pH, or the type of Methocel used for coating (e.g., see Figure 12). However, the diluted latexes were usually allowed to stand in the coated capillary for about 30 minutes before the measurements were made. The zero or near-zero electrophoretic mobilities, along with the 30 minutes elapsed time between loading and measuring, suggests that the methylcellulose molecules desorb from the capillary walls and adsorb on the surface of the latex particles (the adsorption of nonionic or steric stabilizers

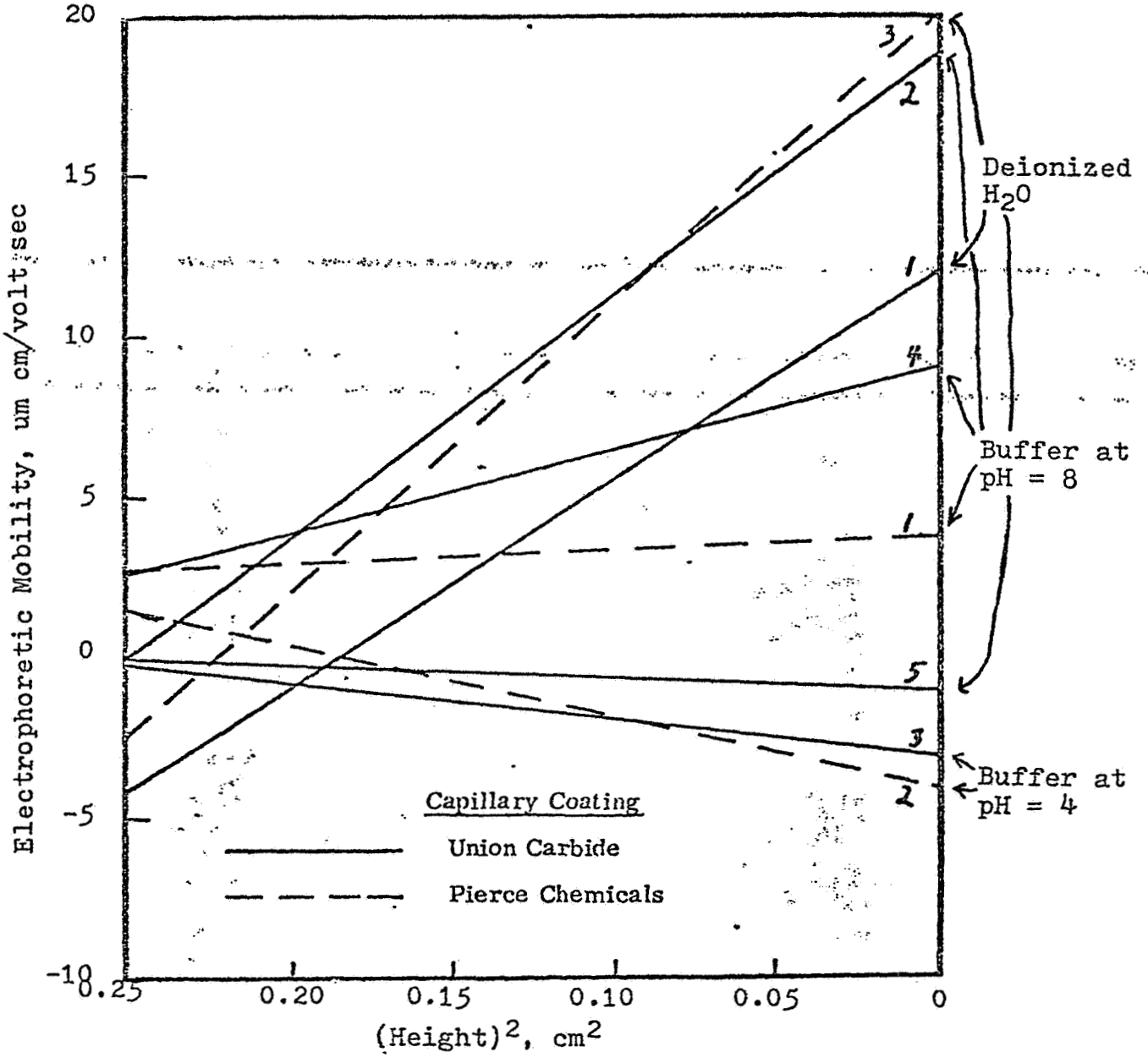

Figure 11. Electroosmotic Flow in Union Carbide and Pierce Chemical Coated Capillaries.

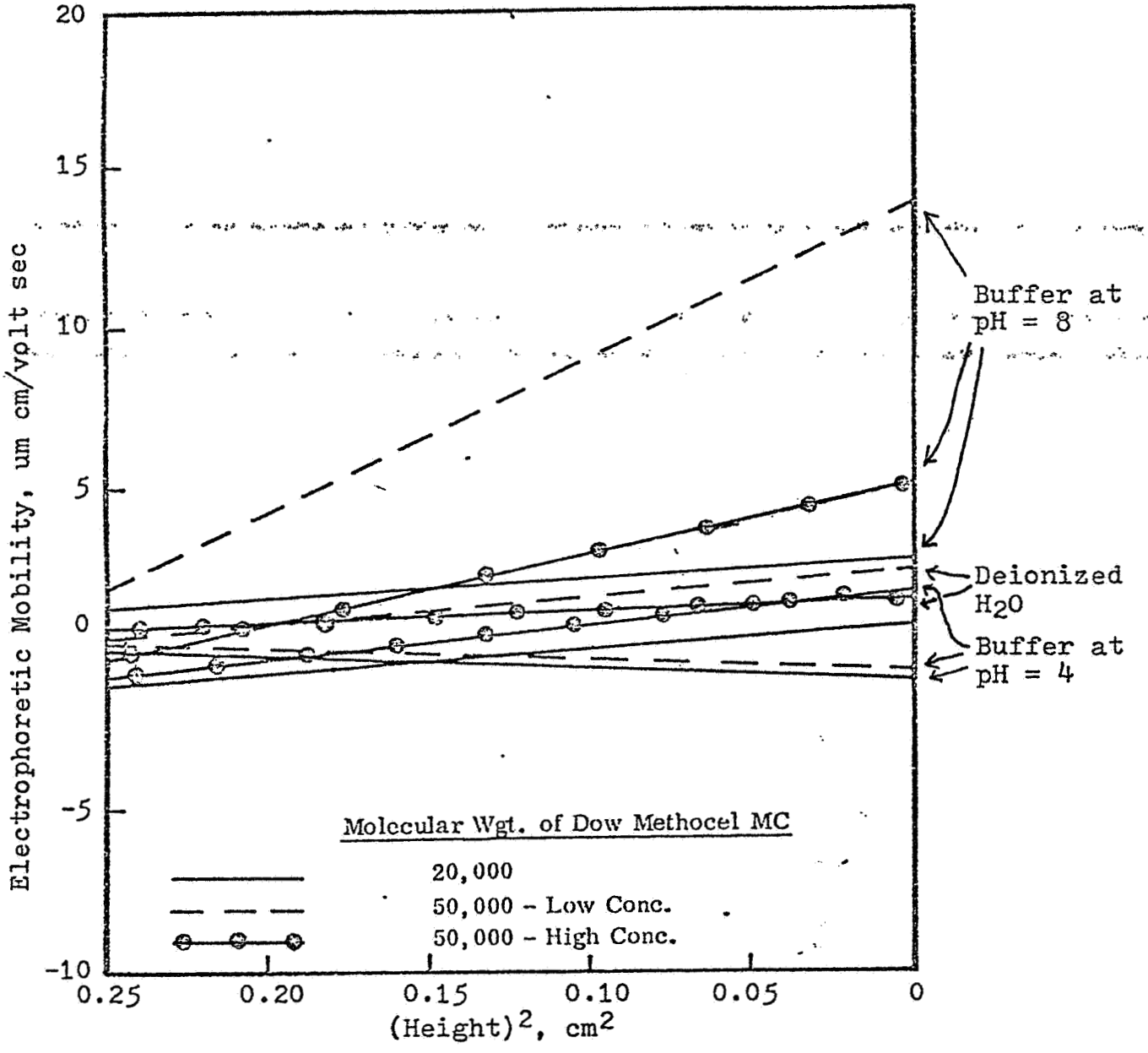

Figure 12. Electroosmotic Flow in Dow Methocel, MC, Coated Capillaries.

is known to reduce the electrophoretic mobility).

Therefore, a technique was developed to begin the measurements within five minutes after loading the cell with the diluted latex. Figure 13A shows that the electrophoretic mobility of the latex particles was initially unaffected by the presence of the methylcellulose coated capillary walls, but gradually decreased to essentially zero upon standing in the capillary. Thus, the methylcellulose is very effective in reducing the zeta potential of the capillary wall-liquid solvent interface and, hence, the electroosmotic flow within the capillary; however, it must be crosslinked or otherwise chemically-bound to the capillary wall so that it cannot desorb and adsorb on the surfaces of the particles in the dispersion. In comparison, Figure 13B shows the results of allowing the latex particles to stand in a capillary treated with the Union Carbide A-1100 coating. The results after 15 hours are comparable to the initial results. In this case the A-1100 coating is irreversibly adsorbed onto the glass surface.

Another approach used (suggested by H. Burrell, Inmont Corp.) to reduce the electroosmotic mobility was to coat the glass with a solution of polyvinyl acetate, allow the solvent to evaporate, leaving a thin film of strongly-adherent polymer, then surface-hydrolyze the polymer film to form a thin layer of polyvinyl alcohol (uncharged and normally water-soluble, but, in this case, chemically-bound to the underlying polyvinyl acetate film). A 4% solution of polyvinyl acetate in methyl ethyl ketone was prepared, and the glass capillary was dipped into this solution for one half hour and then dried in air. The polyvinyl acetate-coated glass surface was then hydrolyzed by heating at 110° C for 30 minutes and then exposing the surface to a 5% sodium hydroxide solution for 10 minutes. Three different molecular weight grades of polyvinyl acetate (specified only as "high, intermediate, and low", obtained from H. Burrell, Inmont Corp.) were applied and hydrolyzed with 5% sodium hydroxide. The results summerized in Table II show that the low-molecular-weight polyvinyl acetate coating (LMW-PVAc) reduced the electroosmotic mobility only slightly; the medium-molecular-weight coating (MMW-PVAc) reduced the electroosmotic mobility to a greater extent; the high-molecular-weight coating (HMW-PVAc) was less effective than the MMW-PVAc. In general, the polyvinyl acetate coating was not sufficiently effective in reducing the electroosmotic flow in glass capillaries.

The most effective material for reducing electroosmosis was found to be methylcellulose, which was shown, however, to desorb from the surface in less than an hour (Figure 11). Therefore, the methylcellulose was irreversibly-adsorbed or chemically-bound to the glass surface by treating the surface with γ-glycidoxypropyltrimethoxysilane (Dow Corning Z-6040), which binds to the glass, then using the epoxide group to link with the hydroxyl groups of the methylcellulose molecules. The mechanism proposed (L. H. Lee, J. Colloid Interface 27, 751, 1968) for the binding of this and other trialkoxysilanes to glass surfaces is as follows:

1. hydrolysis of the trialkoxysilane to the corresponding silanetriol;

2. chemisorption of the silanetriol on the glass surface (interaction between a hydroxyl group of the glass with one of the hydroxyl groups of the silanetriol);

3. formation of hydrogen bonds between hydroxyl groups of adjacent chemisorbed silanetriol molecules;

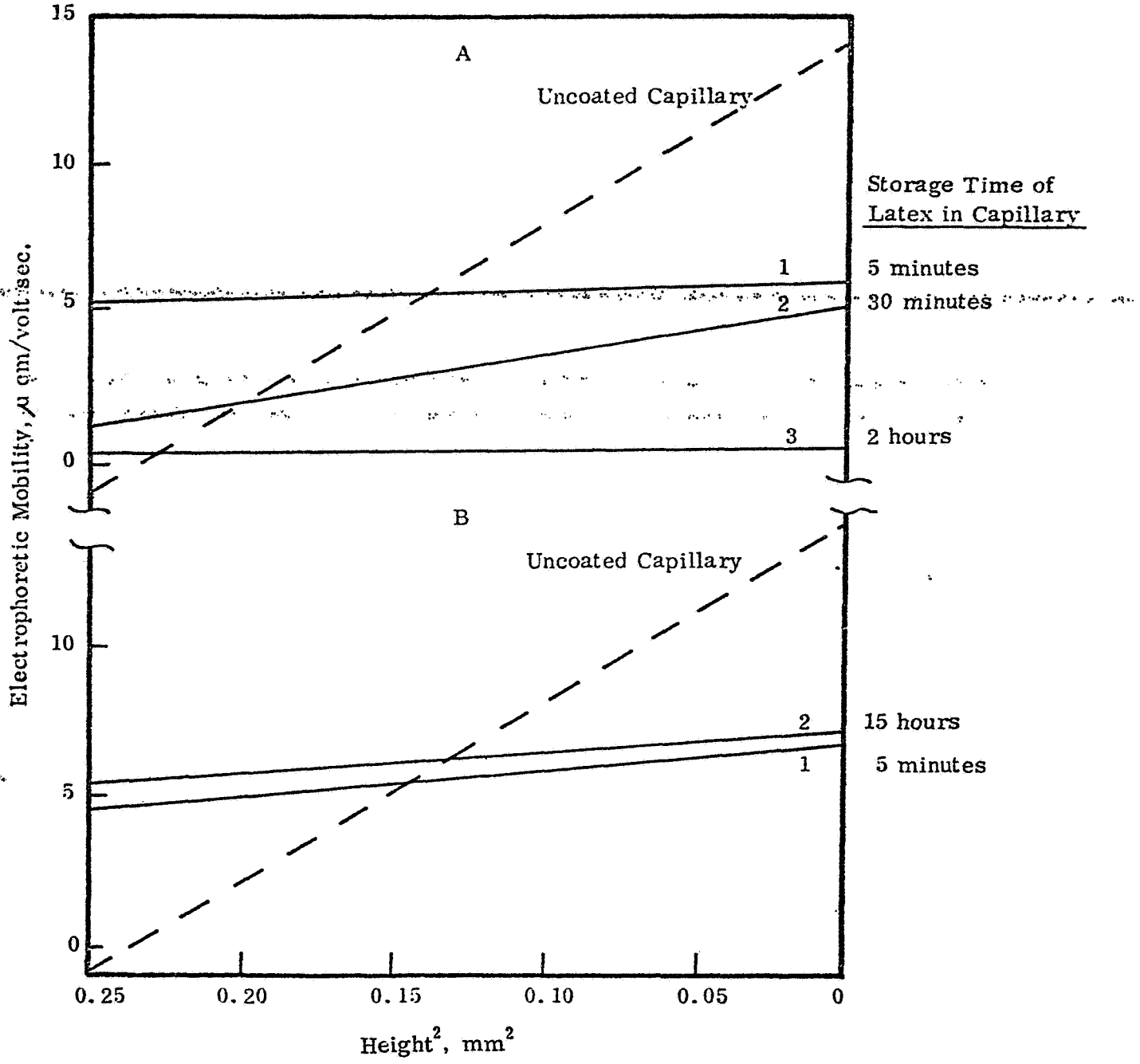

Figure 13. Electroosmotic Flow in Coated Capillaries
A, 110,000 M.W. of Methocel MC
B, Union Carbide Coating

Table II

Electroosmotic Flow in Coated Glass Capillaries

Capillary Coating*	Solvent	U_{os}, μm-cm/volt-sec	U_{os} Ratio $\frac{\text{Coated}}{\text{Uncoated}}$	U_e, μm-cm/volt-sec
LMW-PVAc	H_2O	5.8	0.6	1.6
MMW-PVAc	H_2O	2.0 (3.1)	0.2 (0.3)	2.1 (1.7)
HMW-PVAc	H_2O	4.8	0.5	2.4
LMW-PVAc	Borate Buffer	5.1	1.0	3.3
MMW-PVAc	Borate Buffer	1.8	0.4	2.8
HMW-PVAc	Borate Buffer	2.9	0.6	4.3
LMW-PVAc	Phosphate Buffer	3.8	1.0	2.0
MMW-PVAc	Phosphate Buffer	1.5 (1.8)	0.4 (0.5)	2.8 (1.9)
MMW-PVAc	Phosphate Buffer	1.8	0.5	1.8

*Coating Identification:

LMW-PVAc Low-molecular-weight polyvinyl acetate
MMW-PVAc Medium-molecular-weight polyvinyl acetate
HMW-PVAc High-molecular weight polyvinyl acetate

(all three PVAc's surface-hydrolyzed to PVA)

4. polymerization of adjacent silanetriol molecules during drying by splitting out water from hydrogen-bonded hydroxyl groups.

For the Dow Corning Z-6040 , such a process would give a polysilanetriol chemisorbed to the glass, with an exposed surface of epoxide groups, which are free to form bonds with compounds containing active hydrogen , such as methylcellulose. The methylcellulose (Dow Methocel MC) is applied over the Z6040-treated surface and heated to form chemical bonds between the epoxide groups of the Z6040 and the hydroxyl groups of the methylcellulose.

Part of this methylcellulose coating can be removed by rigorous washing--this is referred to as "physically adsorbed"--and part is removed only with difficulty--this is referred to as "chemically bound". This distinction is important because the "physically adsorbed" methylcellulose apparently is governed by an adsorption-desorption equilibrium and thus, when a colloidal sol with partially covered surfaces is added to the cell, the methylcellulose can desorb from the cell wall and re-adsorb on the colloidal particles, reducing their electrophoretic mobility to that of methylcellulose (zero). Such desorption and re-adsorption would obviate the electrophoretic separation. Fortunately, the "physically adsorbed" methylcellulose can be removed by rigorous washing, leaving the "chemically bound" methylcellulose, which does not desorb under these conditions.

The methylcellulose forms a layer of uncharged hydrated polymer on the surfaces of both the colloidal particles and the cell walls, and thus effectively reduces the zeta potential to zero. The mechanism proposed for this reduction in zeta potential comprises an increase in viscosity at the distance δ from the surface (usually the distance of the slipping plane) such that the slipping plane is moved outward from the surface to a distance where the potential is close to zero.

This report presents results for this Z6040-MC coating system which show that the electroosmotic mobility of glass capillaries (used in microcapillary electrophoresis cells) is reduced from the usual 3.5 μm-cm/volt sec to about 0.1 μm cm/volt sec.

The procedure used to coat the glass capillaries with the Z6040-MC combination was as follows:

1. prepare the Z6040 solution by adding 80 gm of methanol to 20 gm of water, then adding 3 gm of Z6040 (as received) and one drop of glacial acetic acid;

2. immerse clean glass capillary tubes in this Z6040 solution for one hour;

3. remove glass capillary tubes from Z6040 solution, position vertically with lower end in contact with an absorbent paper towel, and dry under vacuum at 60°C for one hour;

4. prepare MC solution by adding 0.175 gm of Dow Methocel HG (8000 cps) to 100 ml of distilled water, stirring for 5 hours, allowing to stand for one hour, and then decanting the clear supernatant layer;

5. immerse Z6040-coated glass capillary tubes in MC solution;

6. remove glass capillary tubes from MC solution, position vertically with lower end in contact with an absorbent paper towel, and dry under vacuum at 60° C for three hours;

7. rinse coated glass capillary tubes with distilled water until "physically adsorbed" methylcellulose is removed and only the "chemically bound" methylcellulose remains.

The glass capillary tubes coated with different variations of the foregoing procedure were inserted in the electrophoresis cell shown in Figure 5 and their electroosmotic mobilities were determined from the parabolic electrophoretic velocity profiles.

Table III shows the results for glass capillary tubes coated with different variations of the Z6040-MC combination and tested using 0.80μm-diameter monodisperse polystyrene latex particles (LS-1117-B). Although many more measurements were made than are listed in Table III, the results given are representative and reproducible to within ± 0.1μm cm/volt sec. The charges on the glass capillary tube walls and on the latex particles were always negative.

These results show that uncoated pyrex glass capillary tube walls (Run No. 1) have a strong negative charge (U_{os} = 3.5μm cm/volt sec), which is halved by coating the surface with Z6040 (Run No. 2).

Coating the glass surface with methylcellulose but omitting the Z6040 undercoat (Run No.'s 3 and 4) gave a low electroosmotic mobility initially, but the introduction of a 1% dispersion of the monodisperse polystyrene latex resulted in complete removal of the methylcellulose from the wall within 2 hours. (These experiments were carried out to determine the feasibility of using a sacrificial polystyrene latex to decrease the rinse time required to remove the excess methylcellulose from the cell; although the experiments were successful, this approach was not developed further because the rinsing procedure was effective and there was a possibility that some polystyrene particles might adhere to the coated glass capillary tube walls).

The pyrex glass capillary tubes that were coated with the Z6040-MC combination according to the foregoing procedure (Run No.'s 5 and 6) showed after extensive rinsing stable low-electroosmotic-mobility coatings that did not lose methylcellulose by desorption, as indicated by the unchanged electrophoretic mobility of polystyrene latex particles in phosphate and A-1 buffers stored in the tube for long periods of time. Similar results were observed when distilled water was stored in the coated capillary tubes for 7 months (Run No.'s 7 and 8); although the electroosmotic mobility was increased somewhat, it did not exceed 1μm cm/volt sec. This Z6040-MC coating was as effective for Kimax glass capillary tubes (Run No.'s 9 and 10) as it was for the pyrex capillary tubes.

All of the foregoing measurements were made in glass capillaries with an ID of one mm because the measurements of the parabolic particle velocity profiles are more precise for small capillaries. The glass columns used on the ASTP electrophoresis experiment, however, had an ID of 6.3 mm. Therefore, a series of measurements were run in large

TABLE III

Electroosmotic Mobility of Coated Glass Capillary Tubes

Run No.	Coating	Buffer Medium	Treatment	Exposure Time of Polystyrene Latex in Tube, min.	Ue*	U_{os}**
1	none	A-1	pyrex control	10	2.50	-3 50
2	Z6040	phosphate	pyrex; no rinse	10	3.40	-1 80
3	MC	phosphate	pyrex; 2 hrs in 1% latex; 1-hr. rinse	10	1.80	-3.20
			4-hr. rinse	10	2.20	-4.80
4	MC	phosphate	pyrex; 16-hr. rinse	10	1.30	-0.10
				120	0.70	-0.10
5	Z6040-MC	phosphate	pyrex; 30-hr. rinse	10	1.60	-0.05
				240	1.60	-0.05
				1320	1.40	-0 10
6	Z6040-MC	A-1	Pyrex; 1-hr. rinse;	10	2.15	-0.35
			3-wk storage in A-1 buffer	10	2.00	-0.40
				120	1.85	-0.20
7	Z6040-MC	phosphate	pyrex; 30-hr. rinse; 7 month storage in water	10	2.05	-0.75
8	Z6040-MC	A-1	pyrex; 30 hr. rinse, 7-month storage in water	10	2.35	-0.80
9	Z6040-MC	A-1	THF***-cleaned Kimax	10	2.10	-0.50
			2-hr. rinse	10	2.15	-0.20
10	Z6040-MC	A-1	THF-cleaned Kimax;	10	1.90	+0.10
			3-week storage in A-1 buffer	240	1.50	-0.10

* electrophoretic mobility (μm cm/volt sec) **electroosmotic mobility (μm cm/volt sec) *** tetrahydrofuran

glass columns in order to verify the coating procedure and especially the rinse procedure developed for the capillaries.

The major problems associated with the measurement of electrophoretic velocities in these relatively large glass columns result from their optical characteristics: 1. the wall thickness is relatively great (about 2 mm), which makes it difficult to determine the exact position of measurement in the channel; 2. the electrophoretic velocity of the particles can be measured down only to the center of the channel because of the limited working distance of the objective. Accurate microcapillary electrophoretic velocity measurements require that the measurement of particle velocities as a function of distance across the capillary be in a plane that intersects the longitudinal axis of the capillary, i. e., the measurements must be made through the exact center of the channel. Since the refractive index of glass is different from that of water, the optical path is displaced as it passes through the glass. Microcapillary electrophoresis cells usually have walls so thin (i. e., less than 100μm) that this optical displacement is small enough to be neglected.

The geometry and wall thickness of the glass electrophoresis columns used in these measurements were not known accurately enough to make precise corrections for the optical displacement. Moreover, the particle velocities could not be measured from one wall to the other. Therefore, the procedure used was to measure the particle velocities from the wall to the approximate center of the channel, where the fastest moving particles were selected for measurement (the fastest moving particles should be in the exact center of the channel). The uncertainty in the values of the electroosmotic mobilities was estimated to be $\pm$ 0.3μm cm/volt sec.

Table IV gives the electroosmotic mobility results for pyrex glass columns coated with the Z6040-MC combination according to the procedure described above and filled with A-1 buffer containing monodisperse polystyrene latex particles. As expected, the uncoated control column (Run No. 1) showed a high electroosmotic mobility and a high electrophoretic mobility of the polystyrene particles placed in it. The coated column which had been subjected to a 4-day static rinse with no water change (Run No. 2) showed a relatively low electroosmotic mobility (0.8μm cm/volt sec), but also the presence of "physically adsorbed" methylcellulose, which at first gave erratic electrophoretic mobilities of the polystyrene particles stored in it and, after 24 hours, a greatly decreased electrophoretic mobility.

In comparison, the columns subjected to the other rinsing procedures (Run No.'s 3-7) all showed electroosmotic mobilities of 0.5μm cm/volt sec or less. A 7-day static rinse with daily water changes (Run No. 3) removed the "physically adsorbed" methylcellulose, while the 4-day static rinse with no water change (Run No. 2) did not. The combination of a dynamic rinse (a continuous flow of water through the column at a rate of one liter/hour) with a static rinse (Run No.'s 4 and 5) also removed the "physically adsorbed" methylcellulose effectively. The dynamic rinse alone (Run No.'s 6 and 7) was effective only if it was continued for a period of at least two days (e.g., a 30-hour dynamic rinse [Run No. 7] still left some "physically adsorbed" methylcellulose).

These results show that a period of at least 3 days is necessary to remove the "physically adsorbed" methylcellulose. The rinsing may be dynamic or static provided that the water is changed frequently, especially in the early stages of the rinse. In these early

TABLE IV

Electroosmotic Mobility of Coated Pyrex Glass Electrophoresis Columns

Z6040-MC coating; A-1 buffer medium

Run No.	O.D. of Column, mm	Treatment	Exposure Time of Polystyrene Latex in Tube, min	U_e*	U_{os}**
1	9	uncoated control	10	3.8	-4.8
2	7	4-day static rinse with no water change	10	1.4	-0.8
			1440	0.3	-0.1
3	7	7-day static rinse with several water changes	10	1.1	-0.3
			1440	1.0	-0.1
4	7	4-day static rinse plus 1-day dynamic rinse	10	2.7	-0.3
			1440	2.1	-0.5
5	7	1-day dynamic rinse plus 3-week soak in A-1 buffer	10	1.0	-0.5
6	9.5	2-day dynamic rinse	10	2.1	-0.5
7	9.5	30-hour dynamic rinse	10	2.6	-0.5
			210	1.6	-0.5

*electrophoretic mobility (μm cm/volt sec) **electroosmotic mobility (μm cm/volt sec)

stages, 1-2 hours is sufficient for the solvent to become saturated with desorbed methylcellulose. After one day of efficient rinsing, several hours are required for the desorbed methylcellulose to attain an equilibrium concentration, which is lower than that of the earlier stages.

The concentration of methylcellulose which desorbs from coated and extensively-rinsed columns filled with A-1 buffer was determined as follows. Two sets of three coated columns were filled with A-1 buffer, sealed, and stored for periods of 3 and 4 weeks, respectively. The A-1 buffer in each set of columns was collected, a small concentration of polystyrene particles was dispersed in each solution, and after a time their electrophoretic mobilities were measured in the Rank microcapillary electrophoresis cell. No significant decrease in electrophoretic mobility was found, which indicates that the concentration of methylcellulose in the A-1 buffer was very small.

2. Plastic Surfaces

Plexiglas was considered by NASA as a possible material of construction for electrophoresis cells in space. Therefore, preliminary experiments were initiated to develop a low-electroosmotic-mobility coating for Plexiglas similar to those developed for glass. The binding of molecules such as methylcellulose to Plexiglas substrates involves different chemical reactions than the corresponding binding to glass or Lexan. Plexiglas is essentially polymethyl methacrylate, sometimes with small proportions of other methacrylate or acrylate esters, or acrylic or methacrylic acid in the case for the high-heat-distortion grades. The obvious method of chemical binding is the partial hydrolysis of surface methacrylate ester groups to form the carboxylate salt, followed by neutralization to the carboxyl form; this would give a random distribution of carboxyl groups over the Plexiglas surface. Possible reactions of these carboxyl groups (and the functional group on the molecule to be chemically-bound) include: (1) esterification with elimination of water (hydroxyl group); (2) hydrogen-bonding (carboxyl group); (3) anhydride formation by heating of hydrogen-bonded carboxyls to eliminate water; (4) salt formation with a di- or trivalent metal ion (carboxyl group); (5) amide formation (amine group).

Rectangular electrophoresis cells of the same configuration shown in Figure 6 were constructed of 1.6-mm-thick Plexiglas G sheet (Rohm & Haas). These cells have an interchangeable center section that can be used to evaluate the electrokinetic properties of different coatings on the Plexiglas as well as other plastic materials which are available only in sheet form.

The interchangeable center sections were treated in the following ways:

1. the cell section was merely rinsed with distilled water and dried, to establish the electroosmotic mobility of the untreated Plexiglas surface;

2. the cell section was filled with 0.01% aqueous Methocel (molecular weight 110,000), allowed to stand for 30 minutes, drained, and dried for a few hours in air at 50°C;

3. the cell section was coated with Dow Corning Z6040 as described earlier;

4. dilute Methocel solution was applied to the Z6040-coated surface as described earlier;

5. the cell section was filled with 0.1N sodium hydroxide, allowed to stand for one hour, drained, rinsed first with 0.1N hydrochloric acid and later with distilled water, then filled with 0.01% aqueous Methocel solution as described above;

6. the cell section coated with Methocel as described above was heated in water at 70°C for 30 minutes.

Table V gives the measurements of electroosmotic mobility for the variously-treated Plexiglas surfaces in distilled water, borate buffer, or phosphate buffer. The Dow Corning Z6040 coating had very little effect on the electroosmotic mobility indicating that little or no reaction with the Plexiglas surface had occurred. All Methocel coatings showed significant decreases in electroosmotic mobility. The best results in phosphate buffer (electroosmotic mobility of 0.6μm cm/volt sec) were obtained by hydrolysis of the Plexiglas surface with sodium hydroxide, followed by neutralization and reaction with the Methocel. The irreversible physical adsorption of Methocel observed with glass surfaces was not observed with Plexiglas, indicating that, in those cases where a significant reduction in electroosmotic mobility was observed, there was some chemical binding of the Methocel to the Plexiglas.

D. Water Permeation Through Lexan and Plexiglas Plates

The Apollo 16 electrophoresis experiment showed that air bubbles had formed in the Lexan tubing during the two-week period from the loading of the cell to initiation of the experiment. Further experimentation in this laboratory demonstrated that Lexan is permeable to water to an extent which is consistent with the size of bubbles found in the Apollo 16 electrophoresis apparatus. This problem of water permeation through plastic materials used in the construction of electrophoresis cells, and the inevitable formation of air bubbles in the cells, has resulted in the initiation of an experimental program to coat and measure the rate of water permeation through plastic materials.

The experimental approach adopted for measuring the rate of water permeation through plastic plates was as follows. A standard glass container, which had an opening of 5 cm^2 was first half filled with water. The specimen to be investigated was then epoxied to the top of the container and stored in a desiccator. The weight loss was then followed as a function of time. It was found that after an initiation period of two or three days the rate of weight loss, or of water permeation, remained constant for several weeks.

One material which is known to have a very low water permeability is a vinylidene chloride copolymer which has the trade name Saran. Samples of Saran lacquer resin were obtained from the Dow Chemical Company. The main experimental problem was to find a suitable solvent for the Saran, which would be a poor solvent for the Lexan and Plexiglas plates which were being investigated. A variety of solvents were used, such as 1,4 dioxane, N,N dimethylformamide, and tetrahydrofuran, all of which attacked Lexan to varying degrees, which were sufficient to destroy its optical properties. Cyclohexanone, however, was found to be an excellent solvent for Saran and, although it does swell Lexan, the rate

Table V

Electroosmotic Flow in Coated Plexiglas Cells

Cell Coating*	Solvent	U_e $\left(\frac{\mu m\ cm}{volt\ sec}\right)$	U_{os} $\left(\frac{\mu m\ cm}{volt\ sec}\right)$	U_{os} Ratio $\left(\frac{coated}{uncoated}\right)$
None	Water	2.60	-3.50	----
MOC	Water	4.05	-1.50	0.43
Z6040	Water	4.10	-6.90	1.95
Z6040 + MOC	Water	2.65	-1.95	0.56
S.T. + MOC	Water	2.60	-2.65	0.76
H.T. + MOC	Water	3.00	-0.20	0.06
None	Borate Buffer	5.00	-5.80	----
MOC	Borate Buffer	5.25	-1.80	0.31
Z6040	Borate Buffer	5.40	-5.60	0.97
Z6040 + MOC	Borate Buffer	4.45	-3.85	0.66
S.T. + MOC	Borate Buffer	5.10	-3.20	0.55
H.T. + MOC	Borate Buffer	5.40	-2.10	0.36
None	Phosphate Buffer	3.15	-3.25	----
MOC	Phosphate Buffer	3.20	-1.00	0.31
Z6040	Phosphate Buffer	2.75	-2.55	0.78
Z6040 + MOC	Phosphate Buffer	2.50	-0.75	0.23
S.T. + MOC	Phosphate Buffer	2.50	-0.60	0.18
H.T. + MOC	Phosphate Buffer	2.80	-1.00	0.31

*Coating Identification:

MOC - methylcellulose (Dow; 110,000 M.W.)

Z6040 - γ-glycidoxypropyltrimethoxysilane (Dow Corning)

S.T. - surface treated with 0.1M NaOH then 0.1M HCl

H.T. - heat treated in H_2O at 70°C for 30 min.

of attack was relatively low with very little loss in optical properties.

Table VI summarizes the results on coated Lexan and Plexiglas plates which were 0.10 cm and 0.16 cm thick, respectively. The dioxane and tetrahydrofuran (THF) solvents had the effect of attacking the Lexan to a much greater extent than the Plexiglas. This results in both of these solvents being suitable for Plexiglas, as opposed to Lexan, both in terms of optical properties and degree of water permeability. The cyclohexanone, however, was found to be the best solvent for Saran and to be compatible with Lexan. These results indicate that the water permeability of both Lexan and Plexiglas can be reduced significantly, probably to a much greater degree than reported in Table VI.

E. Conclusions

The following conclusions can be drawn from this work:

1. The Z6040-MC coating on pyrex glass columns or plastic surfaces decreases their electroosmotic mobilities to small negative values, most likely 0.2 ± 0.1 μm cm/volt sec;

2. This coating gives both "physically adsorbed" and "chemically bound" methylcellulose;

3. The "physically adsorbed" methylcellulose must be removed because otherwise it might desorb from the cell wall and re-adsorb on the particles to be subjected to electrophoretic separation;

4. Extensive rinsing of the coated columns for a period of at least 3 days is required to remove the "physically adsorbed" methylcellulose from the surface;

5. Rinsing of the coated columns over much longer periods of time eventually results in the removal of part of the "chemically bound" methylcellulose, resulting in an increase in the electroosmotic mobility.

6. The permanency of the Z6040-MC coating is suitable for free-fluid electrophoretic separations such as the ASTP experiment but its suitability for continuous particle electrophoretic separations, e.g., the Beckman CPE, has not yet been demonstrated.

Table VI

Water Permeation Results

Plate	Coating	Steady State Weight Loss mg/day	Observation Period, days	Optical Appearance
Lexan	uncoated	0.83	20	Clear
Lexan	1% Saran in Dioxane	1.34	15	Cloudy
Lexan	10% Saran in THF	0.56	15	Cloudy
Lexan	10% Saran in Cyclo-hexanone	0.54	16	Clear
Lexan	20% Saran in Cyclo-hexanone	0.11	83	Clear
Plexiglas	uncoated	1.25	15	Clear
Plexiglas	1% Saran in Dioxane	0.33	15	Clear
Plexiglas	10% Saran in THF	0.10	23	Clear

CHAPTER III

RESOLUTION OF SEPARATION OF FREE-FLUID ELECTROPHORESIS

A. Introduction

The success of free-fluid electrophoresis in separating biological cells in space depends upon the degree to which particles of different electrophoretic mobilities can be separated. An accurate prediction of the results of such an experiment depends upon a knowledge of experimental parameters, such as applied potential gradient and dimensions of the channel wall, as well as of the values for the true electrophoretic mobilities of the particles to be separated. One of the major problems encountered thus far is that the biological systems proposed for separation in space are those in which the particles have not yet been separated on earth by electrophoretic separation techniques. Although there is reason to believe that biological differences in cell populations may be reflected by differences in their electrical double-layer properties, these differences must be relatively small or else the problem of separation would not exist. Therefore, the three major goals of this research program have been to define, develop, and verify the experimental parameters that will lead to a maximum separation of particles which have a minimum difference in electrophoretic mobilities. The subject of this theoretical approach is to define the conditions which lead to maximum resolution in free-fluid electrophoretic separations in cylindrical tubes.

B. Theory of Electroosmotic Flow

The observed velocity V_{obs} of a charged particle exposed to an applied potential in a closed channel of circular geometry may be defined by the equation:

$$V_{obs} = V_e + V \tag{26}$$

where V_e = electrophoretic velocity of the particle
V = the solvent velocity due to electroosmosis.

The solvent velocity under these conditions is defined by the equation:

$$V = U\left(\frac{2r^2}{a^2} - 1\right) \tag{27}$$

where r = distance from center of channel
a = radius of channel
U = electroosmotic velocity at channel wall, i. e., where r = a.

Combining Equations 26 and 27 yields:

$$V_{obs} = V_e + U\left(\frac{2r^2}{a^2} - 1\right) \tag{28}$$

or

$$V_{obs} = U_e E + U_{os} E \left(\frac{2r^2}{a^2} - 1 \right) \tag{29}$$

where U_e = electrophoretic mobility

U_{os} = electroosmotic mobility

E = applied potential gradient.

Equation 29 predicts that, for values of U_{os} less than zero, the particle velocity is at a maximum in the center of the channel (i. e., when $r = 0$), and decreases as r increases. The controlling factor that determines whether or not separation of two different types of particles will occur is the velocity of the trailing edge of the faster particles relative to the velocity of the leading edge of the slower particles. If the velocity of the latter is less than that of the former, separation will occur. If the two velocities are equal, or if the velocity of the latter is greater than that of the former, separation will not occur. If the sample plug has a radius of d, the velocity of interest for the faster particles (the trailing edge; subscript 1) is at $r = d$, and the velocity of interest of the slower particles (the leading edge; subscript 2) is at $r = 0$. Equation 29 may now be used to define these velocities of interest:

$$V_{obs1} = U_{e1} E + U_{os} E \left(\frac{2d^2}{a^2} - 1 \right) \tag{30}$$

$$V_{obs2} = U_{e2} E - U_{os} E \tag{31}$$

Although V_{obs1} must be greater than V_{obs2} for a separation to be experimentally feasible, the limit occurs when $V_{obs1} = V_{obs2}$. Thus, Equations 30 and 31 may be equated and rearranged to yield:

$$\Delta U'_e = -2R^2 U_{os} \tag{32}$$

where $\Delta U'_e = U_{e1} - U_{e2}$ when $V_{obs1} = V_{obs2}$, and

$R = d/a$.

The physical significance of $\Delta U'_e$ is that it represents the absolute minimum difference in particle mobilities which may be separated under <u>any experimental conditions</u>. Equation 32 predicts that $\Delta U'_e$ is directly proportional to both the electroosmotic mobility and the ratio of sample plug radius to the channel radius squared (i. e., R^2). Furthermore, Equation 32 is independent of the applied potential and implies an unlimited time and distance for the separation. Figure 14 shows the variation of $\Delta U'_e$ as a function of R for different values of U_{os}. The importance of the value of R for an electrophoretic separation experiment is evident, especially for low values of $\Delta U'_e$. For example, if the particles to be

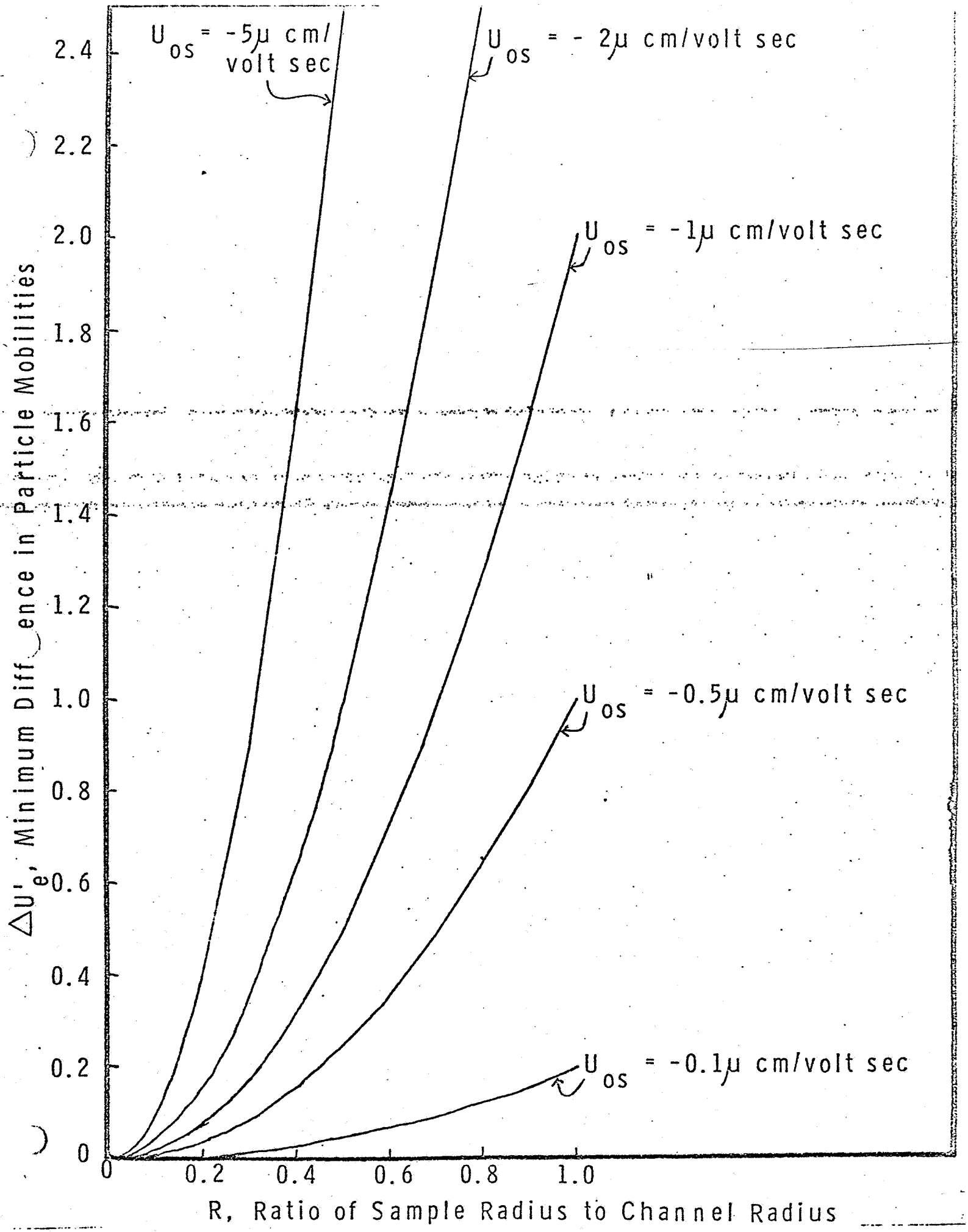

FIGURE 14 Minimum Difference in Particle Mobility Required for Separation as a Function of Relative Size of Sample Plug

separated have electrophoretic mobilities differing by only 0.2μm-cm/volt-sec, they can be separated, even though the electroosmotic mobility may be as high as 2μm-cm/volt-sec, if the R value is 0.2.

Although Equation 32 is extremely useful for predicting whether or not a given separation is possible, it in no way indicates its experimental practicality. For this, the distance between particle bands as a function of all the experimental variables including separation time is of primary importance. Equation 30 gives the velocity of the trailing edge of the faster particles, V_{obs1}, while Equation 31 gives the velocity of the leading edge of the slower particles, V_{obs2}. The separation distance between particle bands, ΔD, may be defined as:

$$\Delta D = V_{obs1}\, t - V_{obs2}\, t - \theta \tag{33}$$

where t is the separation time and θ is the initial thickness of the sample plug. Equations 30 and 31 may now be substituted into Equation 33 to yield:

$$\Delta D = \Delta U_e E t + 2 U_{os} E R^2 t - \theta \tag{34}$$

where ΔU_e is the difference in electrophoretic mobility between particles 1 and 2. Equation 34 may be used to calculate the distance between sample bands as a function of time, sample plug thickness and radius, applied potential, electroosmotic velocity, and the difference in electrophoretic mobility of the particles to be separated.

The primary concern for any planned free-fluid electrophoretic separation of colloidal particles where the results are recorded photographically, is a prediction of whether or not the particles will separate into distinct bands. From this point of view, the limiting separation occurs when: ΔD from Equation 34 is set equal to zero; ΔU_e represents the minimum difference in electrophoretic mobility, $\Delta U_{e_{min}}$; and t represents the maximum time allowed for the separation under a given set of experimental conditions, t_{max}. Equation 34 may now be rearranged to yield:

$$\Delta U_{e_{min}} = \frac{\theta}{E t_{max}} - 2 U_{os} R^2 . \tag{35}$$

Although Equation 35 is useful, it does not contain all the experimental variables expressed explicitely. The maximum time allowed for the separation t_{max} is a function of the length of the channel L, the electrophoretic mobility of the particle with greatest velocity $U_{e_{max}}$, the applied potential E, and the electroosmotic mobility U_{os} according to the equation:

$$t_{max} = \frac{L}{(U_{e_{max}} - U_{os})\, E} . \tag{36}$$

Equation 36 assumes that the separation must end when the first particle reaches the end of the channel (and also that U_{os} is negative, an initial assumption of the derivations). Substituting Equation 36 into Equation 35 yields:

$$\Delta U_{e_{min}} = \frac{\theta U_{e_{max}} - (\theta + 2R^2 L) U_{os}}{L}, \tag{37}$$

or

$$\Delta U_{e_{min}} = \frac{\theta}{L} U_{e_{max}} - \left(\frac{\theta}{L} + 2R^2\right) U_{os}$$

Equation 37 expresses the minimum difference in particle mobilities that may be separated into separate bands as a function of the controlling experimental parameters.

Equation 37 was derived with the assumption that the channel wall has the same charge as the particles. A more general derivation yields the following equation:

$$\Delta U_{e_{min}} = \frac{\theta}{L} U_{e_{max}} + \left(\frac{\theta}{L} + 2R^2\right) \left| U_{os} \right| \tag{38}$$

where $\left| U_{os} \right|$ is the absolute value of U_{os}.

Equation 38 was derived with the assumption that no temperature gradient exists in the electrophoresis column. All of the electrokinetic terms in this equation will now be defined to be those corresponding to 25° C. If it is assumed that no temperature gradient exists along the axis of the electrophoresis column, but that a radial temperature gradient may exist from the center to the channel wall, there are three parameters which must be defined in order to calculate $\Delta U_{e_{min}}$: the temperature at the channel wall $\underline{T}_1$, i. e., at $\underline{R} = 1$; the temperature in the center of the channel $\underline{T}_2$, i. e., at $\underline{R} = 0$; and the temperature at the maximum distance of the particles from the center of the channel $\underline{T}_3$, which is defined by $\underline{R}$ in Equation 38. If the temperature gradient is now assumed to be continuous (e.g., a linear or parabolic temperature gradient), Equation 38 can be re-stated as the following general equation:

$$\Delta U_{e_{min}} = U'_{e_{max}} - U'_e = \frac{\theta}{L} U'_{e_{max}} + \left(\frac{\theta}{L} + 2R^2\right) \left| U'_{os} \right|, \tag{39}$$

where all the primed electrokinetic terms are defined as the values at any one, or combination, of the three temperatures $\underline{T}_1$, $\underline{T}_2$, or $\underline{T}_3$.

Two conditions of electrophoretic separation must now be defined and treated separately. The first is when the electroosmotic flow is in the opposite direction to the electrophoretic velocity, i. e., the sign of the charge on the channel wall is the same as on the particles and parabolic velocity profile is in the direction of the particle travel. The second is when the electroosmotic flow is in the same direction as the particles, i. e., the sign of the charge on the channel wall is opposite to that of the particles and the parabolic velocity profile is inverted, in the opposite direction to the travel of the particles.

The first condition of the parabolic velocity profile will be considered first.

The electrophoretic mobility of a particle is defined by the von Smoluchowski equation:

$$U_e = \frac{\zeta \epsilon}{4 \pi \eta} \quad , \tag{40}$$

where ζ is the zeta potential, and ϵ and η are the dielectric constant and viscosity of the liquid medium. If it is assumed that the zeta potential is independent of temperature:

$$U_e = K \frac{\epsilon}{\eta} \quad , \tag{41}$$

where $K \neq f(T)$. The convention adopted earlier, i.e., that the unprimed electrokinetic terms are applicable only to 25° C, leads to the following expressions:

$$U_e = K \frac{\epsilon_{25}}{\eta_{25}} \text{ (41a)}; \qquad U_{e_{max}} = K_{e_{max}} \frac{\epsilon_{25}}{\eta_{25}} \text{ (41b)}; \qquad U_{os} = K_{os} \frac{\epsilon_{25}}{\eta_{25}} \text{ (41c)}.$$

Since the temperature conditions in the channel are not defined, Equation 39 must be related to Equation 38 in order to define the resolution of separation of 25° C, which is the temperature of the experimental electrophoretic measurements.

The driving force for electroosmotic flow is at the channel wall, which is defined above as being at temperature $\underline{T}_1$. The electroosmotic mobility at temperature $\underline{T}_1$ is:

$$U'_{os} = K_{os} \frac{\epsilon_1}{\eta_1} \quad , \tag{42}$$

or combining with Equation 41c:

$$U'_{os} = \frac{\epsilon_1 \eta_{25}}{\eta_1 \epsilon_{25}} U_{os} \quad , \tag{42a}$$

The resolution of separation of the slower moving particles is controlled by the position of these particles at the apex of the parabola in the center of the channel, which is defined above as being at temperature $\underline{T}_2$. The electrophoretic mobility of the slower moving particles at temperature $\underline{T}_2$ is:

$$U'_e = K \frac{\epsilon_2}{\eta_2} \tag{43}$$

or combining with Equation 41a:

$$U'_e = \frac{\epsilon_2 \eta_{25}}{\eta_2 \epsilon_{25}} U_e \, . \tag{43a}$$

REPRODUCIBILITY OF THE ORIGINAL PAGE IS POOR

The temperature in the center of the channel $\underline{T}_2$ also controls the effective separation distance through $U'_{e_{max}}$ expressed in the right-hand side of Equation 39, so that:

$$U'_{e_{max}} = K_{e_{max}} \frac{\epsilon_2}{\eta_2} , \tag{44}$$

or combining with Equation 41b:

$$U'_{e_{max}} = \frac{\epsilon_2 \eta_{25}}{\eta_2 \epsilon_{25}} U_{e_{max}} \tag{44a}$$

The faster moving particles as expressed in the definition of $\Delta U_{e_{min}} = U'_{e_{max}} - U'_e$ (Equation 39), at the trailing edge of the parabola, which is defined above as being at temperature $\underline{T}_3$. The electrophoretic mobility of the faster moving particles at temperature $\underline{T}_3$ is:

$$U'_{e_{max}} = K_{e_{max}} \frac{\epsilon_3}{\eta_3} \tag{45}$$

or combining with Equation 41b:

$$U'_{e_{max}} = \frac{\epsilon_3 \eta_{25}}{\eta_3 \epsilon_{25}} U_{e_{max}} , \tag{45a}$$

Substituting Equations 42a, 43a, 44a, and 45a into Equation 39 yields:

$$\frac{\epsilon_3}{\eta_3} U_{e_{max}} - \frac{\epsilon_2}{\eta_2} U_e = \frac{\theta}{L} \frac{\epsilon_2}{\eta_2} U_{e_{max}} + \left(\frac{\theta}{L} + 2R^2\right) \frac{\epsilon_1}{\eta_1} U_{os} . \tag{46}$$

The electrophoretic resolution of separation is defined by the equation:

$$\Delta U_{e_{min}} = U_{e_{max}} - U_e , \tag{47}$$

which may be substituted into Equation 46 to yield:

$$\Delta U_{e_{min}} = \left(1 + \frac{\theta}{L} - \frac{\eta_2 \epsilon_3}{\epsilon_2 \eta_3}\right) U_{e_{max}} - \left(\frac{\theta}{L} + 2R^2\right) \frac{\eta_2 \epsilon_1}{\epsilon_2 \eta_1} U_{os} , \tag{48}$$

Equation 48 defines the resolution of separation for the forward parabolic velocity profile as a function of temperature in terms of the temperature variation of the dielectric constant and viscosity of the fluid medium.

A similar derivation for the second condition, an inverted parabolic velocity profile, which occurs when the charge on the particles and the channel wall are the same, gives the following equation:

$$\Delta U_{e_{min}} = \left(1 + \frac{\theta}{L} - \frac{\eta_3 \epsilon_2}{\epsilon_3 \eta_2}\right) U_{e_{max}} + \left(\frac{\theta}{L} + 2R^2\right) \frac{\eta_3 \epsilon_1}{\epsilon_3 \eta_1} U_{os}, \tag{49}$$

where the symbols have the same meanings.

C. Variation of Viscosity and Dielectric Constant With Temperature

The viscosity of the A-1 buffer was measured in the temperature range 0-30° C using a Brookfield viscometer equipped with an UL adapter. The viscosity was found to vary from 2.5 to 1.0 cps over this temperature range. Figure 15 shows the variation of reciprocal viscosity with temperature for A-1 buffer and water. The points represent the experimental values, while the solid lines represent the best linear fit through the experimental points. The equation for the A-1 buffer is:

$$\frac{1}{\eta} = 0.0184\,T + 0.4, \tag{50}$$

where η is the viscosity in cps and T is the temperature in °C.

The dielectric constant temperature variation of the A-1 buffer has not yet been measured. However, Figure 16 shows the literature values for pure water; again points represent the experimental values and the solid line represents the linear fit according to the equation:

$$\epsilon = -0.371\,T + 87.85. \tag{51}$$

Equations 50 and 51 may now be substituted into Equations 48 and 49 in order to express the resolution of separation, $\Delta U_{e_{min}}$, as a function of temperature.

D. Nature of the Temperature Gradient

The only problem which remains for a complete analysis of the electrophoretic resolution is to determine the nature of the temperature gradient. For example, if the channel wall is at 10° C and the center of the channel is at 15° C, then $\underline{T}_1 = 10°$ C and $\underline{T}_2 = 15°$ C. The value of $\underline{T}_3$ is not known and must be determined by experiment or from a mathematical expression which gives the temperature gradient as a function of distance from the center of the channel. The temperature-distance variation can be assumed to be linear or parabolic. The parabolic assumption, which is considered to be the more realistic, gives the following expression for $\underline{T}_3$:

$$T_3 = T_2 - R^2 \,(T_2 - T_1). \tag{52}$$

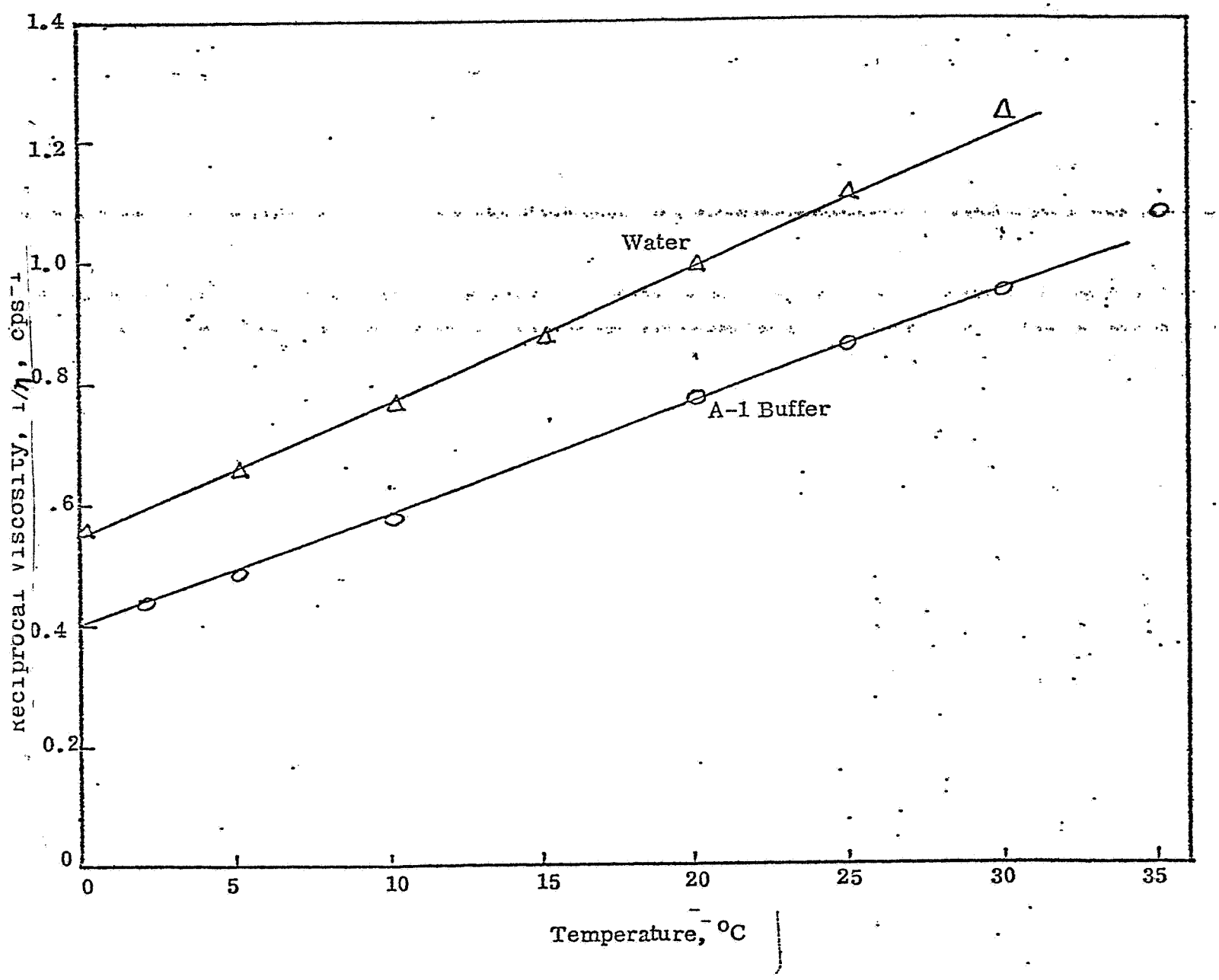

Figure 15. Variation of Reciprocal Viscosity with Temperature for Water and A-1 Buffer

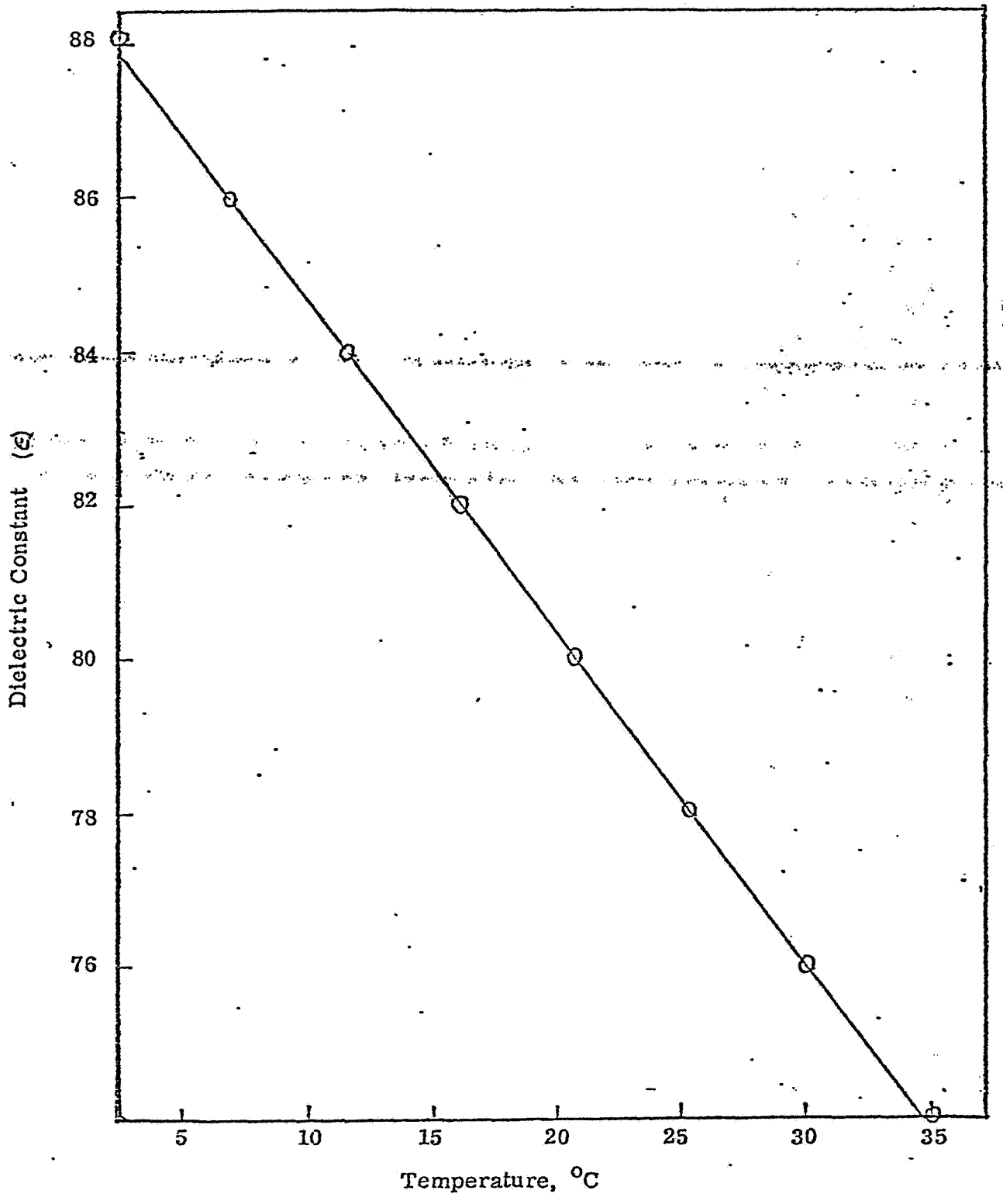

Figure 16. Variation of Dielectric Constant of Water with Temperature

E. Prediction of Resolution of Separation

The electrophoretic resolution of separation $\Delta U_{e_{min}}$ may now be calculated from the following parameters: the dimensions of the electrophoresis column; the dimensions of the sample plug; the electrophoretic mobility of the faster moving particles; the electroosmotic mobility at the channel wall; and the temperatures at the channel wall and in the center of the channel.

The maximum resolution, i. e., the minimum value of $\Delta U_{e_{min}}$, is equal to $U_{e_{max}}\,\theta/L$; it occurs when U_{os} is zero and there is no temperature gradient in the channel. The maximum resolution may also occur when U_{os} is not zero; in this case, the electroosmotic mobility is exactly counter-balanced by the effects of the temperature gradient. This condition may be expressed mathematically by setting the left-hand side of Equations 48 and 49 equal to $U_{e_{max}}\,\theta/L$ and solving for all the terms which are a function of temperature. An explicit solution has not yet been derived because of the complex nature of the resulting equations; however, an approximate solution can be obtained by forcing a linear fit of ϵ/η as a function of temperature according to the equation:

$$\frac{\epsilon}{\eta} = 1.276T + 35.7. \tag{53}$$

Figure 17 shows that Equation 53 (dotted line) is a reasonable representation of the experimental values (solid line) in the temperature range of 0-30° C.

Equations 48 and 49 may now be solved for the conditions of maximum resolution and expressed as a function of temperature through Equations 52 and 53. The resulting equation is:

$$T_2 = T_1 + (T_1 + 30)\left(\frac{\theta}{LR^2} + 2\right)\frac{U_{os}}{U_{e_{max}}}, \tag{54}$$

where U_{os} is negative for a forward parabolic velocity profile and positive for an inverted parabolic velocity profile, predicts the temperature gradient conditions which are necessary to yield maximum resolution. It is interesting to note that the temperature gradient conditions are not functions of the absolute values of U_{os} and $U_{e_{max}}$, but rather of their ratios. Equation 54 has been used to calculate the temperature gradient conditions when $\theta = 0.0$ cm, $L = 14$ cm and $R = 0.75$. Figure 18 shows the results of these calculations for different values of the ratio $U_{os}/U_{e_{max}}$ for both forward and inverted parabolic velocity profiles according to Equation 54. The resolution of separation will be improved, at least initially, when the channel-wall temperature is higher than the center temperature for a forward parabolic velocity profile, and when the center temperature is higher than the wall temperature for an inverted parabolic velocity profile. Furthermore, maximum resolution is obtained with a smaller temperature gradient in the case of an inverted parabolic velocity profile.

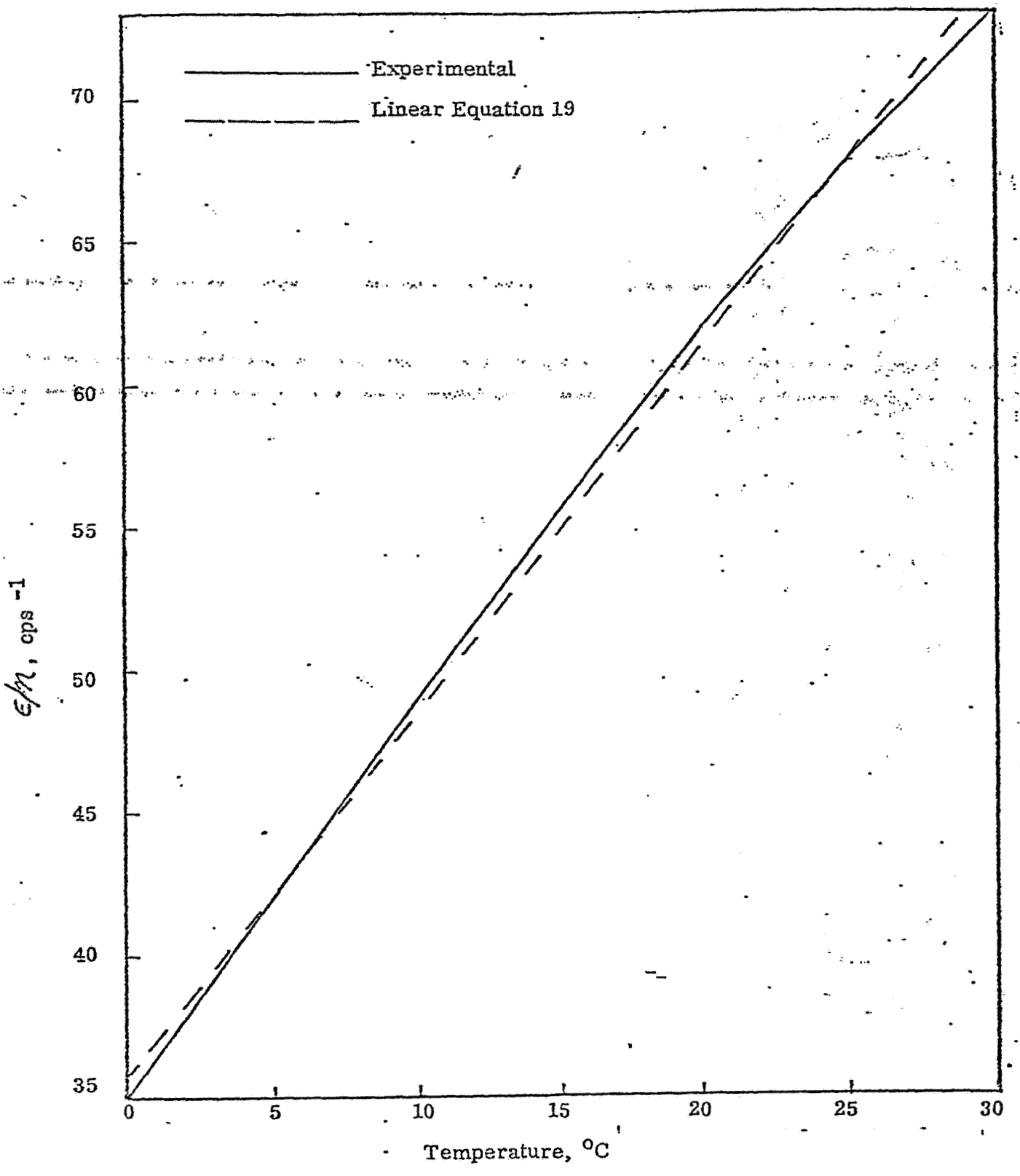

Figure 17. Variation of Ratio of Dielectric Constant to Viscosity Ratio with Temperature for A-1 Buffer

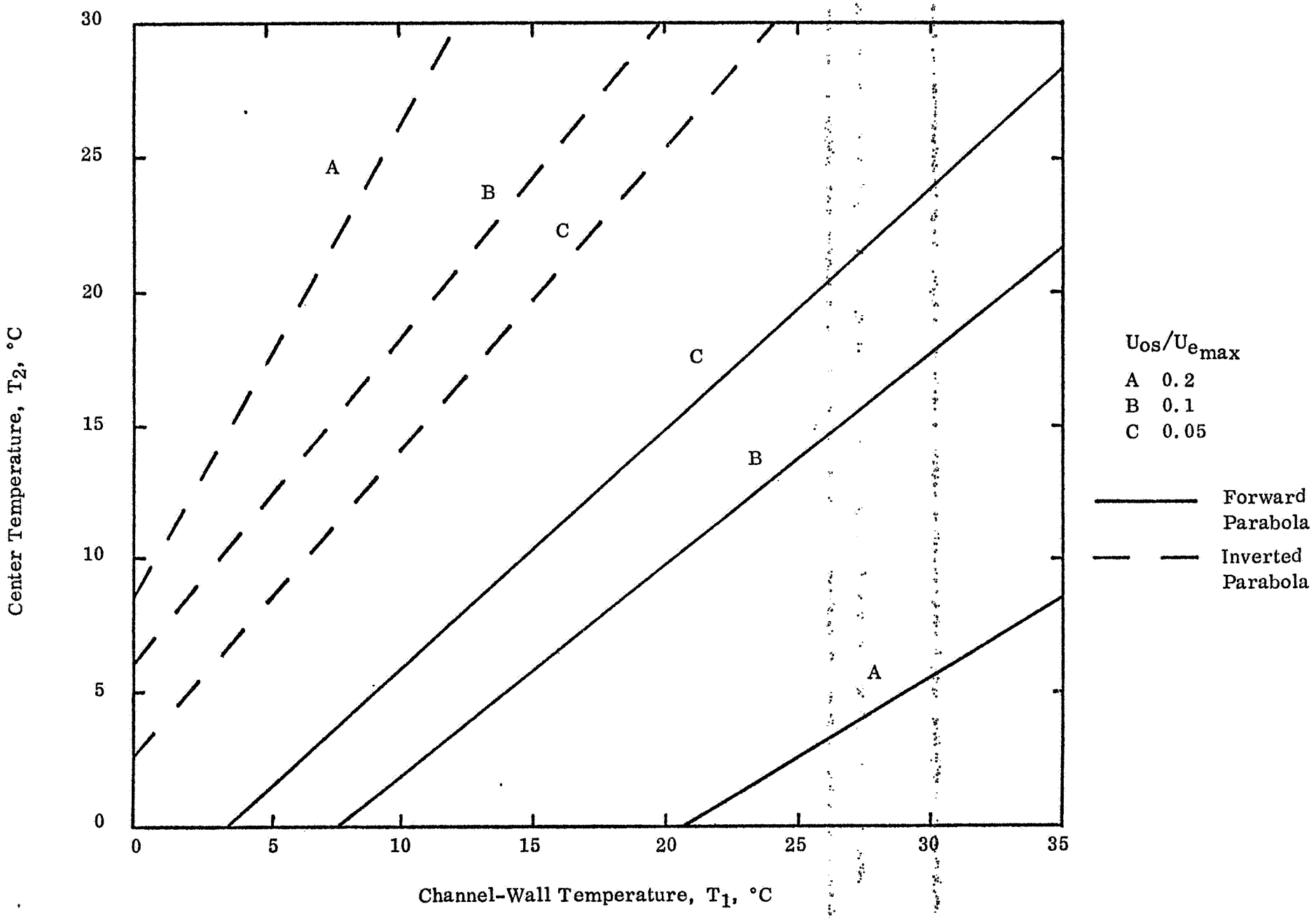

Figure 18 Temperature Grandient Conditions Necessary for Maximum Resolution for Different Values of $U_{os}/U_{e_{max}}$

Equations 48-52 may now be used to calculate the resolution of separation for different values of U_{os} and $U_{e_{max}}$, assuming the following values of the experimental parameters which represent the best values available for the ASTP experiment: $\theta = 0.3$ cm, $\underline{L} = 14$ cm; $\underline{R} = 0.75$; $\underline{T}_2 = 15°C$. Figures 19 and 20 show the variation of resolution of separation with channel-wall temperature for a forward and inverted parabolic velocity profiles, respectively. Figure 19 also contains two curves (C and E) which show the effect of a temperature gradient in the absence of electroosmosis. It is obvious from these results that the temperature gradient should be kept to a minimum. Also, since the channel-wall temperature is expected to be lower than the center temperature because of external cooling, an inverted parabolic velocity profile in which the channel wall has a relatively small charge of sign opposite to that of the particles should give an improved resolution of separation.

Figure 21 shows the variation of resolution of separation with electroosmotic mobility when the channel wall is at 13°C and the center temperature is 15°C for different values of $U_{e_{max}}$. As $U_{e_{max}}$ increases, maximum resolution of separation occurs at increasing, but low, values of U_{os} in the positive direction. This means that if the faster moving particles have a negative charge with an electrophoretic mobility of 3μm-cm/volt-sec, then the maximum resolution of separation will occur when the channel wall has a positive charge with an electroosmotic mobility of 0.06μm-cm/volt-sec.

The foregoing theoretical derivation shows that the resolution in free-fluid electrophoretic separations depends upon the temperature gradient. If the cell dimensions, the temperatures at the center and wall of the cell, and the electrophoretic mobility of the faster moving particles are known, the electroosmotic mobility that would give maximum resolution can be calculated. Thus far, our experiments have been directed toward minimizing the electroosmotic mobility, and values as small as 0.1-0.4μm-cm/volt-sec (negative) have been achieved consistently. However, with external cooling of the cell wall (i.e., the temperature of the channel wall is lower than that of the center of the column), the resolution of separation would be enhanced if the channel wall bore a slight charge opposite in sign to that of the particles. Therefore, assuming that the samples proposed for separation comprise negatively charged particles, it would be desirable to develop coatings which would have a slight positive charge.

F. Computer-Calculated Prediction of Free-Fluid Electrophoretic Separation

The equations which were derived in the above analysis define the resolution of electrophoretic separation as a function of the physical and experimental parameters such as: length and diameter of the electrophoresis column; thickness and diameter of the sample plug; electroosmotic mobility at the cell wall/liquid interface; maximum electrophoretic mobility of the particles to be separated; and the radial temperature gradient generated in the electrophoresis column by joule heating. Although this analysis is useful for making a judicious choice of the experimental parameters and for matching the experimental parameters to the electrophoretic characteristics of the particles to be separated, it does not define completely the results of a separation. Therefore, the model adopted in the above analysis was used to construct a computer program which would predict the position and concentration of particles in free-fluid electrophoresis as a function of time.

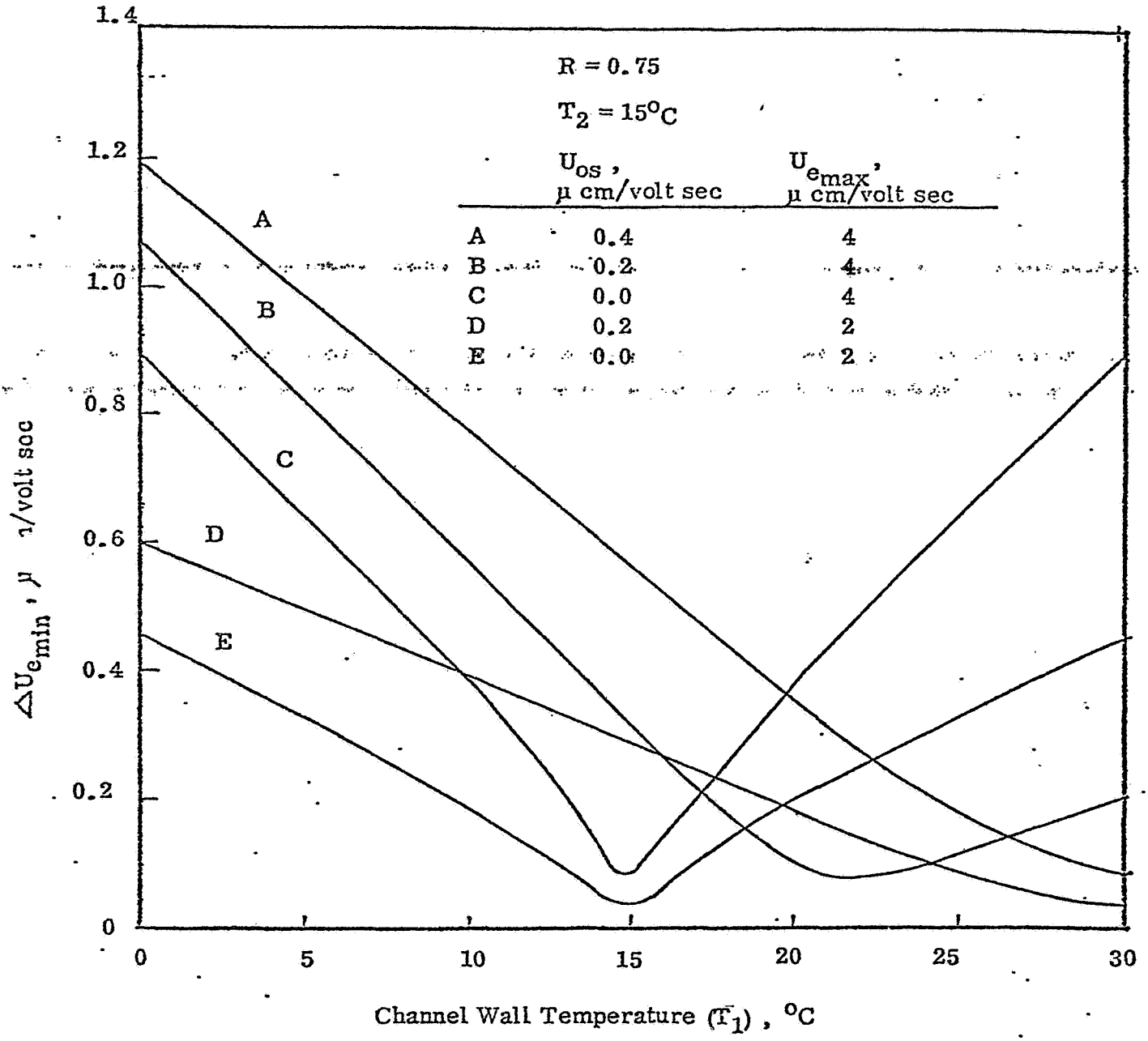

Figure 19. Variation of Resolution of Separation with Channel Wall Temperature for Forward Parabolic Velocity Profile as a Function of Electroosmotic Mobility and Maximum Electrophoretic Mobility of the Particles

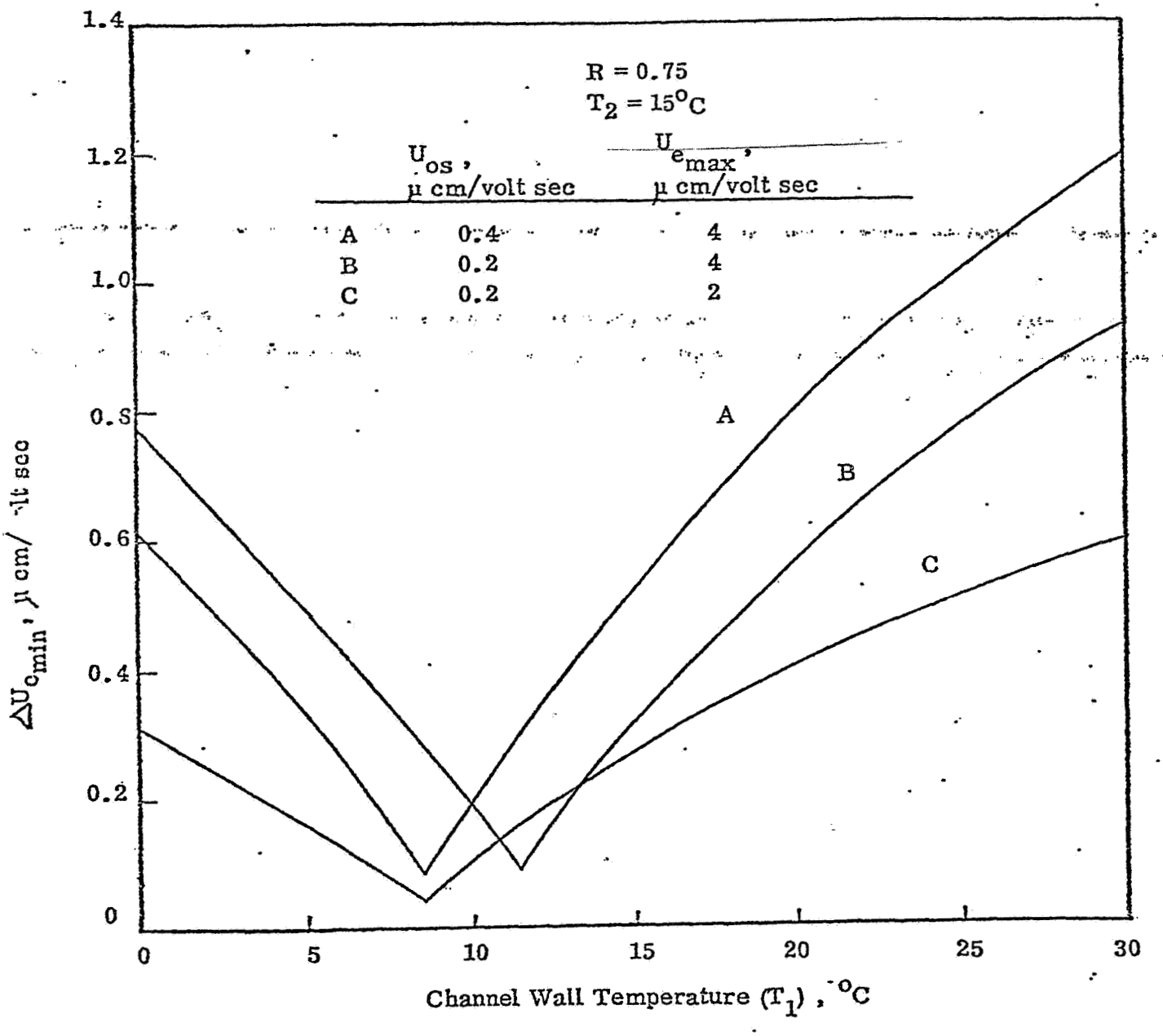

Figure 20. Variation of Resolution of Separation with Channel Wall Temperature for Inverted Parabolic Velocity Profile as a Function of Electroosmotic Mobility and Maximum Electrophoretic Mobility of the Particles

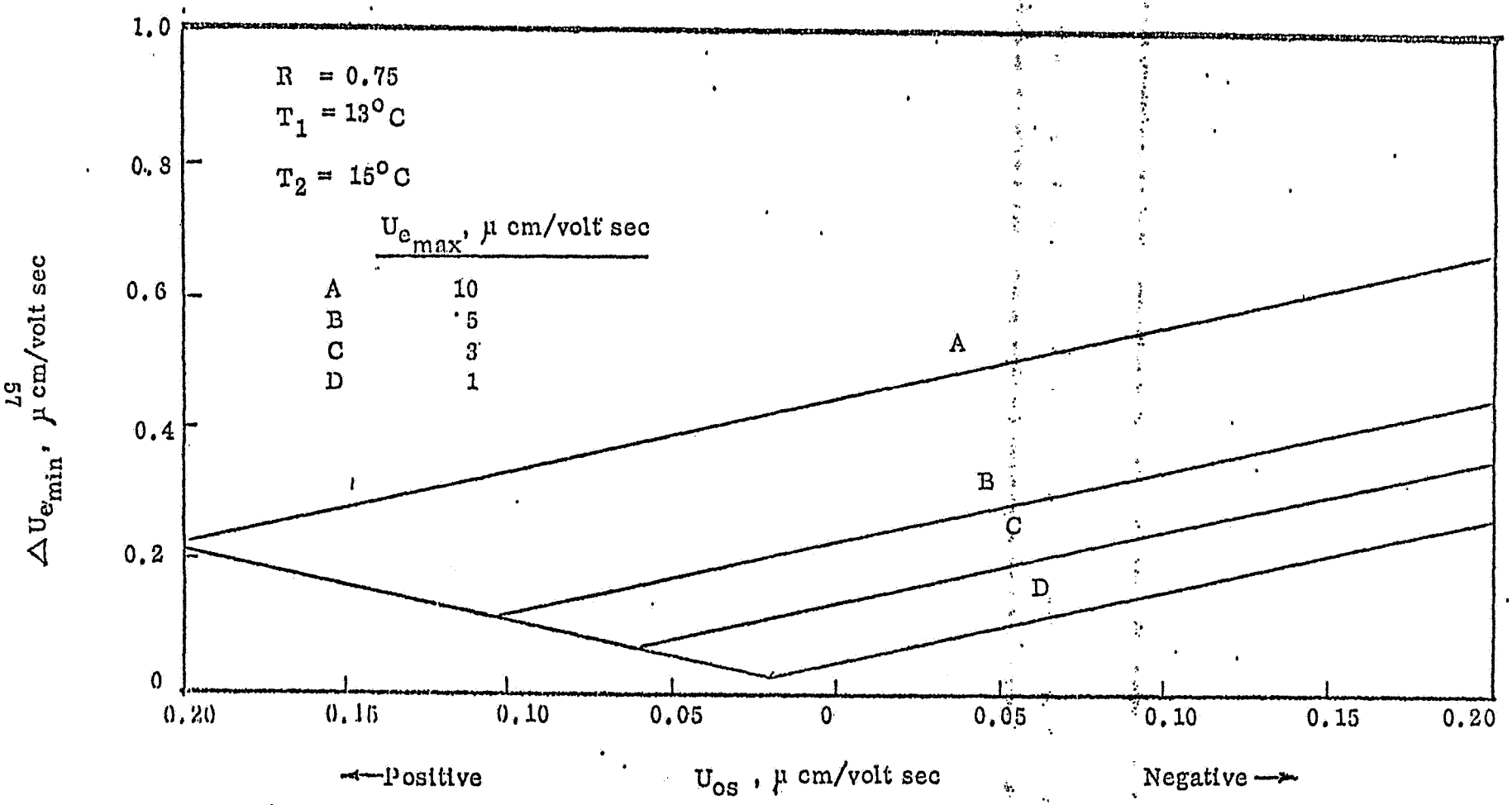

Figure 21 Variation of Resolution of Separation with Electroosmotic Mobility as a Function of Maximum Electrophoretic Mobility of the Particles.

The computer program results were calculated using the following experimental parameters:

Length of the electrophoresis column..... 14 cm
Sample plug thickness..... 0.3 cm
Ratio of sample plug radius to column radius..... 0.75
Temperature at center of column..... 15° C
Temperature at column wall..... 13° C
Electroosmotic mobility..... 0.20μm cm/volt sec

Included in the computer program are the following assumptions: the radial temperature gradient in the column is parabolic; the electrophoretic mobility of the sample particles is temperature-dependent only with respect to the dielectric constant and viscosity of the electrolyte medium; the temperature is independent of the length of the column and does not vary with time; and the potential gradient is uniform throughout the column.

The input for the electrophoretic mobility of the sample particles was designed to use not only single values, but also the complete electrophoretic mobility distribution, provided it can be expressed mathematically. A prerequisite for predicting the results of an electrophoretic separation, therefore, is a knowledge of the electrophoretic mobility distribution of the sample particles. Since one of the objectives of formulating this computer program was to aid in the analysis of the ASTP fixed red blood cell mixture experiment, the fixed red blood cells of rabbit, human, and horse were used for the initial computations. The electrophoretic mobility distributions for rabbit, human, and horse fixed red blood cells were measured in this laboratory by micro-capillary electrophoresis. These results are the solid lines of Figure 22; the bar graphs are the results reported by Dr. Knox, (Monthly Report, September 1975, NAS8-30887). The mobility distributions were then expressed by parabolic, straight line, and gaussian distribution functions.

The computer-calculated electrophoretic separations are shown in Figures 23, 24 and 25 for the parabolic, straight-line and gaussian distributions, respectively. The computer-calculated separations are presented in two different ways. The lower curve shows the concentration of particles as a function of length of the column. This lower curve gives no information concerning the radial distribution or position of particles in the column. The upper printout of each figure shows the cross-sectional position of particles in the column. This printout shows the location of particles in the column, but does not represent their concentration, i.e., each symbol does not have the same weight in terms of concentration. The combination of both types of computer outputs would be necessary to give a complete prediction of a FFE separation.

The results of Figures 23, 24, and 25 show the position of the particles after they had undergone electrophoretic migration for a distance of 14 cm. The time of migration is not important here because an arbitrary value of 10 volts/cm was used for the potential gradient. These results, furthermore, are not intended as a prediction of the ASTP fixed red blood cell separation since the experimental conditions were not the same. The results do show, however, the effect of different distributions on the degree of separation. While the parabolic and straight-line distributions yield practically identical results, the Gaussian distribution results in a somewhat poorer separation. This result is due to the fact that a

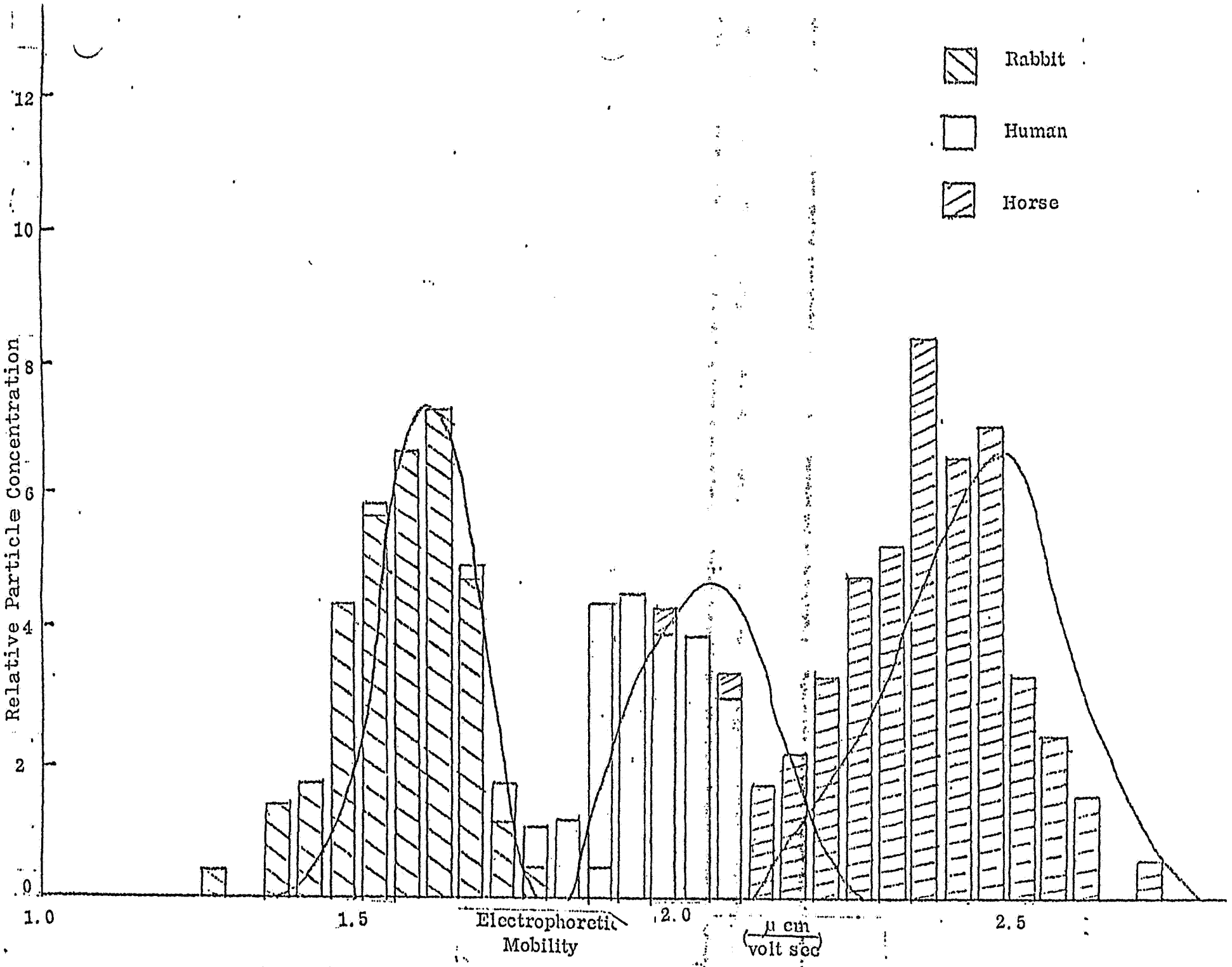

Figure 22 Electrophoretic Mobility Distributions of Fixed Red Blood Cells.

REPRODUCIBILITY OF THE ORIGINAL PAGE IS POOR

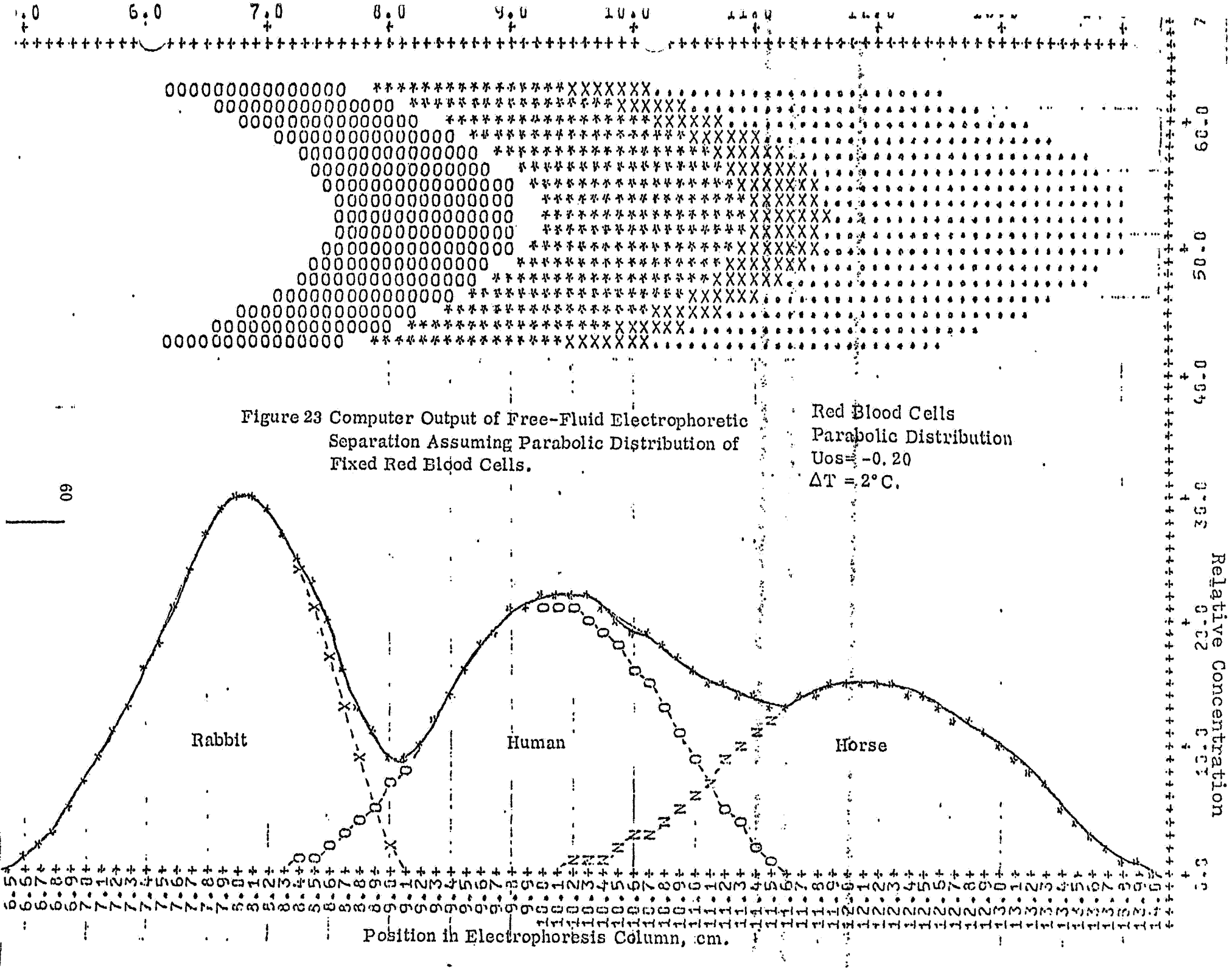

Figure 23 Computer Output of Free-Fluid Electrophoretic Separation Assuming Parabolic Distribution of Fixed Red Blood Cells.

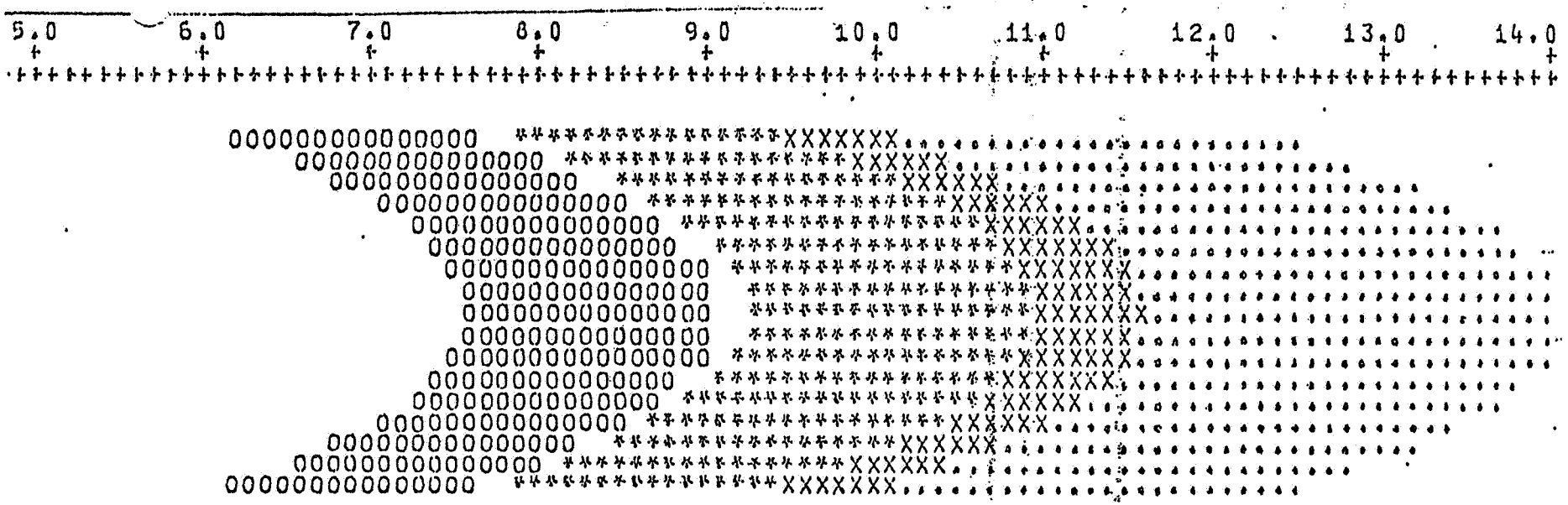

Figure 24 Computer Output of Free-Fluid Electrophoretic Separation Assuming Straight Line Distribution of Fixed Red Blood Cells.

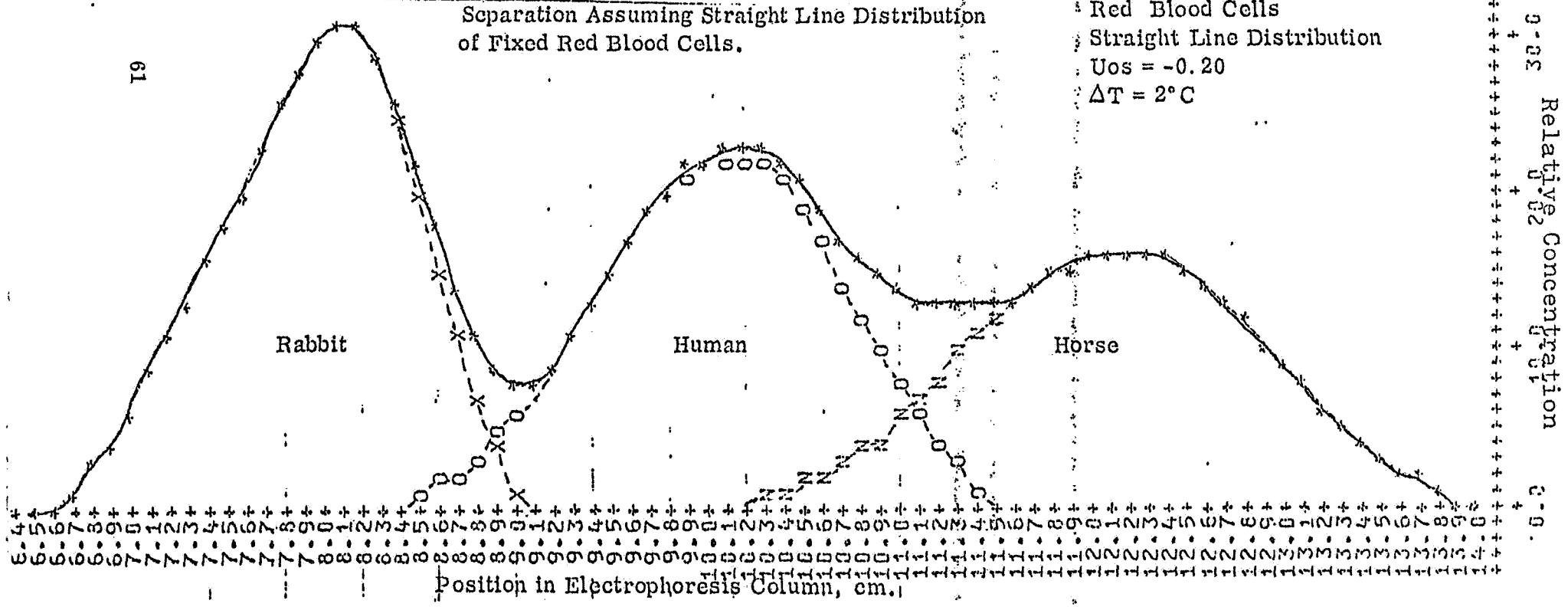

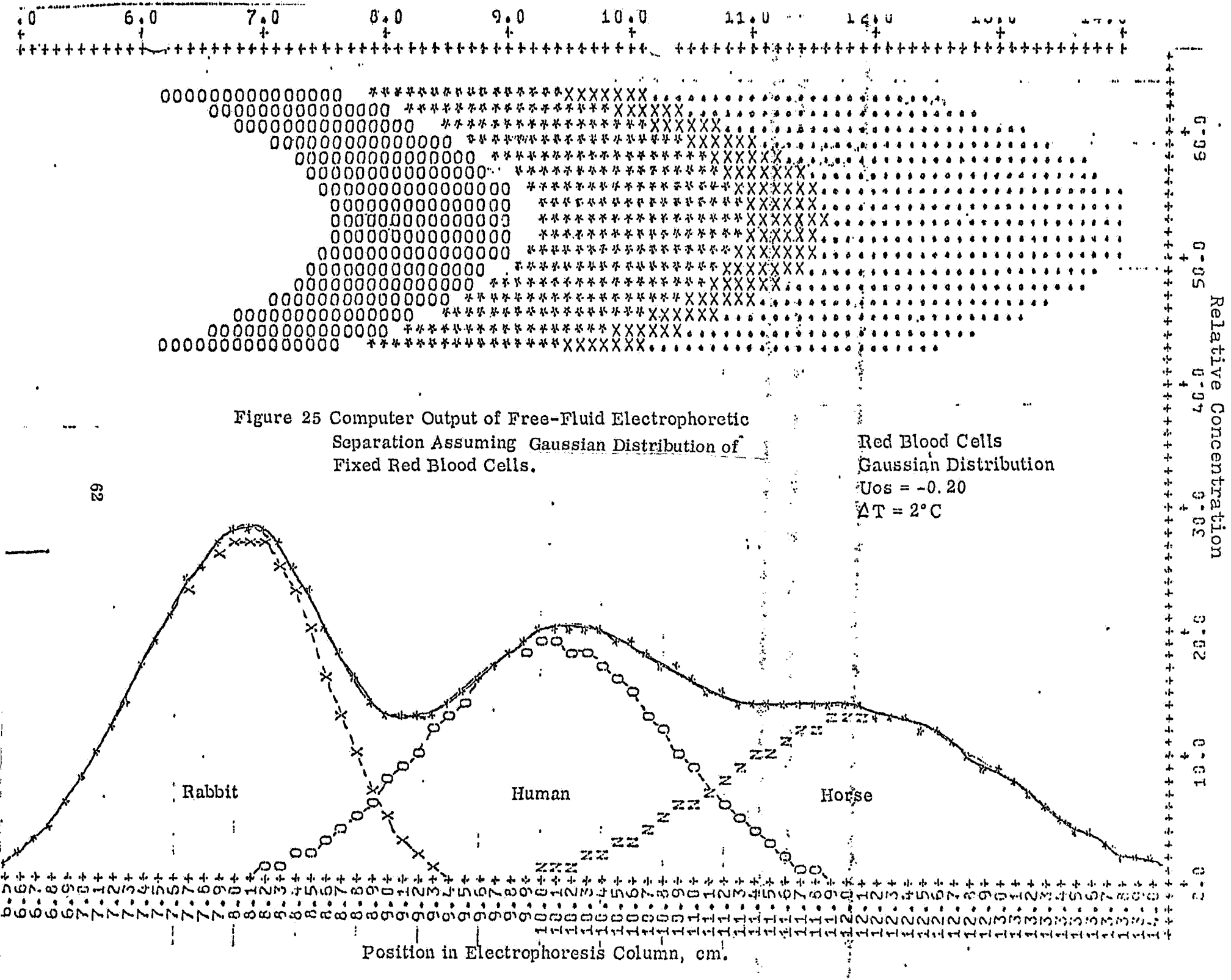

Figure 25 Computer Output of Free-Fluid Electrophoretic Separation Assuming Gaussian Distribution of Fixed Red Blood Cells.

Gaussian distribution fitted to the experimental results leads to a more gradual decrease of the particle concentration to zero at high and low electrophoretic mobilities than predicted by the straight line and parabolic distributions. Since the Gaussian distribution shows "tails" larger and smaller than those of the experimental data, it is unrealistic and therefore shall not be used for future analysis of fixed red blood cells.

The two experimental variables which were investigated were the electroosmotic mobility and the radial temperature gradient ΔT, where ΔT is equal to the temperature in the center of the column minus the temperature at the column wall. The computer printout results with ΔT at a constant value of 2° C and varying U_{os} are reproduced in Figures 26-30 for U_{os} values of -0.3, -0.2, -0.1, 0.0, and +0.05μm-cm/volt-sec, respectively. The results show that, as the magnitude of U_{os} decreases, the degree of separation of the fixed red blood cells increases, with the maximum separation occuring at a U_{os} value of +0.05μm-cm/volt-sec. These results are in agreement with previously reported results which showed that the maximum resolution (i.e., minimum value for $\Delta U_{e_{min}}$) for these experimental conditions occurs at a U_{os} value of +0.05μm-cm/volt-sec.

The computer printout results with U_{os} at a constant value of -0.2μm-cm/volt-sec and varying ΔT are reproduced in Figures 31, 32, and 33 for ΔT values of 5°, 0° and -5° C, respectively. The results show that as ΔT decreases the degree of separation increases. Negative values of ΔT means that the temperature in the center of the column is lower than at the column wall. Although a negative temperature gradient is unrealistic, the results do show the effect which a temperature gradient has on the degree of separation in FFE.

The computer program which has been developed for predicting the electrophoretic separation of particles in FFE can predict the degree of electrophoretic separation as a function of the different physical and experimental parameters. The computer printout results predict the position of particles in the column and the concentration profile of the particles along the length of the column as a function of time. This information can be useful for the design of the experiment itself and for evaluating candidate samples for this type of separation. This type of analysis is also expected to be useful for evaluating the ASTP fixed red blood cell experiment. The information necessary for a valid evaluation of the ASTP results is a knowledge of the electrophoretic mobility distribution of the rabbit, human, and horse fixed red blood cells, the absolute concentrations of each of these cells, a knowledge of the minimum concentration of cells which can be photographed under identical experimental conditions, and the flight film information such as the velocities of the leading and trailing edges of all visible bands.

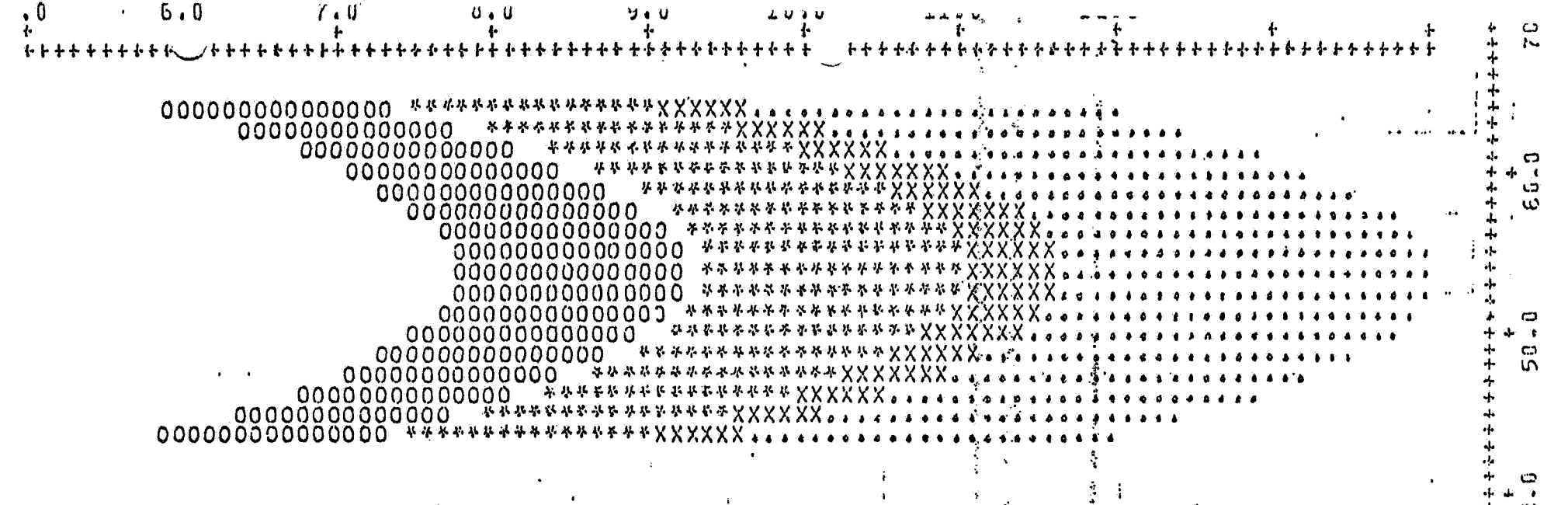

Figure 26 Computer Output of Free-Fluid Electrophoretic Separation Assuming Parabolic Distribution of Fixed Red Blood Cells with $U_{os} = -0.3\ \mu$ cm/volt sec and $\Delta T = 2$ C.

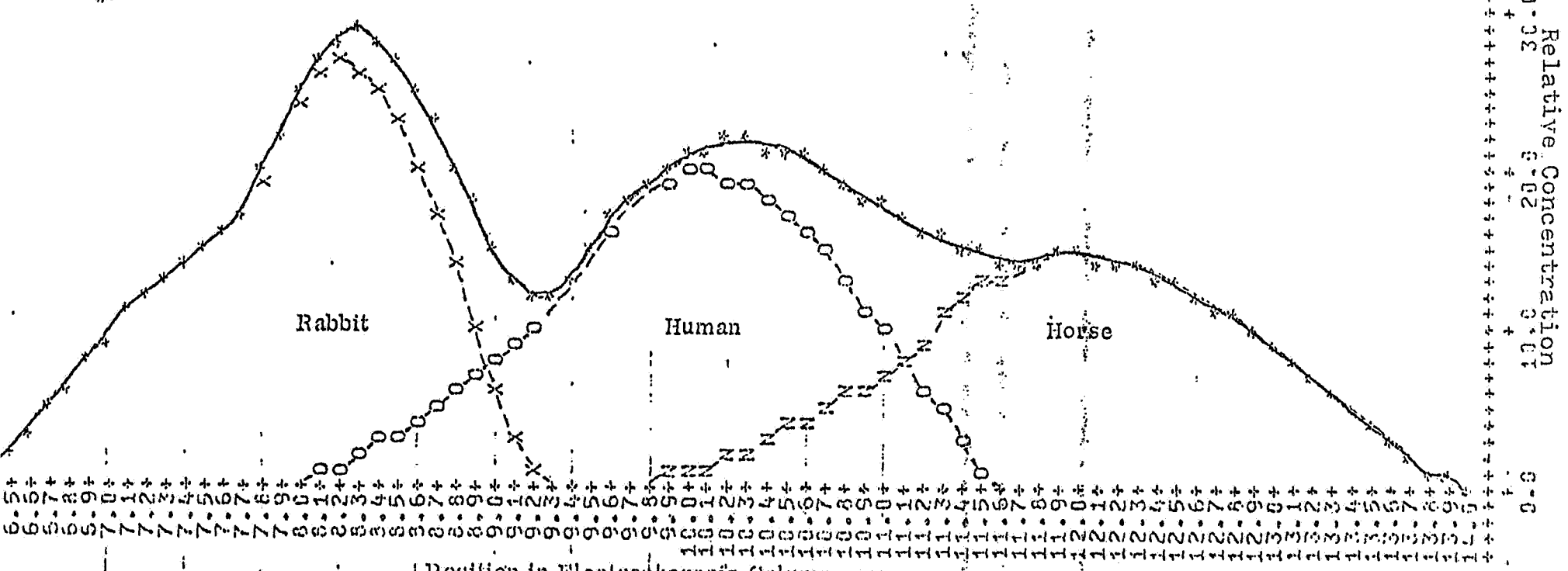

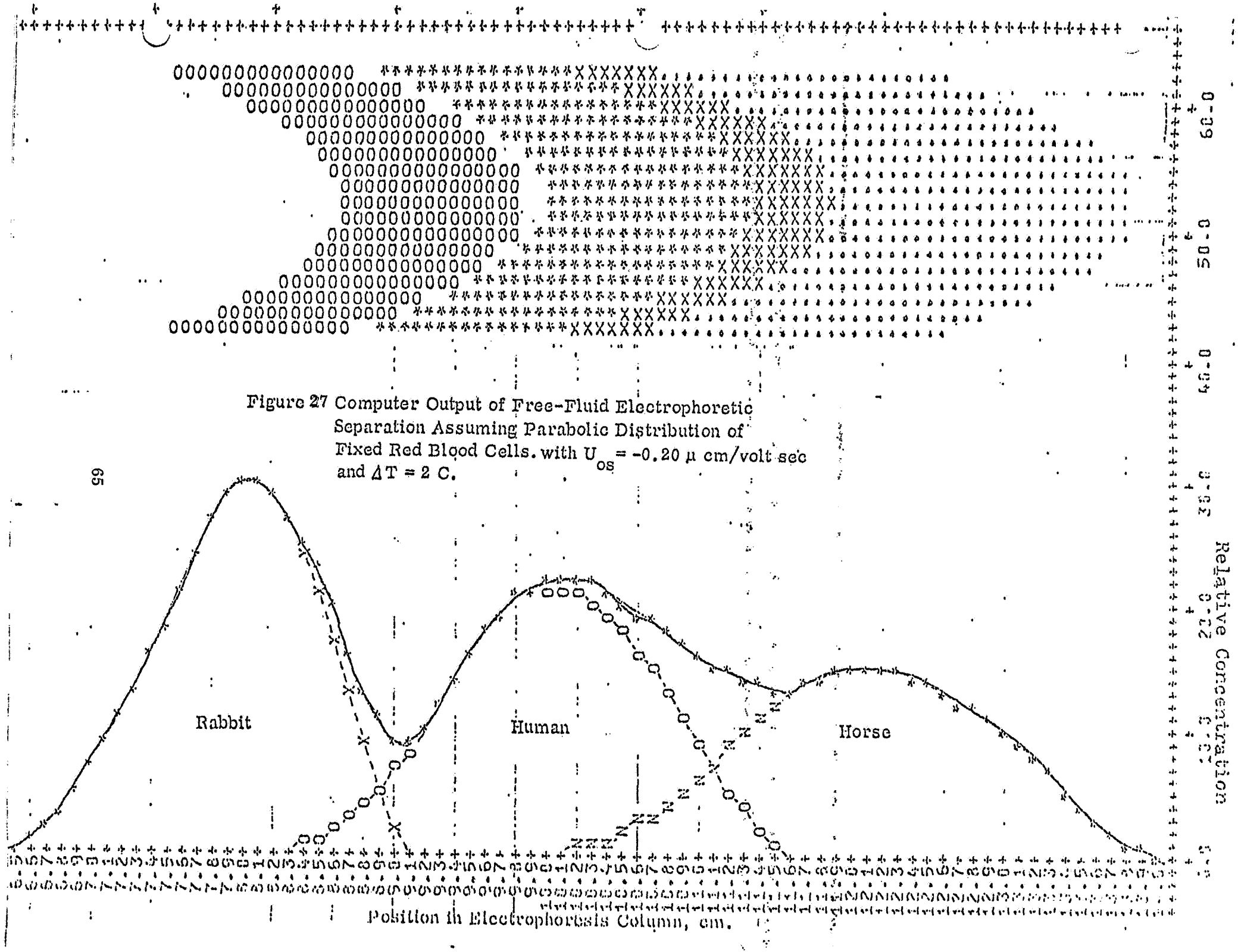

Figure 27 Computer Output of Free-Fluid Electrophoretic Separation Assuming Parabolic Distribution of Fixed Red Blood Cells. with $U_{os} = -0.20\ \mu$ cm/volt sec and $\Delta T = 2$ C.

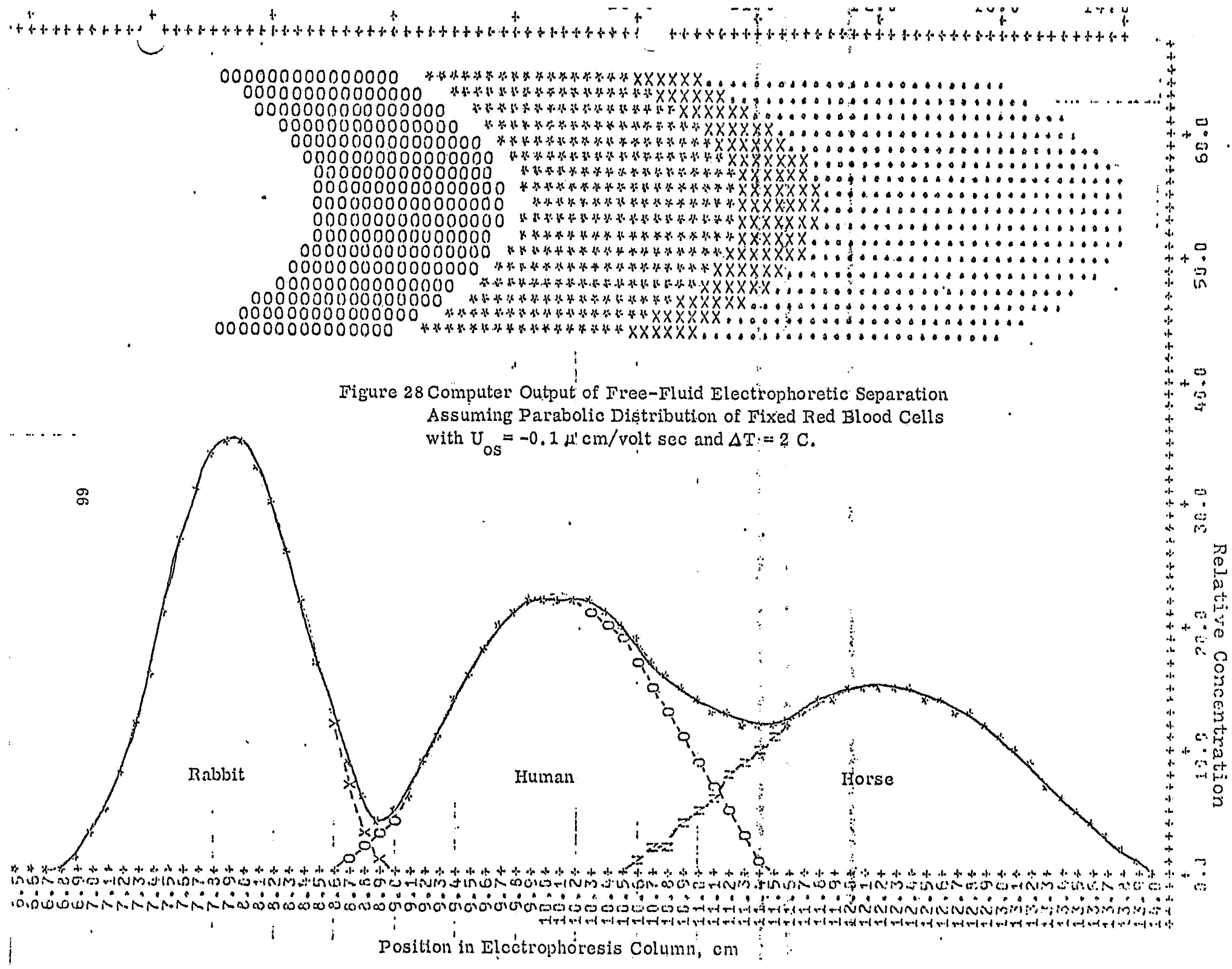

Figure 28 Computer Output of Free-Fluid Electrophoretic Separation Assuming Parabolic Distribution of Fixed Red Blood Cells with $U_{os} = -0.1\ \mu$ cm/volt sec and $\Delta T = 2$ C.

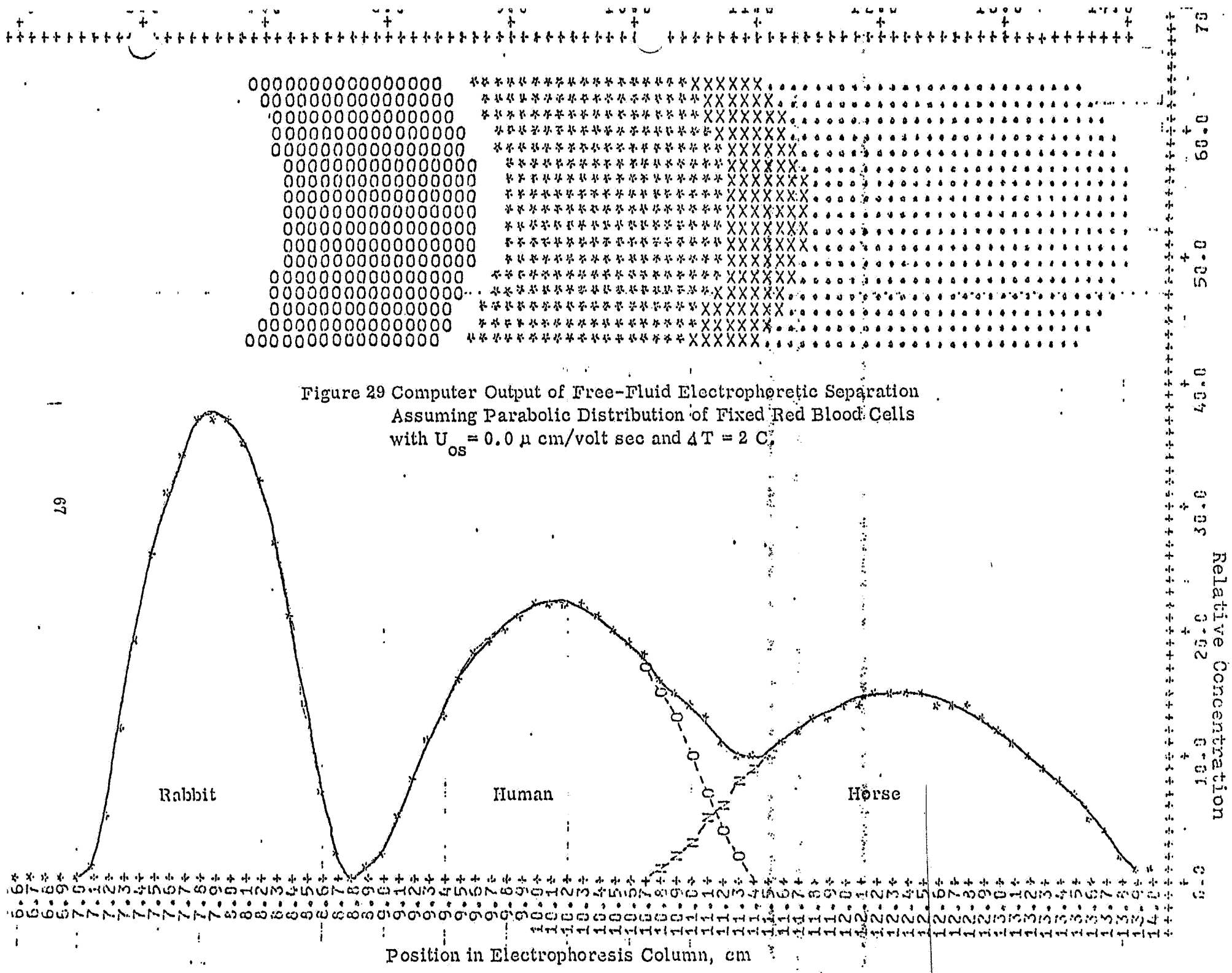

Figure 29 Computer Output of Free-Fluid Electrophoretic Separation Assuming Parabolic Distribution of Fixed Red Blood Cells with $U_{os} = 0.0\ \mu$ cm/volt sec and $\Delta T = 2$ C.

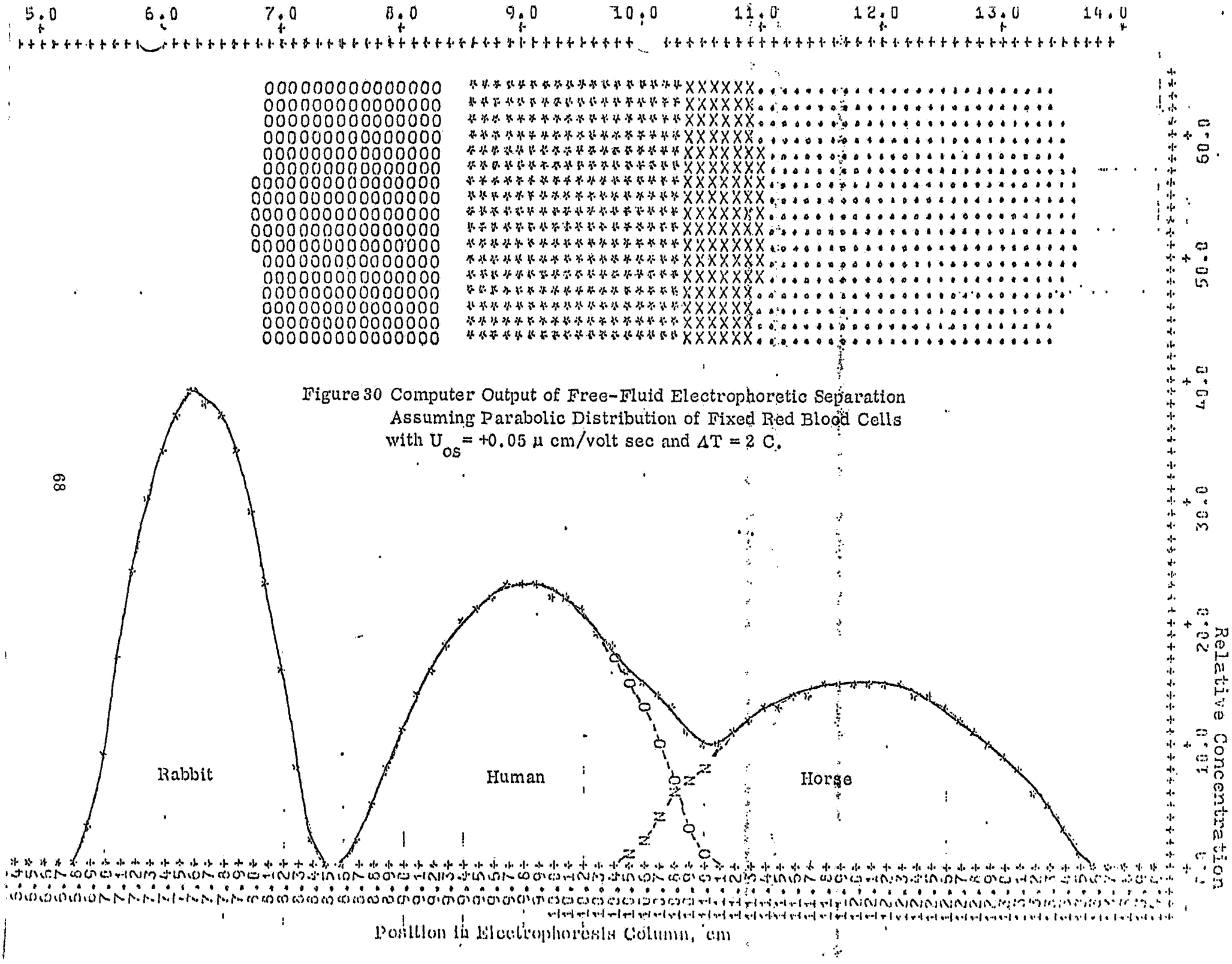

Figure 30 Computer Output of Free-Fluid Electrophoretic Separation Assuming Parabolic Distribution of Fixed Red Blood Cells with $U_{os} = +0.05\ \mu$ cm/volt sec and $\Delta T = 2$ C.

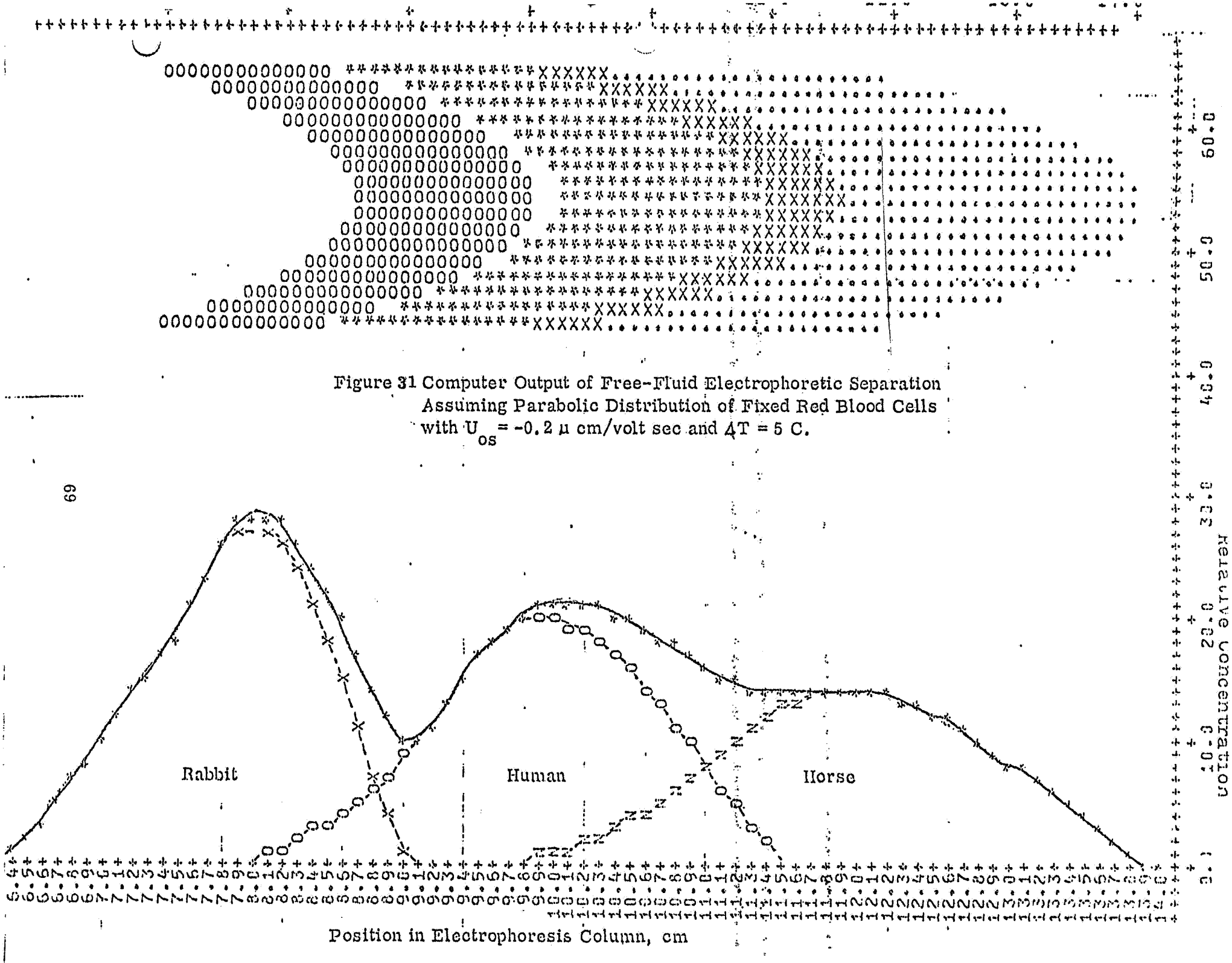

Figure 31 Computer Output of Free-Fluid Electrophoretic Separation Assuming Parabolic Distribution of Fixed Red Blood Cells with $U_{os} = -0.2\ \mu$ cm/volt sec and $\Delta T = 5$ C.

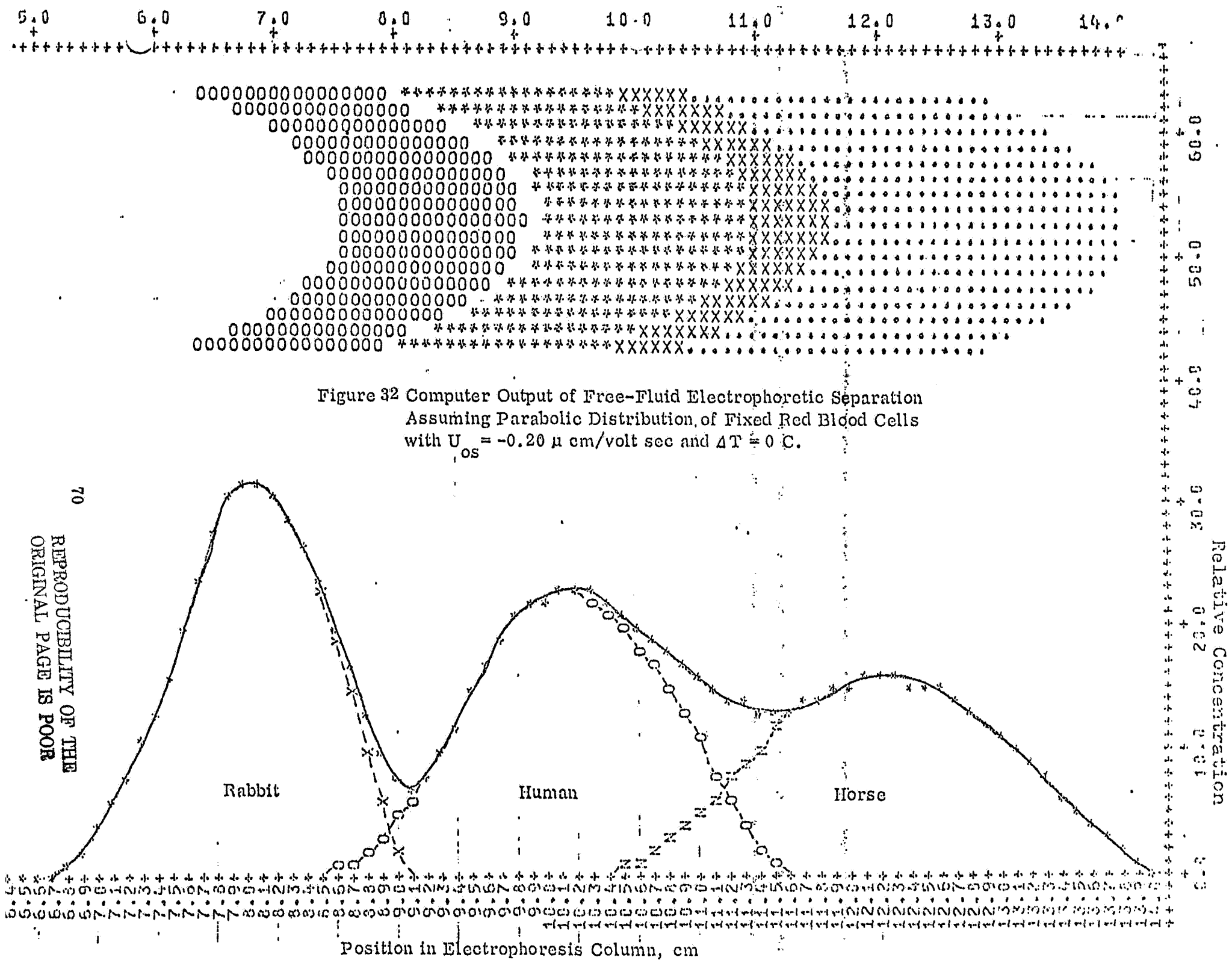

Figure 32 Computer Output of Free-Fluid Electrophoretic Separation Assuming Parabolic Distribution of Fixed Red Blood Cells with $U_{os} = -0.20\ \mu$ cm/volt sec and $\Delta T = 0$ C.

REPRODUCIBILITY OF THE ORIGINAL PAGE IS POOR

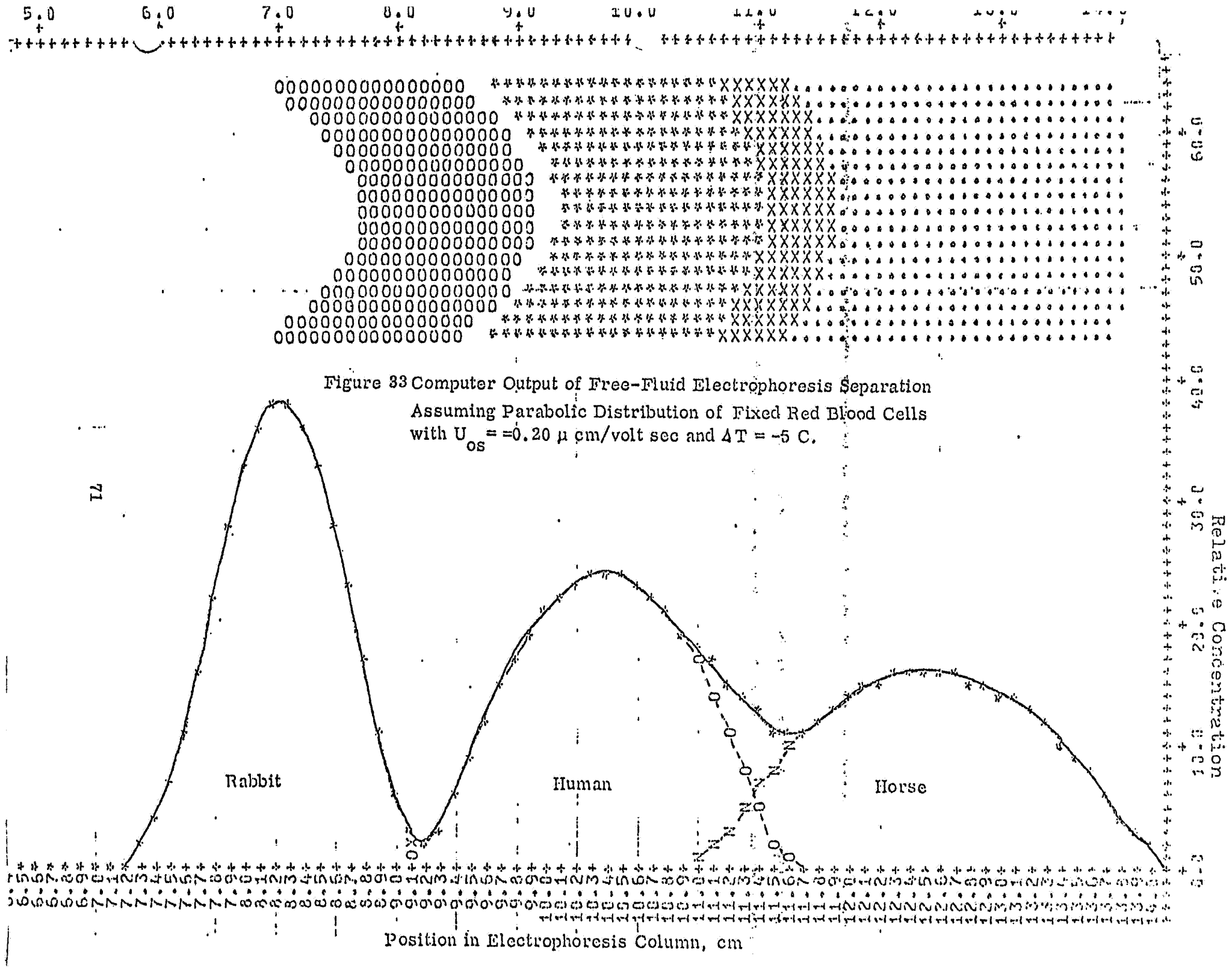

Figure 33 Computer Output of Free-Fluid Electrophoresis Separation Assuming Parabolic Distribution of Fixed Red Blood Cells with U_{os} = =0.20 μ cm/volt sec and ΔT = -5 C.

CHAPTER IV

EVALUATION OF THE BECKMAN CPE WITH STANDARD PARTICLES

A. Introduction

The Beckman CPE (continuous particle electrophoresis) apparatus was modified and evaluated for its potential use as an analytical instrument to determine the absolute values of the electrophoretic mobility of particle mixtures as well as the electrophoretic mobility distributions. During the course of this work, a series of monodisperse polystyrene latex particles, some of which were dyed different colors, were evaluated for their potential use as standard particles. The use of dyed latex particles of known electrophoretic mobilities was considered important for evaluation of the Beckman CPE because the colors of the separated fractions could be easily observed and thus the need for collecting and measuring the different fractions was obviated.

B. Experimental

The Beckman CPE was modified so that the displacement of the particle stream due to electrophoresis can be recorded accurately and reproducibly. The Plexiglas window, which is located at the bottom of the separation cell and which is used for the visual observation of the sample stream by means of reflected light, was replaced by a quartz window, which is transparent to ultraviolet light. A small optical-bench with an ultraviolet light source and slit for control of beam dimensions was placed in front of the window. The optical bench was attached to a motor, which moves it horizontally across the window to scan the particle stream after the separation and a resistance box, to establish the precise position of the ultraviolet light beam electronically. A UV-sensitive phototube was located in a fixed position on the other side of the window. A Houston Instruments Model 2000 X-Y recorder was used to record the intensity of ultraviolet radiation on the Y-axis and the horizontal position of the optical bench on the X-axis. The electrolyte used in the initial investigation was sodium barbital (Veronal) buffer, which has a pH of 8.6.

The particles used in this investigation were monodisperse polystyrene latexes. The electrophoretic mobilities of the particles were measured using the Rank Brothers Microcapillary Electrophoresis apparatus. The following procedure was used for dyeing the latex particles. An oil-soluble dye was dissolved in benzene; the resulting solution was emulsified in water and added to the latex in a 1:1 benzene solution-latex polymer ratio. Benzene is water-immiscible and a good solvent for polystyrene-type polymers; therefore, it should swell the particles by diffusion from the emulsion droplets through the aqueous phase. Polystyrene latex particles display equilibrium swelling values for good solvents of about 2-3:1 solvent-polymer ratios (the equilibrium swelling ratio increases with increasing particle size and decreasing polymer-water interfacial tension). The swelling of the latex particle by the benzene is expected to take the dissolved dye along with it, provided the dye is also a "solvent" for the polymer. Once the particles are swollen with the benzene-dye solution, the benzene is removed (and the dye left behind) by steam distillation, preferably at reduced pressure. Two requirements for the success of this experiment

(which are not a priori predictable) are: 1. the latex must remain stable during the solvent-swelling and solvent-removal steps; 2. the latex particles must not reject the dye.

The 0.109μm and 1.01μm monodisperse polystyrene latexes were dyed with Calco Oil Blue and Calco Oil Red (American Cyanamid Co.), respectively. The solutions (5%) of dye in benzene were added to a small sample of latex in 1:1 benzene solution-latex polymer ratio, and the samples were agitated in various ways to facilitate mixing. In all cases, the benzene solutions were sorbed into the latex, which took on the color of the dye. In some cases, the sorption of the benzene solution left some colored matter (perhaps rejected dye) on the top of the latex; this was removed and the experiment was continued. Examination of the latex samples by optical microscopy (1000X) showed the presence of latex particles and no other particles, i.e., if any particles of dye were present outside the latex particles, they were too small to be resolved under these conditions. The samples were subjected to steam distillation under vacuum to remove the benzene.

C. Theoretical

The principles of flow in the continuous-flow electrophoresis system have been described by Strickler and Sacks (Ann. N.Y. Acad. Sci., 209, 497, June 1973). A schematic representation of the electroosmotic flow and induced flow in the curtain is presented in Figure 34. The parabolic flow profile due to electroosmosis is in the x-y plane and is either positive or negative in the y direction, while the induced parabolic flow profile is in the x-z plane and is always positive in the z direction. The sample is injected into the center of the stream with a cylindrical configuration and moves with a constant electrophoretic velocity in the y direction in the presence of an applied potential. The migration of the particles is affected by two factors, both of which are a function of their position in the x direction: the electroosmosis of the electrolyte medium which affects the net particle velocity; and the induced parabolic flow profile which affects the velocity of the particle in the z direction and hence the time of exposure of the particle to the electric field. Both factors ultimately affect the migration distance of the particles and the configuration of the sample stream. Both the electroosmotic and induced parabolic flow profiles of the electrolyte medium have compensating effects, i.e., as the particle position increases from the center of the channel the net particle velocity decreases in both the y and z directions. This means that the slower-moving particles will be subjected to electrophoretic migration for a longer period of time than the faster-moving particles in the center of the curtain flow. In principle, therefore, it is possible to match the electroosmotic flow to the induced flow so that the sample streams will remain undistorted after separation. Under these conditions, the displacement of the sample stream will be controlled by the particles in the center of the curtain where the velocity of buffer in the z direction and the positive velocity of buffer in the y direction are both at a maximum. The displacement of the sample bands under these conditions may be defined by the equation:

$$d = kE\ (U_e + U_b), \tag{55}$$

where k = time of separation, sec,
E = applied potential gradient, volts/cm,

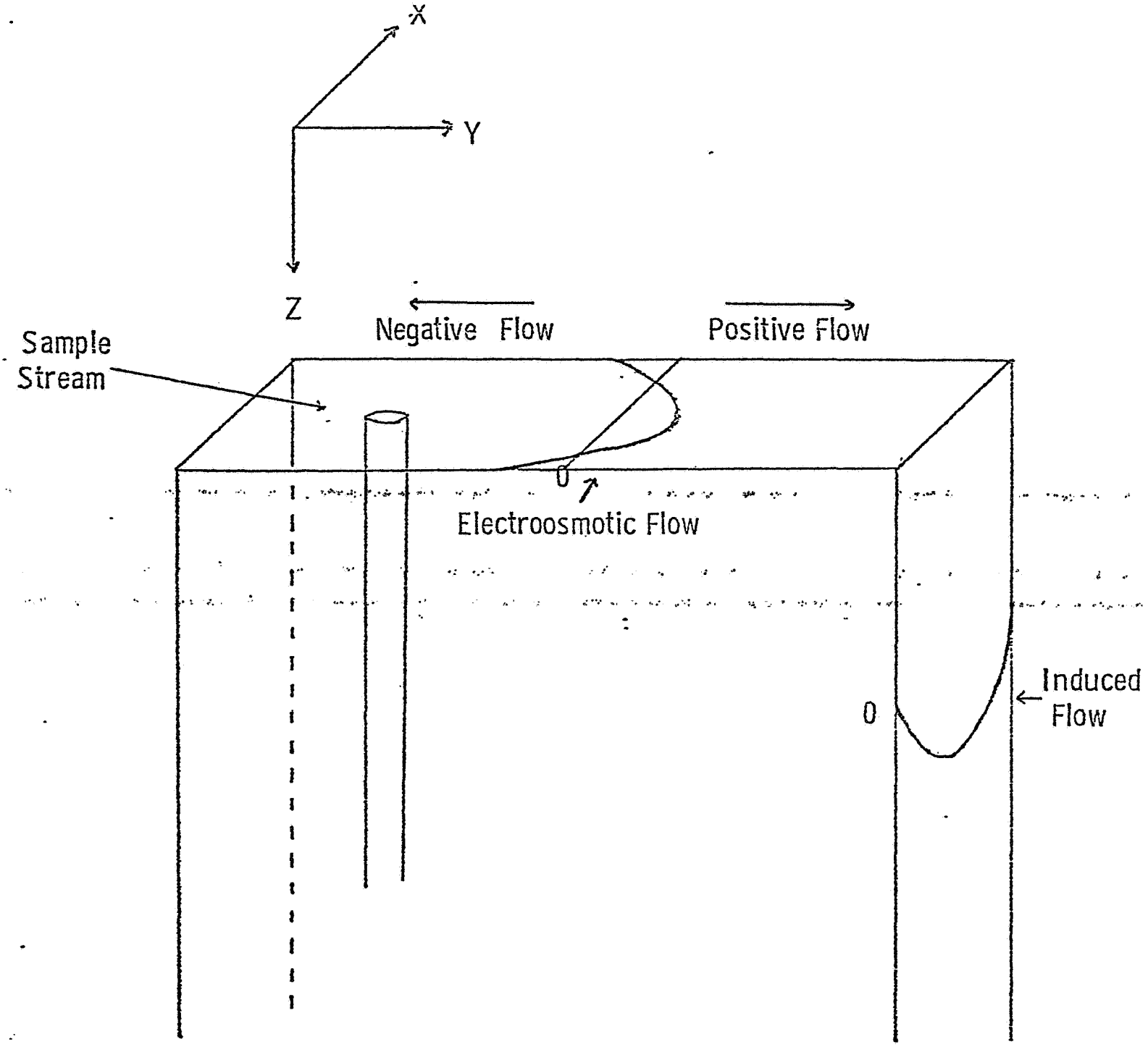

Figure 34 Schematic representation of flow profiles present in electrolyte curtain of CPE.

U_e = electrophoretic mobility of the particles, μm cm/volt sec,
U_b = the effective electrophoretic mobility of buffer in the center of the channel, μm cm/volt sec,
d = displacement of sample band, μm

Equation 55 may be defined in terms of the instrument parameters of the CPE system. Since the current flow is in a cell of rectangular geometry, the electrolyte velocity in the center of the channel can be related to the electroosmotic velocity by the Komagata Equation. Under the conditions present in the CPE, the velocity in the center of the channel is equal to one-half the electroosmotic mobility so that $U_b = U_{os}/2$, where U_{os} is the electroosmotic mobility at the cell wall/liquid interface. It can also be shown from hydrodynamic equations that the velocity of a fluid in the center of a rectangular channel is equal to 1.5 v_{av}, where v_{av} is the average linear velocity. The time of separation k, therefore, is equal to $L/1.5\ v_{av}$, where L is the length of the channel which is exposed to the applied field. Since $v_{av} = F/A$, where F is the rate of volume flow and A is the cross-sectional area of the channel, Equation 55 may be expressed as:

$$d = \frac{L\,A\,E}{1.5\,F}\left\{U_e + \frac{U_{os}}{2}\right\} \qquad d = (L\,A\,E/1.5\,F)\left[U_e + (U_{os}/2)\right] \tag{56}$$

The Beckman CPE instrument used in this investigation has the following instrumental parameters: L = 30.5 cm, A = 0.675 cm^2, F = 0.417 cm^3/sec, so that:

$$d = 32.9\ E\left\{U_e + \frac{U_{os}}{2}\right\} \qquad d = 32.9\ E\left[U_e + (U_{os}/2)\right] \tag{57}$$

D. Experimental Results

The displacement of the sample stream displayed on the X-Y recorder was calibrated in terms of the actual displacement by allowing the UV light source to scan across a transparent ruler which was imprinted with 1-mm divisions. The magnification factor on the recorder was found to be 18.2X. A series of monodisperse polystyrene latexes dispersed in Veronal buffer was used to evaluate the CPE by measuring the displacement distance as a function of the applied potential gradient in the range 20-100 volts/cm. Although the separation distance was proportional to the applied potential gradient, some scatter was observed; this was attributed to experimental problems such as maintaining a constant flow rate for both the curtain buffer and sample injection. Figure 35 shows the results for the 1.01μm diameter latex where the displacement of the sample stream is recorded for different applied potentials.

Although there are both experimental and theoretical problems in using the CPE as an analytical tool to determine the absolute electrophoretic mobility of particles, the instrument is ideally suited for determining the relative electrophoretic mobilities of a mixture of particles. A mixture of six different monodisperse latexes with particle sizes in the

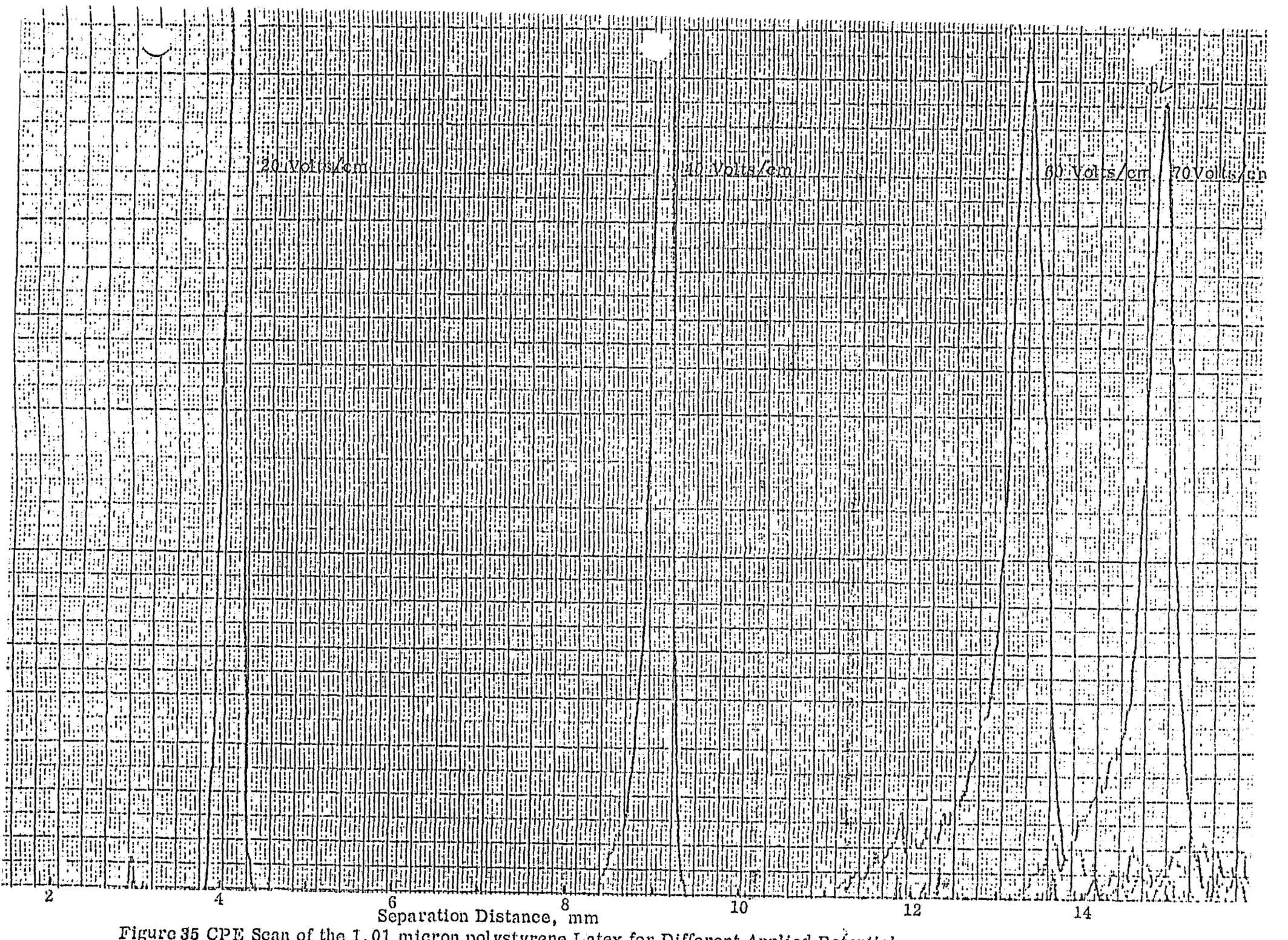

Figure 35 CPE Scan of the 1.01 micron polystyrene Latex for Different Applied Potentials.

range of 0.088 - 2.02μm was dispersed in sodium barbital buffer and separated in the CPE. The separation at an applied potential of 50 volts/cm is shown in Figure 36. The six different peaks were also observed at other applied potentials. Although these results indicate the extreme sensitivity of the CPE for determining relative electrophoretic mobilities of a mixture of particles, they also show that the ability of the instrument to separate particles is limited. This conclusion is deduced from the fact that although the 0.088, 0.109, and 0.357μm particles are distinguishable, their respective peaks all fall within a distance of 1 mm, which is beyond the limits of resolution of the collection tubes.

Several monodisperse polystyrene latexes were investigated to determine their electrophoretic mobilities in A-1 buffer, and three with measured electrophoretic mobilities of 4.0, 3.2 and 2.7μm cm/volt sec were colored red, white and blue, respectively. The three latex samples were then mixed in equal concentrations and separated in the Beckman CPE at an applied potential of 30 volts/cm. Figure 37 shows that the sample was indeed separated into three separate bands, which were visually identifiable according to their color. The separation distances of the red, white and blue particles were 5.9, 5.1 and 4.4 mm, respectively. The displacement of the red particles, along with the measured electrophoretic mobility of the same sample, was substituted in Equation 57 to calculate the value of U_{os} in the CPE. The calculated U_{os} value was 3.95μm cm/volt sec. This value, which is valid only for the A-1 buffer, can now be substituted into Equation 57, which is then solved for U_e:

$$U_e = \frac{d}{32.9\ E} - 1.975 \qquad U_e = (d/32.9\ E) - 1.975 \qquad (58)$$

The separation distances $\underline{d}$ for the white and blue particles were then substituted in Equation 58 to calculate $\underline{U}_e$. The values for the white and blue latexes were 3.19 and 2.48μm cm/volt sec, respectively, which are in good agreement with the values of 3.2 and 2.7μm cm/volt sec, respectively, determined by microcapillary electrophoresis measurements.

E. Conclusions

The Beckman CPE can be used as an analytical tool to measure the absolute electrophoretic mobilities of particles. Likewise, the separation distance of the sample stream can be calculated when the electrophoretic mobilities of the particles are known. The simplified equations and conclusions presented in this report, however, are only valid when the sample stream is not distorted by electroosmosis and induced parabolic flow. A more detailed theoretical analysis is necessary to take into account the various experimental parameters.

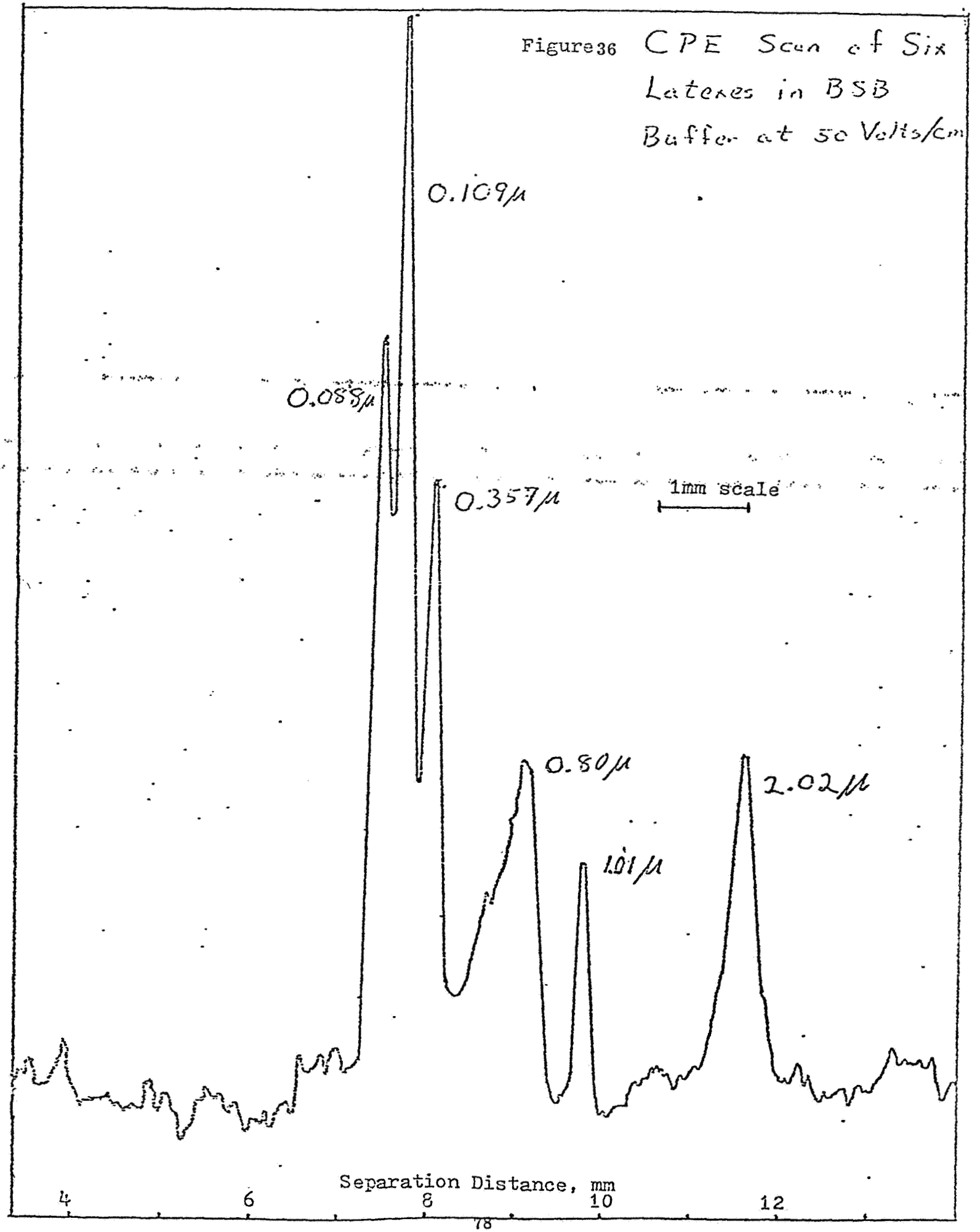

Figure 36 CPE Scan of Six Latexes in BSB Buffer at 50 Volts/cm

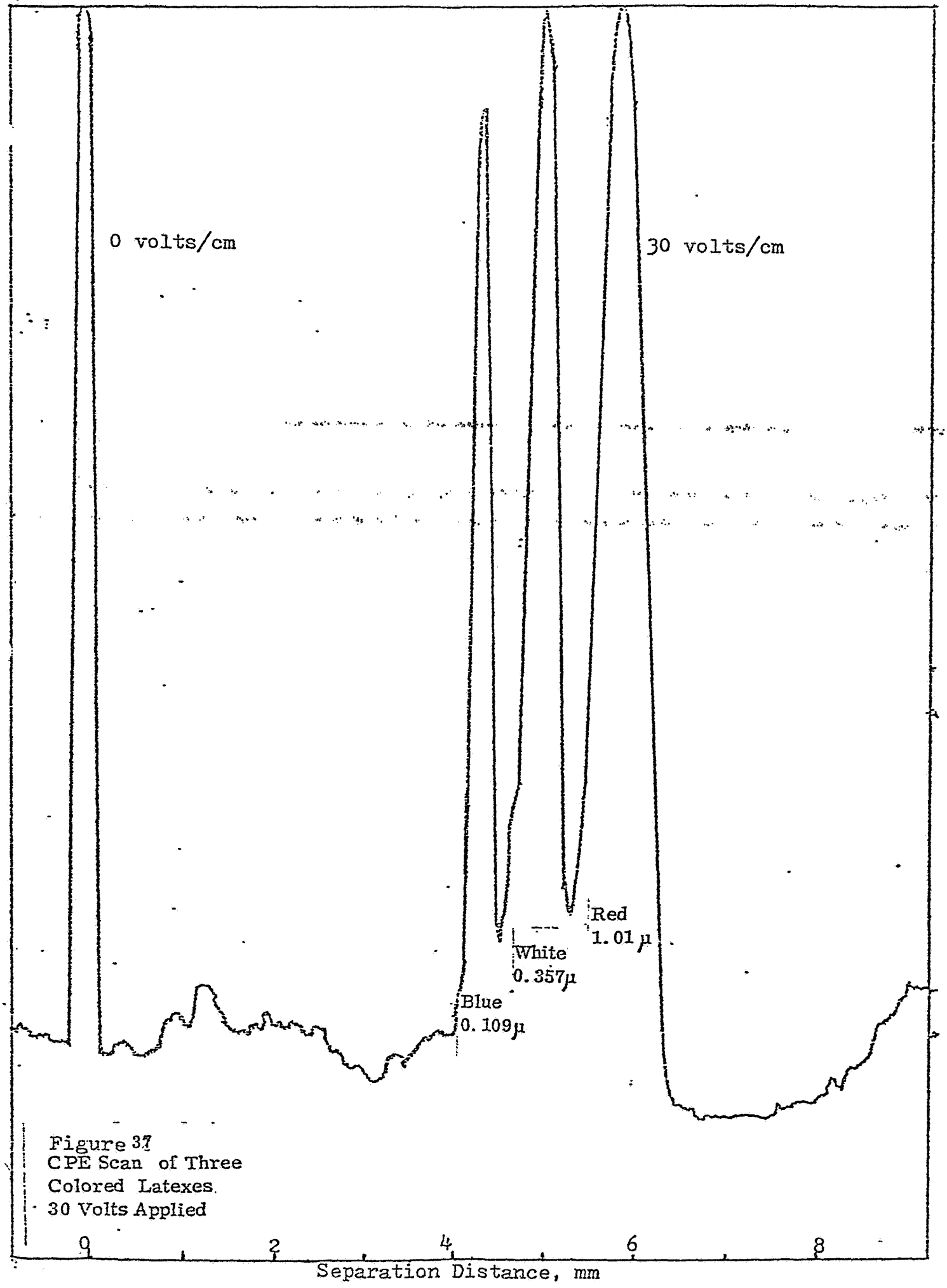

Figure 37
CPE Scan of Three
Colored Latexes.
30 Volts Applied

CHAPTER V

SUMMARY AND CONCLUSIONS

The Apollo 16 electrophoresis experiment demonstrated that separation of the two different-size monodisperse latexes did indeed take place, but that the separation was obscured by the pronounced electroosmotic flow of the liquid medium. The results of this experiment, however, were dramatic in the sense that it is impossible to carry out a similar separation on earth. The most practical conclusion which can be drawn from the Apollo 16 experiment is that a free-fluid electrophoretic separation is possible in space, whereas such a separation is not possible on earth. Also, it can be stated unequivocally that any electrophoretic separation will be enhanced under microgravity conditions. The only question is the degree of this enhancement, which can be expected to vary from one experimental technique to another.

The low-electroosmotic-mobility coating (Z6040-MC) which was developed under this program was found to be suitable for a free-fluid electrophoretic separation such as the experiment designed for the ASTP flight. The problem with this coating, however, is that its permanency is limited because of the slow desorption of the methylcellulose from the coated surface. This property of the Z6040-MC coating renders it less effective for continuous electrophoretic separation systems which are being designed for future space applications. Since any electrophoretic separation technique requires control, if not the elimination, of electroosmotic flow, more work is required to develop coherent coatings of the desired magnitude and sign of the cell-wall zeta potential.

The success of any electrophoretic separation of biological materials in space depends upon the degree to which particles of different electrophoretic velocities are separated. It would be desirable to predict the results of an electrophoretic separation for all techniques as a function of the various experimental parameters. This prediction would aid in the design and evaluation of the different experimental approaches. The development of the theory and resolution of separation in this report is limited only to consideration of the static free-fluid electrophoresis experiment designed for the ASTP flight. This same approach can and should be applied to all proposed electrophoretic separation techniques in order to evaluate and define the limits of application.